A Study on Modeling Downstream Influence in Signal Controlled Arterials

ZHU, Hong

A Study on Modeling Downstream Influence in Signal Controlled Arterials

（信号制御された幹線道路における下流影響モデリングに関する研究）

ZHU, Hong

(朱 宏)

Doctor of Engineering
Graduate School of Environmental Studies
Nagoya University
（名古屋大学大学院環境学研究科　博士（工学））

2020

Abstract

Signalized arterial is the core traffic facility of the urban road network and its performance is directly related to citizens' commuting convenience. The signalized intersection is one of the key components of signalized arterials. Their operations considerably affect the performance of the whole road system. Spillback describes the situations that downstream queues extended over upstream stoplines so that upstream platoons cannot be discharged normally. It is a common traffic issue on signalized arterials when traffic is extremely congested. However, even before spillbacks, the capacity of each intersection can be influenced especially on the signalized arterial on which intersections are closely spaced and undertake high input volume. This effect is called the downstream influence which is a visual and psychological impact on upstream drivers. While waiting to be discharged in an approach, drivers observe the size of the downstream queue and estimate the duration of the downstream queue. Base on this, then they will know whether their forward routes can be interfered by downstream traffic. If they noticed that their desired driving speed cannot be achieved, they may sacrifice the efficiency to pursue safety and comfort. As a result, the performance of the discharge flow is discounted. Meanwhile, this impact can be propagated and amplified towards the upstream direction. This is the reason why, in peak time, congestions occurred in upstream sections of designed bottlenecks.

However, in current practice, existing traffic simulators cannot capture this phenomenon properly, because they ignore the capacity drop before spillback happens. Meanwhile, estimation methodologies in existing manuals do not include factors comprehensively explaining the downstream influence. Correspondingly, the primary objective of this research is to theoretically model the downstream influence and propose a procedure that can properly estimate the influenced saturation flow rate (SFR, hereinafter) and start-up lost time (SLT, hereinafter). Several questions should be answered before achieving this target. How to measure and quantify the downstream influence? How to introduce the downstream influence into the traffic simulation on signalized arterials? More importantly, how to produce estimation methodologies for SFR and SLT that can be applied in practice? However, fundamental research regarding the above questions is very rare so far. Moreover, empirical cases of discharged flow with downstream influence are important and not easy to be observed. Finding

proper survey sites is another challenge of this study. To solve the above questions, the effort of each chapter is highlighted below.

As an initial step of this research, fundamental philosophies of the discharge process at signalized intersections are introduced in ***Chapter 2***. Also, attention is also given to reviewing literature about related researches. Existing methodologies about SFR and SLT estimations are listed and compared. Also, previous researches about downstream influence are summarized, which aims to provide a deep understanding of current research gaps and pave the way for this research.

Chapter 3 quantifies impacts of the downstream traffic on the discharge flow at upstream through lane by both empirical study and theoretical model. Utilizing the data collected at an experimental site of Yasukuni-tori in Tokyo City, SLTs and SFRs of 5 approaches at 3 signalized intersections are statistically studied with several downstream factors (queue length, segment length, and offset). Results show that long queues in the short downstream segment under large positive offset may lead to low SFR and large SLT. Based on these findings, a virtual speed (v_{op}) is created to measure the downstream influence, v_{op} is the speed by which the upstream platoon joins the downstream queue just at the time when the last vehicle starts to move. v_{op} is a function of queue length, segment length, and offset. By using this variable as the core indicator, the intelligent driver model (IDM) is improved and the new model is named as IDM+ in this study. A micro-simulation platform is designed based on the IDM+. Moreover, simulated trends are generalized and summarized into a two-step model by doing the regression analysis on data that were produced from the simulation experiment. In this two-step model, v_{op} is firstly calculated based on downstream factors. Influenced SFR and SLT are then derived based on the v_{op}. Firstly, the new model completely coincides with the experiment data. More importantly, it shows a similar trend and has a good fit with what was observed from the survey site.

Chapter 4 analyzes the downstream influence on signalized arterials. The cell transmission model (CTM) is a popular model of simulating traffic propagations and modified CTM improved the basic theory so that it can simulate realistic discharge features (SFR and SLT). In this study, downstream impacts are introduced into the modified CTM letting its parameters be governed by models of influenced SFR and SLT (from ***Chapter 3***). Firstly, the performance of the proposed CTM is proved to have equivalent performances as the IDM+. In

order to further test the new CTM, a CTM based platform is created for simulating a real-world arterial, the Hirokoji-tori in Nagoya. The comparison result shows that the modified CTM model considering downstream influence fits the observed traffic flow on signalized arterials better than the existing CTM. Especially in predicting the traffic congestion, the newly proposed CTM has a very outstanding performance. This conclusion emphasized the important role of downstream influence in modeling traffic propagation along signalized arterials. Finally, the proposed model is tested through a sensitivity analysis by which it is pointed out that high traffic demand, high entry flow from the minor streets, short segment links, large positive values of both downstream and secondary downstream intersections' offsets may result in the upstream congestion of signalized corridors.

Chapter 5 mainly proposes a methodology that can estimate adjustment factors for SFR and SLT by the long-term traffic demand profile instead of the real-time queue length data. In the beginning, another CTM based platform is created by use proposed CTM to simulate the discharge process at a signalized intersection. By utilizing the data from simulations, the relationship between traffic demand and queue length is modeled by the regression analysis. Following the hint of models of influenced SLT and SFR in ***Chapter 3***, the estimation model for adjustment factors is structured into a two-step model as well. Firstly, v_{op} is calculated by the estimated queue length along with other downstream factors. Secondly, another regression analysis is done to determine the relationship model between simulated adjustment factors and newly calculated v_{op}. Then, CTM based platform and the proposed estimation procedure are performed for 6 specially designed scenarios. Results are shown in contour line figures. They revealed that lower green ratio, smaller cycle length, and more flow from minor streets result in more serious downstream impacts. Finally, the proposed estimation procedure is further applied in real-world approaches comparing with the methodology prescribed in MTSCJ. Results indicate that proposed adjustment factors are reasonable and necessary to be included in practice.

Chapter 6 highlights the major findings of this research. Consideration of multi-lane Arterials, the stochastic features of calibrated parameters in the car-following model, clearing vehicles influence, clearance lost time, and autonomous vehicle flow are suggested as significant future study points in order to reach the final goal of dynamic network traffic control considering downstream influence.

Acknowledgement

I would like to express my gratitude to all those who helped me during my three years of studies at Nagoya University.

My deepest gratitude goes first and foremost to Professor Hideki Nakamura from Nagoya University, my supervisor, for his constant encouragement and guidance. He illuminated the road ahead for me when I was the most confused in my life. He has walked me through all the stages of the three years. He provided a very blessed research environment and many opportunities to discuss with many overseas scholars to improve my academic knowledge and practical skills. Without his consistent and illuminating instruction, I could not successfully complete my researches.

I am also greatly indebted to Associate Professor Miho Iryo-Asano from Nagoya University and Associate Professor Hirokazu Kato from Nagoya University for serving my doctoral committee and for their significant suggestions and useful comments.

I owe my deepest gratitude to Assistant Professor Xin Zhang from Nagoya University. She has helped me a lot since I entered this laboratory. While studying in Japan, she guided me carefully like a sister, regardless of the difficulties of living in Japan or the problems of studying. No matter when I asked her questions, she always answered me patiently.

Thanks to the staffs from my laboratory Assistant Professor Yuji Kakimoto, Assistant Professor Nan Kang, and Technical Assistant Ayaka Imai who I have been busy helping me for my graduation. I also owe my sincere gratitude to my friends and my fellow classmates who gave me their help and time in listening to me and helping me work out my problems during the difficult course of the study.

Last thanks would go to my beloved family for their loving considerations and great confidence in me all through these years. I hope my daughter and wife can smile to every dawn and sunset.

Table of Contents

List of Tables

List of Figures

CHAPTER 1 INTRODUCTION

1.1 Research Background

As an important facility, signalized arterials play a critical role in collecting traffic from minor roads and delivering them to expressways. Especially during peak time, signalized arterial carried a large amount of commuter flow. Signalized intersections are fundamental components of signalized arterials and its operations significantly affect the performance of the whole arterial. Therefore, signalized arterials and intersections have been paid widespread attention.

It is undoubted that increasing the capacity of the discharging process at network nodes can enhance the performance of the whole signalized arterial effectively. For a typical signal cycle, vehicles would arrive randomly at any time following the demand profile and queued vehicles will be accumulated during the red time. Once the signal indication turns green, the queued vehicles will pass the stop line one by one and then gradually be discharged with a saturation flow rate (SFR). Transition stage from parking condition (0 flow rate) to saturation flow may (maximal flow rate) takes several seconds during which period, they shall react to the green signal, press the pedal and accelerate. Normally, the discharge process is defined by three variables, saturation flow rate (SFR, hereinafter), start-up lost time (SLT, hereinafter) and clearance lost time (CLT, hereinafter). They play main roles in traffic engineering studies and practice applications because they are foundation variables for capacity estimations at signalized intersections and determining signal phasing.

Especially in the urban area, congestion on signalized arterial is becoming a common problem in majority metropolis, which are influencing society, environment, and economy significantly. For decades, considerable attention has been paid to establishing methods to solve arterial congestion and improve operational efficiency. Some researchers and

practitioners introduced signal coordination into signalized arterials to improve overall traffic flow propagation along urban arterials. Green waves have been recognized as one of the most efficient methods to avoid or mitigate traffic congestion which is letting the green signal on before the upstream traffic flow arrives so that vehicles can keep running without stop. For instance, bandwidth maximization is one of the most popular methods in arterial signal coordination control following this idea (Little, 1981). However, its effect is always discounted for shortly spaced intersections under high traffic demand. Because the presence of queue in the downstream segment may slow down the vehicle platoon from the upstream approach and the upstream intersection is always influenced and works in a low capacity condition.

Considering this, traffic scholars suggested that under high traffic demand the existing queue in the downstream segment should be discharged for a few seconds firstly before the upstream green by shifting the offset. However, there is no systematic research on how traffic propagation is hindered by downstream traffic. Accordingly, no specific calculation procedure is proposed to define the shifted offset. In order to overcome this research gap, understanding the influenced capacity of the upstream intersection is the first important issue to be solved.

1.2 Problem Statement

The presence of long-length and long-duration queues in the downstream may negatively reduce the discharge performance of the upstream approach. Ideally signalized intersections with large cycle length under high traffic pressure need longer link length to accommodate a large amount of queued vehicles. For a short road segment, a large portion of the downstream space may be occupied by queued vehicles and only a small available space can be left for upstream discharging. Once the above situation is accompanied by positive offsets, the duration of the downstream queue can be further extended.

For understanding the downstream impact, the discharge flow is roughly divided into three types. First is the uninfluenced discharge flow, upstream platoon discharges into a downstream segment with ideal traffic conditions (short queue or even no queue). In this case, the capacity of upstream is limited by road conditions such as geometry design. Secondly, spillback is an extreme case of the downstream impacts when the downstream queue is quite long and last for

long durations. Vehicles of upstream intersection cannot pass the stop line because of the extension of the downstream queue. This phenomenon will waste effective green time and significantly reduce the efficiency of the upstream intersection. It has been referred to in Highway Capacity Manual (HCM, hereinafter) 6th Edition (TRB, 2016) and added into the estimation model as a reduction parameter. At last, recently, it has been widely recognized that even before spillback occurs the capacity of the upstream intersection will be deteriorated by the downstream conditions. Therefore, between uninfluenced discharge flow and spillback, there is another type of discharge flow named influenced discharge flow. In this influenced discharge flow, the upstream platoon can pass the stop line without stopping. However, facing the downstream queue, especially for the through movement, most of the drivers may hesitate to quick start-up and choose a lower speed than free start in order to have a more comfortable and safer trip. It is expected that the longer the downstream queue is, the greater such an impact. Furthermore, if the queue in the downstream segment is still waiting for the traffic signal to turn green, the drivers departing from the subject intersection approach would be further discouraged because a red indication of the next signal means the long duration of the downstream queue.

On the other hand, during peak hours along urban arterials, if congestion happens, researchers usually attribute it to traffic demands higher than bottleneck capacities or problematic signal timing. However, at some intersections which their designed capacities satisfy the demand and should not be the bottleneck of signalized arterials, congestion still can be frequently observed. What's more, traffic flows freely in downstream intersections at the same time. Through observation and analysis, we claimed that congestions on signalized arterials should not simply be blamed on reaching capacity or wrong signal timings. Cumulative interactions between multiple consecutive intersections such as the above-mentioned downstream influence have inescapable responsibilities. This part will be detailed introduced in ***Chapter 4***.

Hence, downstream influence is an important issue not only for estimating the capacity of a single intersection but also for accurately simulating the real traffic propagation along a signalized arterial. However, the existing estimation methods for capacity do not fully consider the downstream influence and they could overestimate the real value. For instance, the estimation model of SFR in HCM only explained the downstream influence when spillback happens but did not cover the capacity drop of influenced discharge flow. What's more, none

of the existing manuals proposed a method to estimate the influenced SLT considering downstream influence. These yield to overestimated capacity, especially in urban dense corridors with closely spaced intersections further result in the inappropriate estimation of vehicle signal green intervals and cycle lengths.

Besides, existing simulators did not properly include the consideration of downstream impacts when modeling discharge behaviors at signalized intersections. This drawback may reduce the simulation accuracy which makes simulators fail to predict the occurrence of congestion. Vehicles in existing simulators (such as VISSIM) can only react to motions of vehicles ahead. Although this interaction can result in a little reduction in discharge performances. However, in the real world, not only a single vehicle ahead but also the whole platoon downstream may influence upstream drivers' judgment and operation. This little reduction described by existing simulators is not enough to explain the actual influenced discharge process. (The detailed analysis will be further introduced in ***Chapter 2*** and ***Chapter 3***) in the capacity of the upstream intersection. Therefore, developing a concrete estimation methodology for the influenced SFR and SLT with proper considerations of downstream impacts is necessary.

1.3 Research Objectives

According to the problem statement above, an overall research framework to reach the global objective is presented in Figure 1.1.

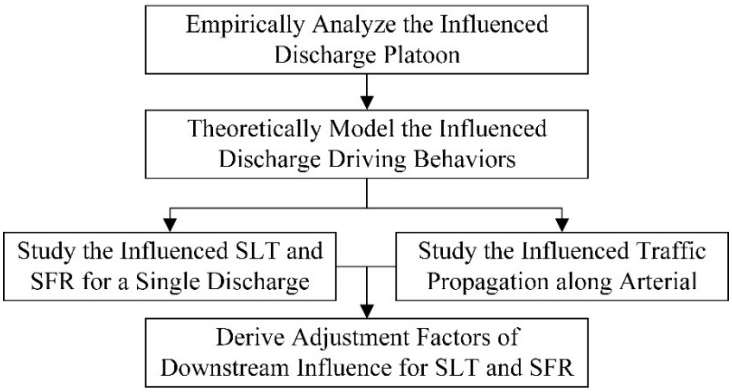

Figure 1.1 The overall research framework

Firstly, though vehicles in the upstream approach can directly observe the downstream queuing conditions with less sight obstruction, they will react to and influenced by the downstream platoon. Theoretically, they are more significant to downstream traffic. Excluding the influence of turning vehicles, this article will mainly focus on the capacity of through lanes before spillback occurs. With the recognition of the study becomes deeper, research objectives are divided into four stages. This research primarily intends to study the influenced discharge procedure empirically. More specifically, this research first of all attempts to distinguish key influencing factors and quantify downstream impacts. Secondly, influenced discharge driving behaviors are planned to be theoretically modeled by an improved car-following model. Thirdly, by adopting the proposed car-following model, the influenced SFR and SLT will be modeled by reproducing a simplified discharging process. Then, how downstream impacts perform along the arterial are intended to be investigated. In the end, a set of adjustment factors for the influenced SLT and SFR is intended to be proposed. The aim of the proposed methodology is mainly to facilitate capacity estimations at the signalized intersections in urban areas under heavy traffic demand.

1.4 Research Flow and Organization of Dissertation

A research flow to complete the tasks shown in Figure 1.1 is presented in Figure 1.2, concurrently with the organization of this dissertation. ***Chapter 2*** mainly goes through some basic terminologies involved in this study and reviews past researches about capacity estimations at signalized intersections. In this Chapter, we also review researches and methodologies about the downstream influence on capacity estimation in existing manuals and simulators. Studies about key technologies involved in this paper such as the car-following model are referred to as well. In ***Chapter 3***, downstream impacts are empirically analyzed firstly to find out key influencing factors and their effect mechanism on the capacity of through movement. By these findings, an existing car-following model, Intelligent Driver Model (IDM, hereinafter) is redesigned to explain the influenced driver behaviors under the downstream influence. Then a simplified discharge process is formulated on the basis of the proposed car-following model to model the influenced SFR and SLT. ***Chapter 4*** further extends the above study from a single intersection level to an arterial level. In this chapter, models of influenced SFR and SLT are further introduced into a meso-level model, Cell Transmission Model (CTM,

hereinafter). Through the experiment study, the mechanism of downstream influence evolving along the arterial is analyzed and the importance of considering the downstream influence in modeling arterials is pointed out as well. Based on the proposed CTM, ***Chapter 5*** proposes a methodology for calculating the adjustment factors on influenced SFR and SLT of through lanes. This chapter pays more attention to the practical ability of the model and discusses a few case studies to preliminarily investigate the application conditions of the proposed methodology. ***Chapter 6*** highlights the major findings of this research and suggestions on future studies.

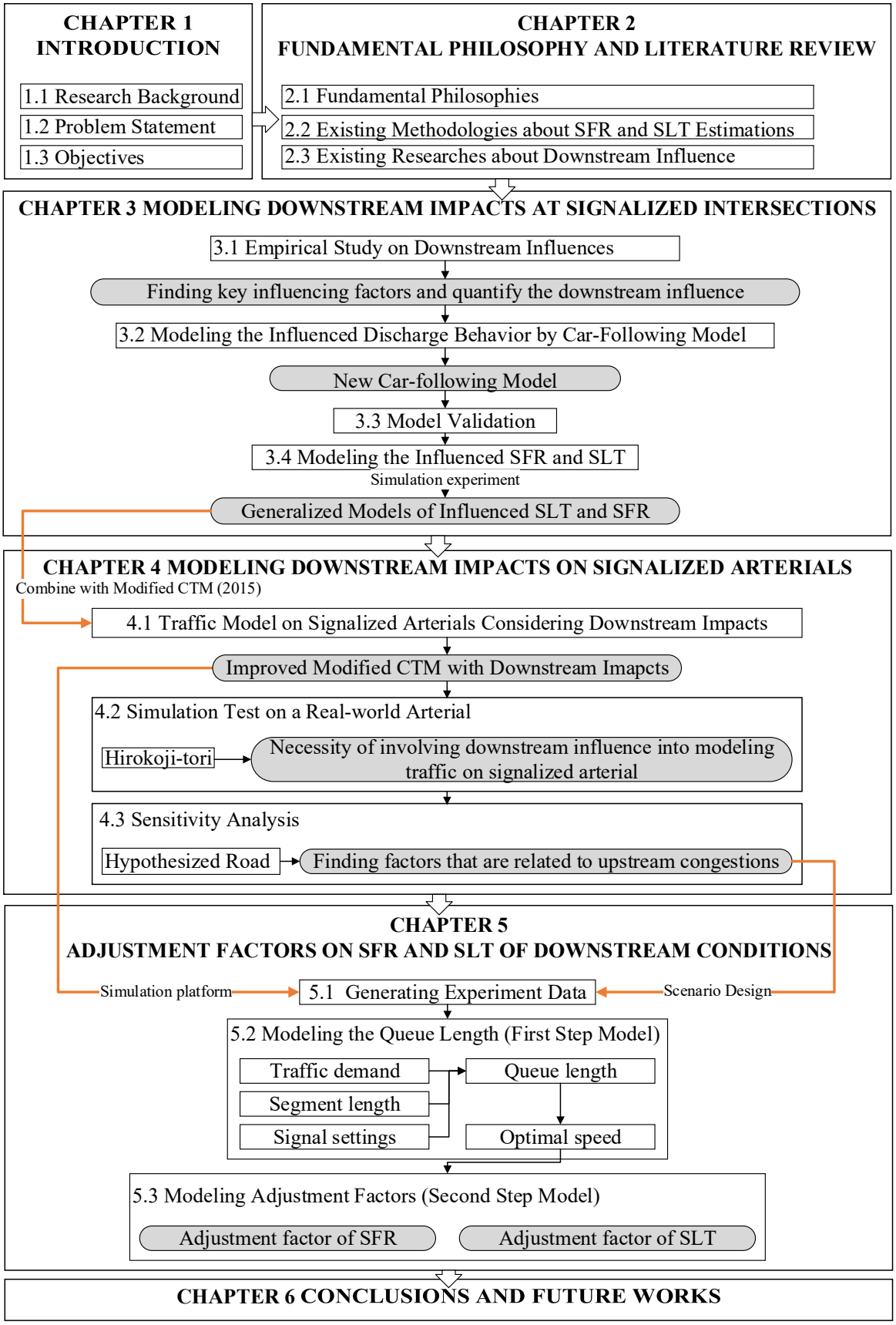

Figure 1.2 Research flow and organization of this dissertation

CHAPTER 2 FUNDAMENTAL PHILOSOPHY AND LITERATURE REVIEW

2.1 Fundamental Philosophies

Basically, signalized arterial consists of several signalized intersections. The performance of one signalized intersection is mainly related to traffic conditions at the directly downstream segment. In some extreme cases, the traffic capacity of an intersection is affected by multiple connected downstream intersections at the same time. For instance, when downstream intersections are closely spaced (intervals are less than 50m) and traffic demand is quite high, queues in multiple road sections can easily merge into one long queue. However, firstly, the above situations are quite rare in reality and generally accompanied by the occurrence of spillback which is beyond the scope of this study. Secondly, vehicles in the next segment occupy most of the visions of upstream drivers and dominate their judgment. To have a better understanding of the capacity reduction phenomenon, this research assumes that driver behaviors of vehicles discharging from the subject intersection are only influenced by traffic conditions in the directly downstream section. A corridor with two signalized intersections is plotted to explain the fundamental philosophy in this research as shown in Figure 2.1.

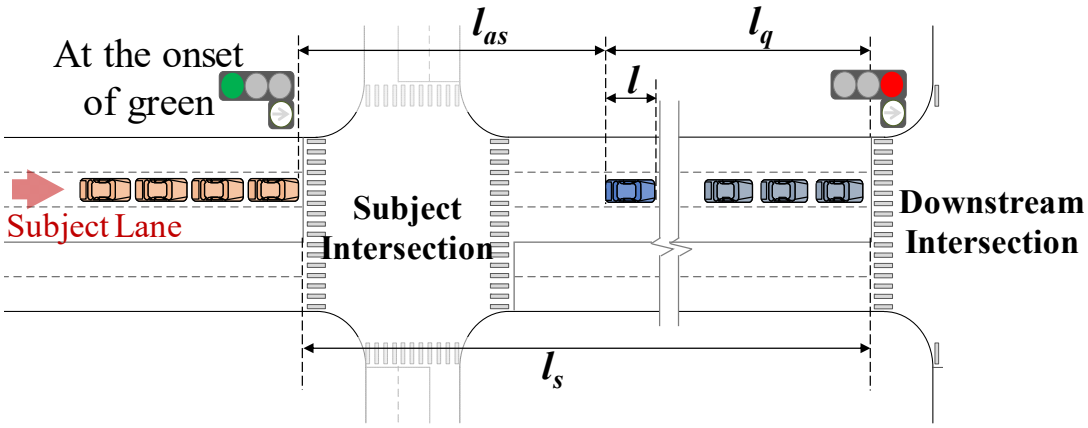

Figure 2.1 Fundamental philosophies and definition of analysis parameters

As shown in Figure 2.1, l_s defines the length of the downstream segment which is the distance from the upstream stop-line to the downstream stop-line. l_q is the queue length in the downstream link which is the distance from the rear bumper of the last queueing vehicle in the downstream link to the downstream stop-line. l_{as} represents the available space ahead of the upstream discharge platoon which is the distance from the rear bumper of the last queueing vehicle in the downstream link to the front bumper of the first queueing vehicle in the upstream platoon. Because this research mainly focuses on the discharge process of upstream through lanes, downstream queue length and available space are measured at the onset of upstream green indication. *offset* is the time difference between the onset of green at the downstream intersection and the onset of green at the subject intersection. According to signs of offset values, it is classified into two types, positive offset, and negative offset. A positive offset means at the onset of upstream green, the downstream signal is still red. Negative offset means at the onset of upstream green, the downstream signal already became green.

As shown in Figure 2.2, for one discharge process in this road system, when the upstream indication turns green, vehicles need to react to the initiation of the green phase and to accelerate. After a few seconds, they reach the maximal departure flow rate. During the acceleration time, the green time is underutilized and it is generally regarded as SLT. Correspondingly, SLT is defined as the additional time consumed by the first few vehicles in a queue at a signalized intersection above and beyond the saturation headway. The maximal departure flow rate generally regarded as SFR. In HCM (TRB, 2016), SFR is defined as, the equivalent hourly rate at which previously queued vehicles can traverse an intersection approach under prevailing conditions, assuming that the green signal is available at all times and no lost times are experienced.

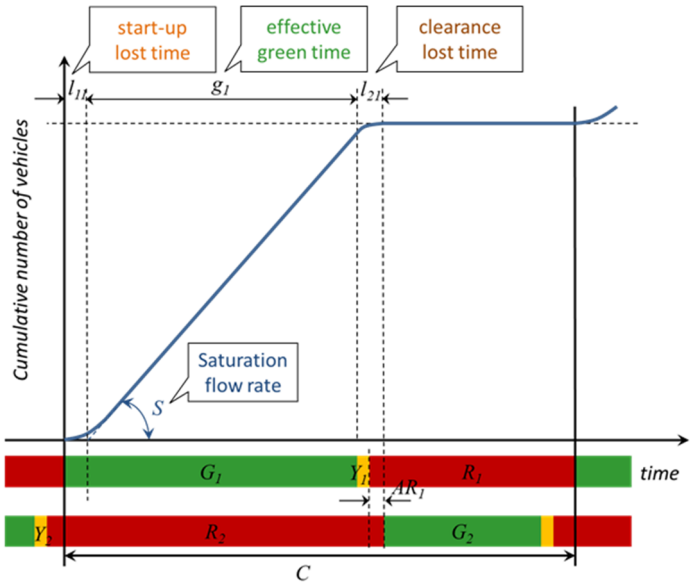

Figure 2.2 Flow rate changing during one discharge process

It is easy to infer that these efficiency factors (SFR and SLT) are related to the above-mentioned downstream condition measurements, l_s l_q, and *offset*. Understanding interactions between upstream discharging, downstream situations, and traffic conditions are the basis of this research. Different traffic demand may yield various downstream conditions and result in different discharge efficiency of upstream platoons. Generally, under low traffic demand, only a few vehicles occur in downstream links and upstream vehicles will pass through the downstream link smoothly. While under high traffic demand, there may be a long queue in downstream and upstream vehicles may stop behind the queue.

2.2 Existing Methodologies about SFR and SLT Estimations

In HCM (TRB, 2016), the capacity of a signalized intersection is calculated separately for each lane group. For the subject lane group, it is defined as the number of vehicles in one hour (veh/h) that can go through the intersection under prevailing geometry conditions, traffic demand profiles, and signalized timings as shown in Equation (2-1).

$$c = s\frac{g}{C} \tag{2-1}$$

where, variables in this equation are defined for each lane group, c is the capacity (veh/h), s is the saturation flow rate (veh/h), g is the effective green time (s), and C is the cycle length (s).

It can be known from Equation (2-1) that capacity is governed by saturation flow rate (s), effective green time (g), and cycle length (c). Green time is the defined time interval for each cycle and discharging vehicles can go through the stop line only during this period. Theoretically, the length of the effective green time (g) should be long enough to satisfy the arrival traffic demand. It is calculated by the following Equation (2-2).

$$g = G + Y - (SLT + CLT) \tag{2-2}$$

where, variables in this equation are defined for each cycle, G is the green time, Y is the amber time, SLT+CLT defines the total lost time (s), SLT is the start-up lost time, and CLT is the clearance lost time.

SFR and SLT are two important parameters for capacity estimation and discussed in this research. The following two sections introduce existing methodologies and researches about these two parameters.

2.2.1 Saturation flow rate (SFR)

SFR estimation is one of the most important study fields in the study on signalized intersections. The most frequently used procedure to estimate the SFR is the one proposed by HCM 6th Edition (TRB, 2016), which is explained through Equation (2-3).

$$\mathrm{SFR}_{\mathrm{est}} = s_0 f_w f_{HVg} f_p f_{bb} f_a f_{LU} f_{LT} f_{RT} f_{Lpb} f_{Rpb} f_{wz} f_{ms} f_{sp} \tag{2-3}$$

$\mathrm{SFR}_{\mathrm{est}}$ is a function that is calculated by letting the base SFR times different adjustment factors (f_{xx}). Where $\mathrm{SFR}_{\mathrm{est}}$ is the adjusted saturation flow rate (veh/h/ln), s_0 is the base saturation flow rate (pcu/h/ln), f_w is the adjustment factor for lane width, f_{HVg} is the adjustment factor for heavy vehicles and grade, f_p is the adjustment factor for the existence of a parking lane and parking activity adjacent to lane group, f_{bb} is the adjustment factor for the blocking effect of local buses that stop within the intersection area, f_a is the adjustment factor for area type, f_{LU} is

the adjustment factor for lane utilization, f_{LT} is the adjustment factor for right-turn vehicle presence in a lane group, f_{RT} is the adjustment factor for right-turn vehicle presence in a lane group, f_{Lpb} is the pedestrian adjustment factor for left-turn groups, f_{Rpb} is the pedestrian-bicycle adjustment factor for right-turn groups, f_{wz} is the adjustment factor for work-zone presence at the intersection, f_{ms} is the adjustment factor for downstream lane blockage, and f_{sp} defines the adjustment factor for sustained spillback.

Recent researches revealed that results from Equation (2-3) are always higher than observed values that are based on field surveys. It indicates that these factors are not sufficient and other adjustment factors should also be considered for more accurate estimation SFR. In urban areas, especially during the peak time, the arrival demand will reach 70%-90% of the intersection capacity. The long queue may generate at each intersection approach. By observation, it is found that SFRs of the departing vehicles are very likely influenced by the downstream longer queue. Hence, it is worthy to confirm whether the impact from downstream queues can be quantified into an adjustment factor for the SFR estimation.

The estimation method prescribed in the Manual on Traffic Signal Control, Japan (MTSCJ, 2006) follows a similar equation as the one in HCM. However, in MTSCJ's equation, only adjustment factors of f_w, f_{HV}, f_{bb}, f_{LU}, f_{LT}, f_{RT}, and f_{Lpb} are considered. However, values of base SFR differ with the HCM method. Also, the values of the 7 considered factors vary in different subject sites considering the geometric conditions and traffic demand profiles. They are defined according to Japanese conditions. On the other hand, adjustment factors like f_a, f_p, f_{LU}, f_{Rpb}, f_{wz}, $f_{ms,}$ and f_{sp} are not included in the equation.

The procedure of observed SFR (SFR_{obs}) that is prescribed in HCM is defined by saturation headway (h_s) observed in each cycle. For one cycle, the h_s is the average value for headways of all vehicles discharged except the first four headways as shown in Equation (2-4) and (2-5).

$$\mathrm{SFR}_{\mathrm{obs}} = \frac{3,600}{h_s} \tag{2-4}$$

$$h_s = \frac{T_n - T_4}{n-4} \tag{2-5}$$

Where, variables in this equation are defined for each cycle, SFR_{obs} is the observed SFR (veh/h/ln), h_s is average saturation headway (s), T_n is the discharge time of n^{th} queued vehicle (s), T_4 is the discharge time of 4^{th} queued vehicle (s), and n is the number of queued vehicles observed.

With the development of new information technologies, the methods of traffic information acquisition are constantly improving. Based on new technologies, some innovative methods for measuring observed SFR were proposed to facilitate the signal timing process. For instance, Wang et al (2019) proposed a new procedure for measuring SFR by Didi drivers' trajectory data. By this method, real-time data of observed SFR can be uploaded without the necessity of field investigation.

In recent year, the effects of different parameters such as taxi blockage and composition of traffic flow on SFR has been investigated by many researchers as well. Davoodi et al. (2015) claimed that motorized two-wheelers have better function of acceleration and maneuverability properties than passenger cars. Traffic flow that is composed of such vehicles can significantly increase the discharge performance. Chand (2017) revealed that the PCU for a certain vehicle type should not be a constant value. For certain traffic flow, PCU values may vary with their corresponding proportions dynamically. The rule of PCU changing is expected to be proposed, whereas, it has not been summarized in this research finally. In order to load or unload passengers, Taxi may park on the roadside or street. Behbahani et al. (2017) investigated this behavior and proposed that the average on-street parking maneuver time (or the average blockage time) of taxies may reduce the SFR at signalized intersections. Results indicated this reduction becomes more obvious when lane width is narrower.

In addition to impacts from taxi blockage and traffic composition, scholars have proved that weather and intersection geometry have significant impacts on the SFR as well. Sun et al. (2013) carried out an empirical analysis at a four-leg signalized intersection under different weather conditions. Research results indicated that SFRs observed on rainy days are approximately 3-7% less than SFRs observed on sunny days. Branston (1979) conducted a comparative analysis under different brightness conditions. He proposed that for the discharge traffic on through lane, SFRs observed in dark environments are 6% less than SFRs observed in light environments. Chodur et al. (2011) investigated negative effects on SFRs from multiple types of bad weather conditions (rain, snow, cloudy, and foggy). They found that long-duration

rain results in a greater reduction in observed SFRs (8.5%-12.3%) than the short-duration rain (3.6% on average). In addition, they indicated that SFR in snowy and cloudy weathers are 10% and 11.4% respectively less in comparison to SFR observed on sunny days.

Regarding studies about intersection geometry, attentions are mainly paid on turning radius, lane width, approach grade, and turning angles. In 2011, Shao et al. (2011) did a comprehensive study on intersection performances involving many influencing factors such as road geometries (lanes number, turning radius, lane width, approach grade), traffic conditions (parking conditions, traffic composition, speed limitation, venerable road users), and city population. They concluded that the capacity of left-turning lanes (right-hand driving) are sensitive to lane width and turn radius. Sando et al. (2009) investigated geometry impacts on SFRs of triple left-turn lanes. They revealed that values of downgrades and turning angles positively influence SFRs. Whereas, one-way streets and curved approaches have negative contributions to SFRs.

2.2.2 Start-up Lost Time (SLT)

Start-up lost time denotes the underutilized time due to the platoon accelerating process (TRB, 2016). Since no estimation methodology for SLT that has been proposed by any manual, the method to calculate the observed value of SLT (SLT_{obs}) is introduced here. The SLT_{obs} is calculating the total time difference between the first four headways and the four times saturation headway.

$$SLT_{obs} = \sum_{i=1}^{4} (h_i - h_s) \tag{2-6}$$

Where, h_i is the headway that measured at stop line for i^{th} vehicle in the discharged queue.

As a small value, the change of SLT is often ignored and is set as constant simply being given a value of 2 or 3 seconds in signal timings. HCM (TRB, 2016) recommends that SLT is generally about 2.0 sec/phase. Nevertheless, small values should also be taken seriously. Tiny errors will result in the mismatch between designed capacity and real traffic demand. This difference may be amplified on traffic corridors, leading to a big problem for the road system. Many factors have been proved that may impact the SLT, such as vehicle type, gradient,

pedestrian behaviors, reaction time, and psychological factors. Minh and Sano (2003) claimed that start-up lost time should be divided into two parts. First is the start response time and second is time lost due to vehicles' acceleration. Start response time (t_r) is the time difference between the green indication (or other recognizable starting indications) and the time when drivers in a queue press the accelerator pedal. It is an indicator of driving characteristics and a key composition of start-up lost time at signalized intersections. Li and Prevedouros (2002), recommended using the following equation (2-7) for representing the relationship between the start-up lost time and the start response time.

$$\mathrm{SLT}_{\mathrm{obs}} = t_r + 4\left(H_{avff} - h_s\right) \tag{2-7}$$

Where H_{avff} is the average queue discharge headways of the first four vehicles in the queue at a signalized approach (s).

For estimating the t_r, different values are proposed in various researches. As early as 1977, Messer and Fambro (1977) revealed that for the first driver in the waiting platoon at a signalized intersection, response time is as much as 2.0s. While for the vehicles in another position, reaction times are recommended to defined as 1.0s. Because before actions the leading vehicle should judge more information than drivers in other sequences. Both Institute of Transportation Engineers (1994) and Akçelik et al. (1999) claimed to define start response time as 1.0s. Whereas, Bonneson (1992) proposed 1.22 seconds for t_r. Li and Prevedouros (2002) claimed to use 1.76s and 1.42s separately for t_r values of through and left-turning vehicles. In the AIMSUN simulator (2010), the default value of t_r for vehicles in a leading position is 1.35s. Tong et al. (2002) proposed that t_r for passenger cars and taxis should be around 1.32s. AASHTO (2004) studied its stochastic feature. Considering drivers may face different situations, they claimed that values of t_r should distribute between 1.0s and 2.5s. In Turkey, Çalışkanelli and Tanyel (2016) suggested defining different values for different maneuver types. They found that mean values for vehicles of through, right-turning, and left-turning maneuvers are separately 1.48s, 1.39s, and 1.26s. Also, an empirical formula is proposed by them for predicting the t_r of drivers in the leading position under different situations, as shown in Equation (2-8).

$$t_r = -0.149MNV - 0.136GN + 0.020C \tag{2-8}$$

Where *MNV* is the maneuver type (through passing vehicles, *MNV*=0; right-turning vehicles, *MNV*=1; left-turning vehicles, *MNV* = 2) and *GN* is the gender of the driver (1 for male drivers and 0 for female drivers).

Base on Equation (2-8), Çalışkanelli, et al. (2017) further proposed an empirical model for estimating the t_r of drivers in the leading position and pointed out that SLT is related to lane width, bus percentage, and queue length, as shown in Equation (2-9).

$$SLT = 8.00 - 1.94W_L + 3.31P_{bus} + 0.07L_q \quad (2\text{-}9)$$

Where W_L defines the lane width (m), P_{bus} bus percentage (%) in the queue and L_q is the queue length of discharging platoon (veh/ln).

2.3 Existing Researches about Downstream Influence

Since the end of the 20th century, scholars realized that the discharge effectiveness at signalized intersections is strongly related to downstream traffic conditions. The first is about the downstream influence explained by HCM (2016) in the SFR estimation (Equation (2-3)). Among all adjustment factors, f_{sp} is the only parameter that explains the adjusting of downstream impacts. Equation (2-10) is the formula in HCM that introduces the calculation of f_{sp} and shows that f_{sp} is subject to the volume-to-capacity ratio (v/c) and f_{ms}. Equation (2-10) reveals that the f_{sp} only represents downstream impacts from sustained spillbacks which is caused by the traffic oversaturation or mid-segment lane blockage. Whereas, it can be observed that capacities of signalized intersection reduced due to downstream queue even when no spillback occurs. Hence, this adjustment factor prescribed by HCM is insufficient to cover all types of downstream queue influence.

$$f_{sp,l} = \left(\frac{dv_u}{c_u}\right)^{0.5} \times f_{ms} \times f_{sp,l-1} \quad (2\text{-}10)$$

Where, variables in this equation are defined for each upstream movement, $f_{sp,l}$ is adjustment factor for spillback for iteration l, dv_u is the maximum discharge rate (veh/h), c_u is

capacity at the upstream intersection (veh/h), and f_{ms} is adjustment factor for downstream lane blockage.

Akcelik and Rouphail (1992) were the first researches to study downstream influence at non-isolated signalized intersections. They established a simple analytical model for simulating queue interaction. Through simulation experiments, they found that even traffic inputs are lower than defined capacity, the whole performance of the paired intersections is strongly related to the queue size in the link between two intersections. Finally, they gave a hint about the future study that SFR reductions due to downstream impacts are worthy to be investigated. Ahmed and Abu-Lebdeh (2005) assumed a hypothetical two neighboring signalized intersection and macroscopically modeled delays for this road section by simulating traffic flow propagations and signal control parameters. It is found that the delay occurred on this assumed road system is relevant to the downstream conditions. They pointed out that downstream conditions should be included in the evaluating level-of-service (LOS) and capacity estimation. Finally, this paper emphasized that properly adjusting offsets and green ratios can reduce delays at two intersections. The Traffic Signal Timing Manual (FHWA, 2008) suggested taking traffic measures for urban arterials during high volume periods with objectives of minimizing the time when intersections are suffering from spillbacks and managing interactions between queue at each intersection. This manual mentioned that downstream queue lengths should also be included in the evaluation of traffic measures at intersections.

Yu and Sulijoadikusumo (2005) did a comprehensive investigation into existing analytical models. They pointed out that in order to represent downstream disturbance current models are far from enough. All of these models required a large amount of data empirical data which can cover all types of traffic and road conditions. This work is quite challenging and hard to be finished. Therefore, a mathematical model requiring a small size of empirical data should be found in the future study. For overcoming this gap, a network-wide simulation model with proper consideration of downstream impacts is necessary. As one of the most advanced simulators, VISSIM is based on Wiedemann 74 and Wiedemann 99 car following models for the longitudinal movement (2015). It has been widely applied in simulating not only the uninterrupted traffic flow but also the interrupted traffic flow. By the test in chapter 3, it was found that this software did not consider the downstream influence properly while simulating the discharge flow at closely spaced intersections. Hashemi et al. (2017) did field surveys and

investigated the downstream impact at two Japanese corridors on which intersections are closely spaced. This paper provided adequate empirical analysis for the influenced SFR. However, he hasn't provided a convincing approach for estimating SFR reductions considering the downstream influence. This paper clearly proved that a long queue in a short downstream link with a large positive offset can lead to a lower SFR at the subject intersection.

2.4 Summary

As introduced in the fundamental philosophy, SLT and SFR are two important parameters for capacity estimation at signalized intersections. From the above literature reviews, it can be concluded that researchers were devoted to making the capacity estimation model more accurate and comprehensive by incorporating more adjustment factors. However, existing models are still problematic because none of them has properly considered the capacity reduction from downstream impacts. Since the 1990s, scholars started to study the interaction effect between two adjacent intersections. It has been gradually recognized that not only the upstream queue length and delay but also the SFR and SLT should be affected by the downstream conditions. However, until now, no systematic research about downstream influence at signalized intersections has been proposed much less the practical application. Therefore, it is an important research gap and this problem is necessary to be addressed.

CHAPTER 3 MODELING DOWNSTREAM IMPACTS AT SINGNALIZED INTERSECTIONS

Downstream impacts happen frequently and especially for streets in the urban area which have closely spaced intersections and high traffic volume. Based on empirical studies, this chapter mainly addresses two issues, how are upstream capacities affected parameters and which are key influencing factors of downstream conditions. The essence of all macroscopic qualitative changes is caused by microscopic quantitative changes. This phenomenon is studied starting from capturing influenced driving behaviors. Firstly, Yasukuni-tori in Tokyo Japan, a typical arterial for this phenomenon is observed in this chapter, which is the foundation work for understanding and capturing this behavior. By several comparative analyses, key influencing factors are determined and a new car-following model is designed with these factors. Base on this new car-following model, downstream impacts at isolated intersections are modeled.

3.1 Empirical Study on Downstream Influence

3.1.1 Assumptions

Firstly, the perspectives of upstream waiting drivers are analyzed. The following figure (Figure 3.1) shows the information that upstream drivers can get from observations while waiting. They can clear know the available space (l_{as}), segment length (l_s), queue length (l_q) by spatial observation. Also, by comparing the time difference between two consecutive signals or simply observe the motion of the downstream platoon, drivers can know the offset.

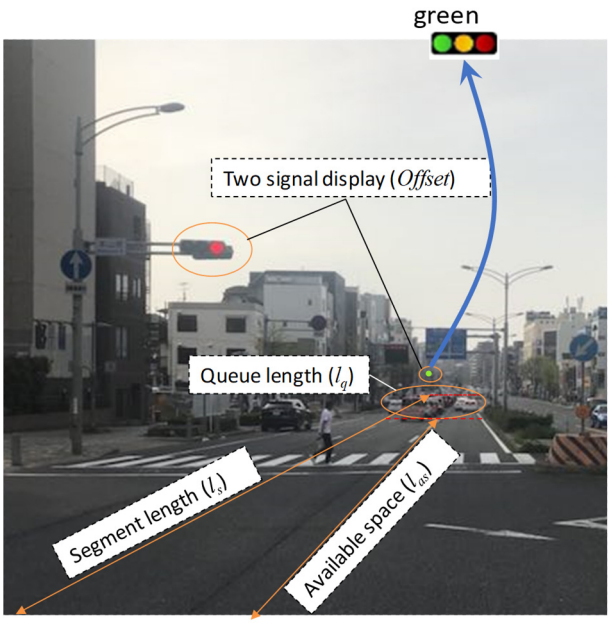

Figure 3.1 Perspectives of upstream waiting drivers

Two different typical downstream conditions are shown in Figure 3.2. Case A shows a good downstream condition, where the queue in the downstream link is short (nearly 30% of downstream space has been occupied by queueing vehicles). The signal of downstream intersection is green which means that the downstream queue will be discharged soon. Case B shows a bad downstream condition where the queue in the downstream segment is long (almost 100% of downstream space has been occupied by queueing vehicles) and the signal of the next intersection is red which indicates that the downstream queue may last for a long time.

(a) Case A (b) Case B

Figure 3.2 Two cases of downstream conditions

For case A, drivers waiting in upstream through lane can anticipate that at the time when they arrive at the downstream link, downstream vehicles may already have gone far away. There is a high probability that their forward routes are not hindered by the downstream queue, so that they may start-up quick and travel fast. In contrast, for case B, drivers may notice that the end of the downstream queue is closed and the red signal indicates that the downstream queue may stay even after their arrival. Upstream drivers can infer that no matter how fast they drive they have to join the downstream platoon. Most of the drivers have the subconsciousness of optimizing their travel processes. Therefore, if drivers understand that they have a high probability of stopping or decelerating after only travel for a short distance, they may not accelerate and travel as quickly as a free discharge. Drivers' behaviors are disturbed worrying about the risk of a crash or wishing to join the downstream queue in a comfortable way.

Accordingly, this research assumed that under negative influence from downstream traffic, the SFR will be lower and SLT will be higher from the through lanes at upstream intersections. Shorter downstream links and longer downstream queues probably result in greater downstream impacts. In addition, if the signal indication at the downstream intersection is red at the onset of green, downstream impacts may further be amplified.

3.1.2 Sites Selection and Data Collection

In the whole study, two roads in Japan were observed and studied. One is the Yasukuni road in Tokyo. Signals on this road are set as actuated traffic signals so that multiple offset values can be observed from this road. The other one is the Hirokoji-tori in Nagoya. Phase timing of traffic each signal along Hirokoji-tori is fixed and their cycle lengths are the same. Therefore, only 4 different offset values can be observed from the Hirokoji-tori. For analyzing downstream impacts under various traffic conditions (different segment lengths with different offset), the Yasukuni road in Tokyo is suggested to be analyzed. The field study of the Hirokoji-tori in Nagoya will be applied for the arterial level study and detailed in Chapter 4. The following paragraph introduces detailed information about the field survey on the Yasukuni road.

Figure 3.3 shows the plane figure of the observed target. Three intersections (a) Jimbocho intersection (b) Sendaimae intersection (c) Manatabashi intersection on this road are closely spaced on a street with a length of 600m. The longest segment between two intersections is 250m and the shortest segment is 116m. 5 observed approaches are located on these three intersections. They are the westbound (WB, hereinafter) and the eastbound (EB, hereinafter) approaches of Jimbocho intersection, the WB and EB approaches of Sendaimae Intersection, the EB of Manaitabashi Intersection. As shown in the plane figure, each approach has two through lanes and shared right-turn lanes. 1, 2, 3, and, 4 approaches also equipped with a left-turn lane. The second through lane of each approach is the main target of the survey.

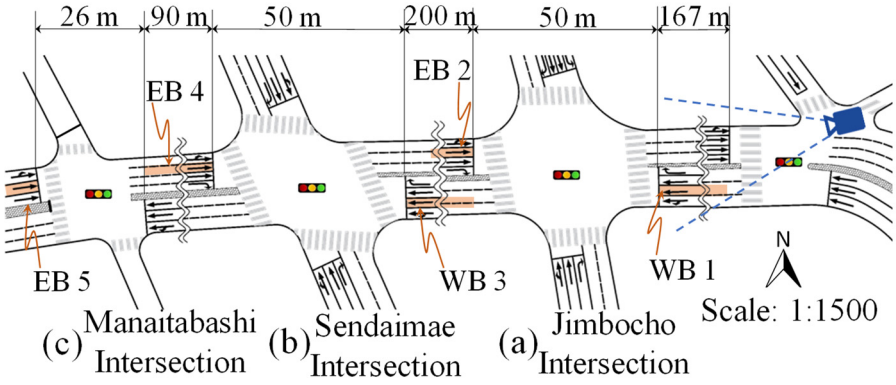

Figure 3.3 Plane figure of Yasukuni road

Tables 1(a), (b), and (c) show base phase plans of these three intersections. They have a common cycle length value (150s). Signal of Jimbocho intersection is set as 4 phasings with two protected-permissive right-turn phases. The signal of Sandaimae intersection is 4 phasing with two protected right-turn phases. Meanwhile, the signal of Manaitabashi intersection is 2 phasing. All signals of the road section are set as actuated. The green time of each cycle changes according to arrival demand. Signal phases of these intersections vary for different cycles on the basis of base phase plans. Accordingly, offset values change with cycles slightly but not breaking the coordination of signals along this arterial.

Table 3-1 Signal setting of each intersection

(a) Jimbocho Intersection

Movement	Signal phasing (s)														Cycle length (s)
	φ_1				φ_2			φ_3				φ_4			
	1	2	3	4	5	6	7	8	9	10	11	12	13	14	
TH&LT															150
Pedestrian															
RT															
TH&LT															
Pedestrian															
RT															
Vehicle movements	61			4	20	2	4	39			4	10	2	4	
Pedestrians	40	10	11	-	-	-	-	18	10	11	-	-	-	-	
Signal Phase Sequence	ϕ_1				ϕ_2			ϕ_3				ϕ_4			

(b) Sendaimae Intersection

Movement	Signal phasing (s)														Cycle length (s)
	φ_1				φ_2			φ_3				φ_4			
	1	2	3	4	5	6	7	8	9	10	11	12	13	14	
TH&LT															150
Pedestrian															
RT															
TH&LT															
Pedestrian															
RT															
Vehicle movements	78			4	7	3	4	34			4	10	2	4	
Pedestrians	57	10	11	-	-	-	-	13	10	11	-	-	-	-	
Signal Phase Sequence	ϕ_1				ϕ_2			ϕ_3				ϕ_4			

(c) Manaitabashi Intersection

Movement	Signal phasing (s)										Cycle length (s)
	φ_1					φ_2					
	1	2	3	4	5	6	7	8	9	10	
Vehicle											150
Pedestrian											
Vehicle											
Pedestrian											
Vehicle movements	98			4	4	36			4	4	
Pedestrians	77	10	11	-	-	15	10	11	-	-	
Signal Phase Sequence	ϕ_1					ϕ_2					

TH: through vehicle RT: right-turning vehicle LT: left-turning vehicle

Green Amber Red

Pedestrian flashing green Exclusive RT phase

Pedestrian movement Vehicle movement

A video survey was conducted on Tuesday, January 31 and Wednesday, February 1, 2017. 3 video recorders were positioned near the window of a tall building where is the office of i-Transport Lab (ITL). They were focusing on recording the Sendaimae intersection, recording the Jimbocho intersection, and covering the whole street separately, as shown in Figure 3.4. So that the movement of each approach can be clearly observed. Survey time on Tuesday starts from 1:00 pm to 6:00 pm covering the off-peak hour and evening peak hour. Survey time on Wednesday starts from 8:00 am to 12:00 am covering the off-peak hour and morning peak hour. At last, 235 cycles were recorded on two consecutive sunny days.

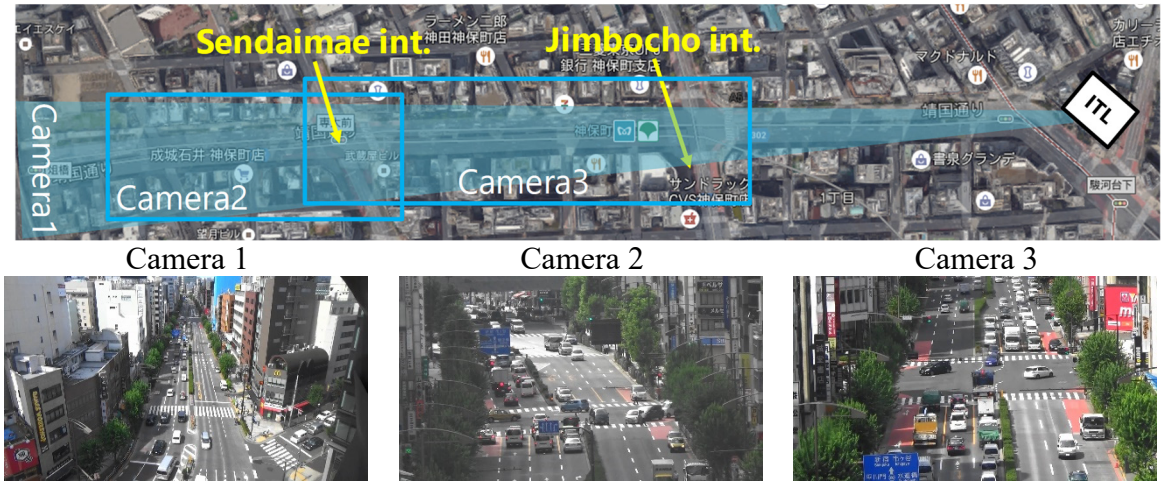

Figure 3.4 Camera positions of the field survey on Yasukuni-tori

3.1.3 Data Processing

Considering the focus point of this research which is to study the influenced capacity of through lanes under different downstream conditions, through lanes that are not influenced by turning vehicles are observed. Considering the actual situation of the survey site, only the 2nd (through) lane of each approach was selected for the data extraction, as shown in Figure 3.3. Throughout the length of the survey time in both two sites surveyed, no accident or any special incident has happened which could interrupt the traffic flow. All video sessions are available for data collection.

In order to extract valid data, only signal cycles with upstream queued platoons that consist of more than 8 queuing vehicles are selected. Meanwhile, we required that in the selected platoon at least the first six vehicles shall be passenger cars. Situations that only one heavy vehicle exists in the platoon are allowed but it should not be in the position of first six

vehicles. The heavy vehicle effect was eliminated by removing their headways and the vehicle behind them from the queue. In red time, the first vehicle may mistakenly wait at the position after the stop line. In this study, the passing time of the vehicle in this situation will be recorded as 0. During data collection, this phenomenon rarely happens at the survey site and most leading vehicles waited at the position 1-3 meters upstream of the stop line. We attribute this to the good driving habits of Japanese drivers. In addition, two other screening rules are set as well in order to eliminate the impact of other variables that are not studied as much as possible. Firstly, treating as invalid cycles, cases were excluded in which vehicles of the subject approach turn into the other lane before going through the intersection or the normally discharging is disturbed by motorbikes, bicycle, and cutting in effect. Secondly, cases were also removed in which vehicle breakdowns, drivers' distraction, and spillback happened at subject approaches. These conditions may lead to extremely strange headways. Furthermore, for properly distinguishing cycles in which spillback occurred, two methods are applied. The first is visual judgments. Cycles in which upstream discharged platoons are obviously hindered by the extension of the downstream queue are screened out firstly. Then, for some ambiguous samples, math judgments are applied which will be introduced in the SFR and SLT calculations.

Furthermore, it is important to mention that at the onset of upstream green, not all downstream vehicles are queuing vehicles. There may be some vehicle from the last phase moving behind the downstream queue. According to the car-following theory, upstream vehicles are directly influenced by them. However, for this research, it is the actual real-world observation at the analysis sites that there were very few moving vehicles. Most of the vehicles in the downstream link joins the queue before the upstream green. We attribute this result to the short link and long all red time between green indications (4s). Based on the above analysis and observation, it can be inferred that the impact of these moving vehicles is very minimal for short-link streets. To simply study the influence of the downstream queue, it is reasonable to remove all samples with moving vehicles and only observed cycles without moving vehicles. For variable-controlling, some influencing factors have been excluded such as heavy vehicles, drivers' distraction, and overtaking behaviors through data screening. However, these factors are important to be reconsidered before this method is applied in practice in the future.

Finally, in every selected cycle, the time of each vehicle passing the stop line and the corresponding downstream, conditions such as queue length, segment length, and offset are recorded. The collected videos are analyzed using an image processing software, "Traffic

analyzer" (Suzuki and Nakamura, 2006) by manually clicking each point of time. Figure 3.5 shows the interface of the analyzer.

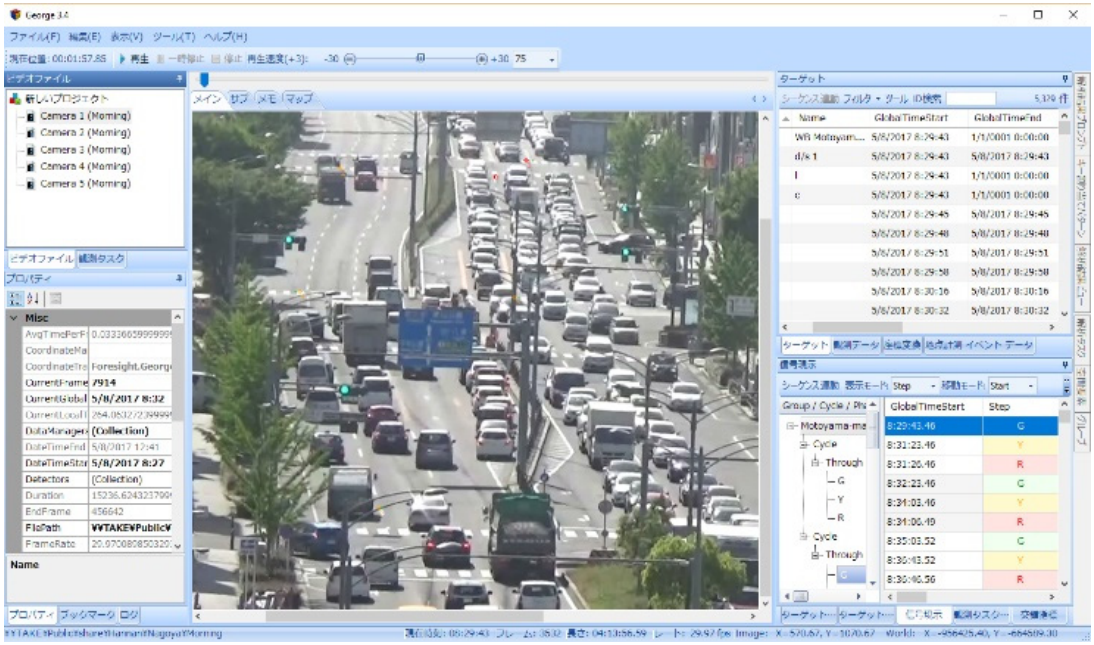

Figure 3.5 Traffic analyzer screen shot

Conventionally, headways reduce gradually with more and more queued vehicles passing through the stop line. Because platoon is still accelerating and hasn't reached the maximal flow rate when the first few vehicles are running through the stop line. HCM claimed that departure headways become saturated when the fifth queued vehicle passes the stop line (TRB, 2016). Accordingly, the saturation headway is the average headway of all queued vehicles except the first four. In this manual, the observed SFR is calculated by letting 3600 (seconds of one hour) divided by saturation headway as shown in Equations (2-4) and (2-5). The observed SLT is calculating as shown in Equations (2-6) and it is the difference between the total time taken for the first four vehicles to pass the stop line and four times saturation headway.

For being easily applied, this equation simply assumed that all discharge platoons reach the maximal flow rate after the fourth vehicle passed the stop line. This assumption cannot explain all cases. Especially in field data, headways fluctuate on vehicle sequence drastically and irregularly which makes it difficult to visually figure out the right position when the flow becomes saturated. In reality, the headway reduction usually ends at or after the fourth vehicle while sometimes before the fourth vehicle. The headway distribution of each cycle varies and the HCM method should not simply be applied in this study. Considering this problem,

measuring the observed SFR and SLT will be done by a newly introduced methodology and it is divided into the following 5 steps.

1. Data points in one cycle are ordered according to time. *i* in this calculation procedure defines the number of data points and n defines the total number of data points. For each selected cycle, plot the cumulative number of discharged vehicles ($Y=\{ y_1, y_2, \ldots y_n\}$) on the elapsed time (after the onset of green time) ($X=\{ x_1, x_2, \ldots x_n\}$) as shown in Figure 3.6,
2. Solve two linear regression curves by the least square method separately for all points and all points except the first points as shown in Equation (3-1) and (3-2);

$$y_i = p_1 x_i + q_1 \left(i = 1, 2, \ldots n\right) \tag{3-1}$$

$$y_i = p_2 x_i + q_2 \left(i = 2, \ldots n\right) \tag{3-2}$$

3. Calculate their x-intercepts and verify whether these two values satisfy the following two criteria;
    a) The values of the two x-intercepts are larger than zero. ($-q_1/p_1>0$ and $-q_2/p_2>0$)
    b) The difference ratio (as shown in Equation (3-3)) is less than 5%.

$$\left| \frac{q_2 p_1 - q_1 p_2}{q_1 p_2} \right| < 5\% \tag{3-3}$$

4. If both two requirements are met, output the first x-intercept value ($-q_1/p_1$) as the SLT_{obs} and the first slope value (p_1) as the SFR_{obs} for this cycle. Otherwise, making new data set by removing the first data point as shown in and turn back to the 2nd step.

$$Y = \left\{ y_1', y_2', \ldots y_{n-1}' \right\} = \left\{ y_2, y_3, \ldots y_n \right\} \tag{3-4}$$

$$X = \left\{ x_1', x_2', \ldots x_{n-1}' \right\} = \left\{ x_2, x_3, \ldots x_n \right\} \tag{3-5}$$

5. If the above two requirements are not satisfied yet after all available data points of a selected cycle have been scanned, it means saturation headway cannot be found in this cycle. This cycle will be identified as an invalid sample and be abandoned. Cycles in which spillback happened or extreme large headways occur due to vehicle breakdowns and drivers' distraction to may have this result.

An example of two successive calculations is provided. Two linear regression curves are shown in Figure 3.6 (Figure 3.6(a) is the fitting curve for 3rd to 14th data points; Figure 3.6(b) is the fitting curve for 4th to 14th data points). The above two requirements are satisfied. Therefore, the SLT (the x-intercept in Figure 3.6(a)) and the SFR (the slope in Figure 3.6(a)) of example is 3.84s and 1560veh/h/ln respectively. By the above procedure, the vehicle sequence where the platoon becomes saturated can be mathematically distinguished as well. In this example, after the 3rd vehicle passes the stop line, this platoon reaches the saturation flow rate. In addition, one of the criteria is "difference ratio is lower than 5%". 5% is set according to the situation of the overall sample. If the headway distribution fluctuates drastically in another field survey, this value can be raised.

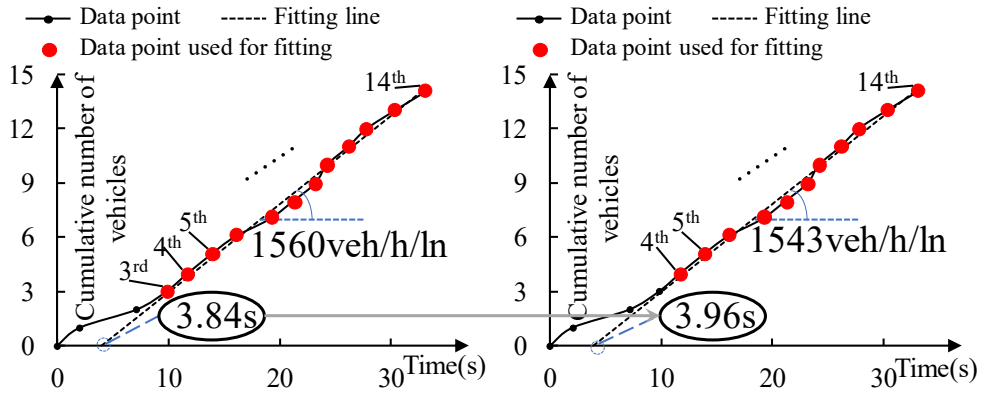

(a) the fitting line for 3rd to 14th data points (b) the fitting line for 4th to 14th data points

Figure 3.6 Example of measuring SLT and SFR

3.1.4 Result and Discussion

After data screening, a total of 294 cycles for all observed approaches are extracted. The methodology mentioned in the last section is used to calculate the observed SLT and observed SFR of each cycle. Based on watching the recorded video and actual driving experiences, it is found that the performance of the upstream platoon and behaviors of upstream drivers differ from different available space (l_{as}) which is the distance from the upstream platoon to the last queuing vehicle in the downstream queue. It can be inferred that when l_{as} is short, vehicles accelerated and ran slowly. On the contrast, while l_{as} is long, the platoon discharged quickly. In order to highlight this point, results are categorized based on the value of l_{as}. "l_{as} =100m" and "l_{as} =200m" are selected as two thresholds. "l_{as}>200m" represents the SLT and SFR of the

cycles which are less affected by downstream conditions. "l_{as}<100m" represents the SLT and SFR of the cycles which are greatly affected by downstream conditions. "200m≥l_{as}≥100m" represents the transitional part between them. Figure 3.7 shows the average SFRs and SLTs of all five approaches for each l_{as} interval.

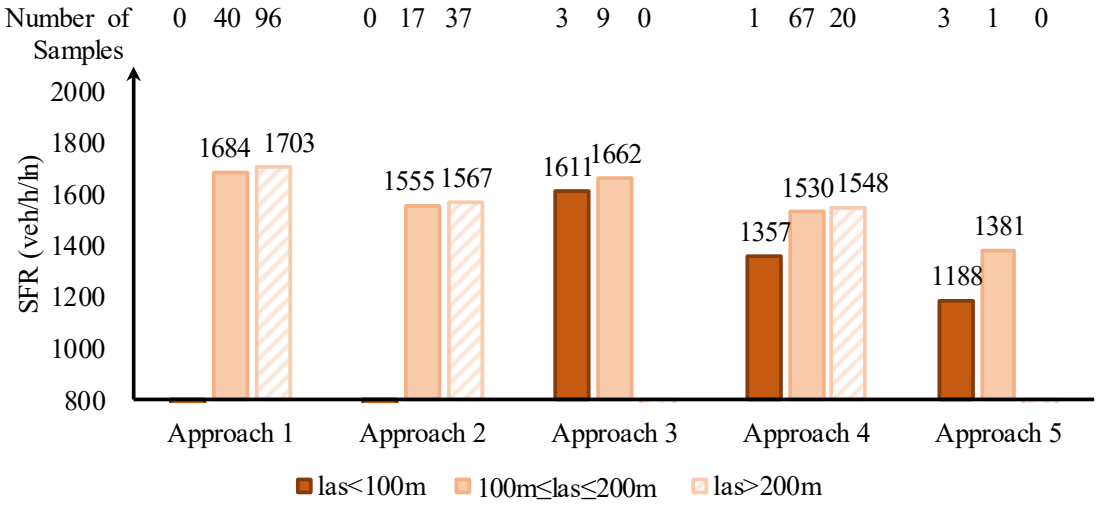

(a) SFR

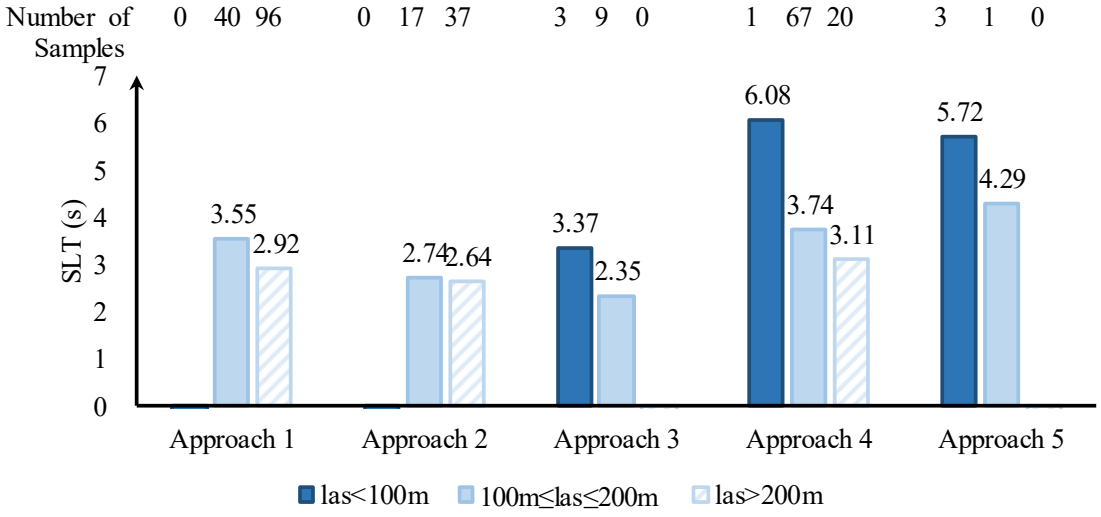

(b) SLT

Figure 3.7 Basic histograms for all five approaches

Firstly, when focusing on the sample size of each approach, it can be easily observed that the number of samples at approach 3 (12 samples) and approach 5 (4 samples) are quite small. It is because that their downstream link lengths are too short (approach 3 is 140m and approach 5 is 116m) that downstream can easily extend to upstream resulting spillbacks. Especially, during data screening, we found that spillbacks happen more frequently for approach 5. It is due to large positive offset values (19s~24s) at approach 5, which always stops the propagation

of the upstream platoon. Also, approaches 1, 2, and 4 have very samples in the category "l_{as}<100m" we inferred that longer segments have better ability in accommodating queuing vehicles and l_s should be one of the key influencing factors. Secondly, while comparing values in each category at different approaches, it is found that average SFRs in "l_{as}<100m" are all lower than them in "200m≥l_{as}≥100m" and average SFRs in "l_{as}>200m" is higher than the other two groups. Average SLTs in "l_{as} <100m" are all higher than values in "200m≥l_{as}≥100m" and average SLTs in "l_{as}>200m" are always the lowest in three categories. The above findings indicate that with l_{as} becomes smaller, the negative influence on upstream capacity from downstream traffic becomes stronger.

The available space (l_{as}) is equal to segment length (l_s) minus queue length (l_q) For further analysis, samples are plotted on values of l_q. As shown in Figure 3.8 (a) and (b), it can be clearly observed that with l_q becomes longer, SFRs tend to decrease and SLTs tend to increase, which reveals that l_q is one of key influencing factors.

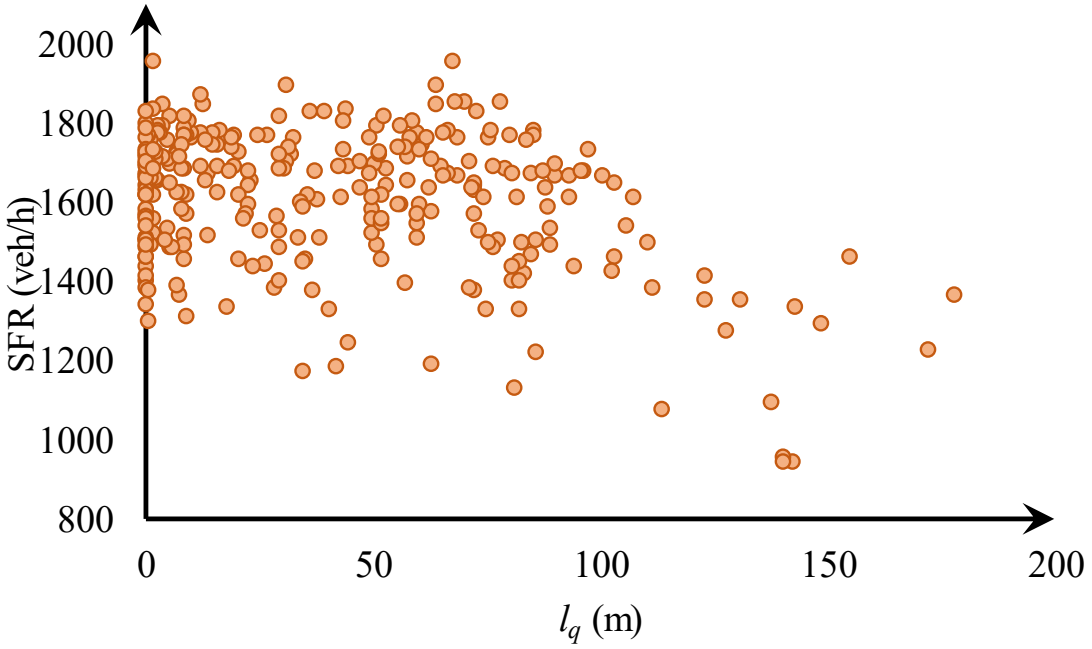

(a) SFR

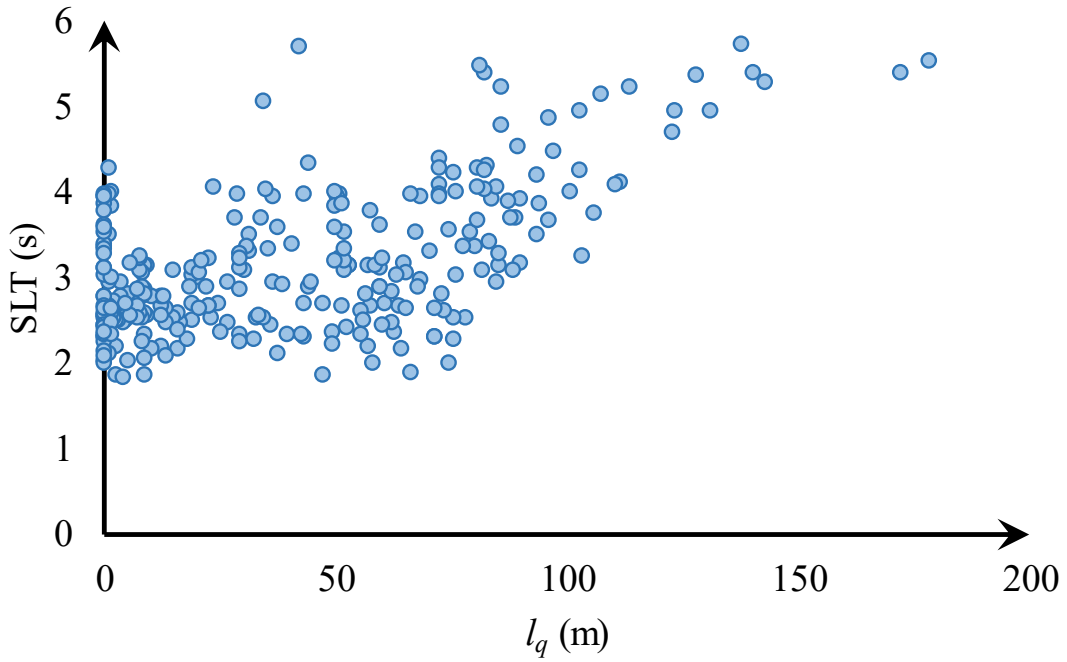

(b) SLT

Figure 3.8 Relationship between SFR(a), SLT(b) with queue length (l_q)

During the above analysis, we can observe both positive and negative offsets in approach 1 and 4. In approach 2 and approach 3, only negative offsets can be observed. In approach 5 only positive offset cases exist. Therefore, for investigating the influence from offset values, samples in approach 1 and 4 are separately plotted. Samples with different offsets are classified into four groups, (-∞, -5], (-5, 0], (0, 5], and (5, +∞]. Four groups are dyed in different colors. With offsets increasing from negative value to positive value, colors of samples (SFR: red, SLT: blue) change from light to dark.

As shown in Figure 3.9 and Figure 3.10, the whole data can be divided into two stages, flat part ($0 \leq l_q \leq 60$m) and reduction part for SFR or upgrading part for SLT ($60 \leq l_q$). as shown in Figure 3.9(a) and (b), most of the data points (both SFR and SLT) are located in flat sections in approach 1. In this stage, SFRs and SLTs in four groups are intermingled. A small sampling of data distributes in decreasing (SFR) or increasing (SLT) parts. In the changing stage, it can be roughly observed that samples with low offsets are lower than ones with high offsets. On the other hand, as shown in Figure 3.10(a) and (b), only a few data points are in the flat stage in approach 4 and they are highly mixed. Almost 80% of the points belong to the decreasing (SFR) or increasing (SLT) sections. We can clearly observe that samples with high positive offset values are lower than points with low offset values. The above findings indicate that

large positive offset values can aggravate the negative influence of long queues and it deserves to be counted as one key influencing factor as well.

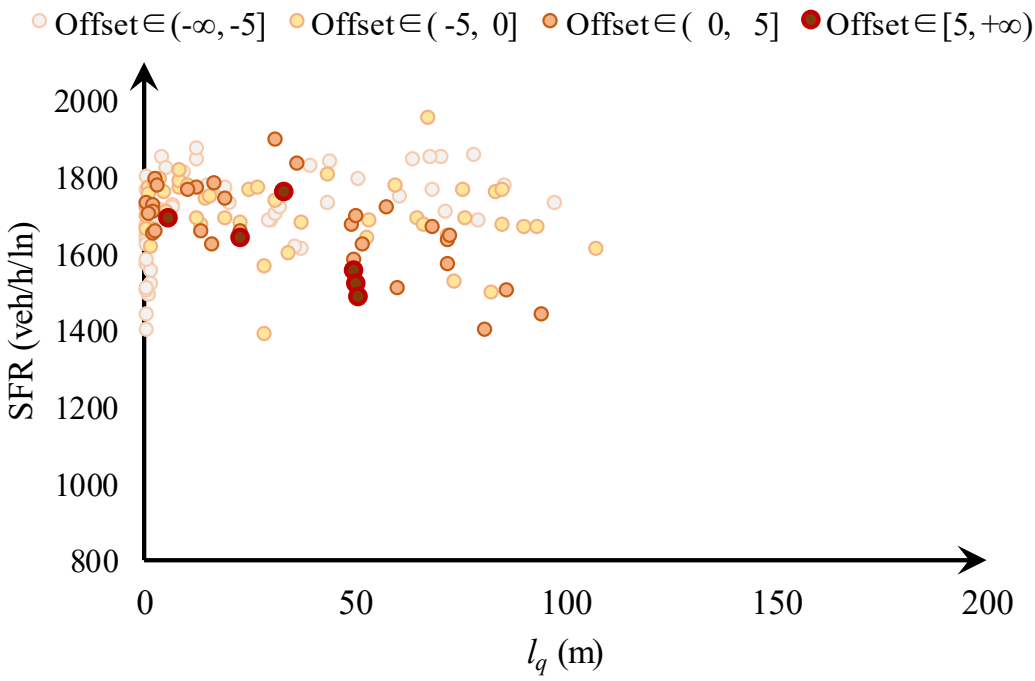

(a) SFR

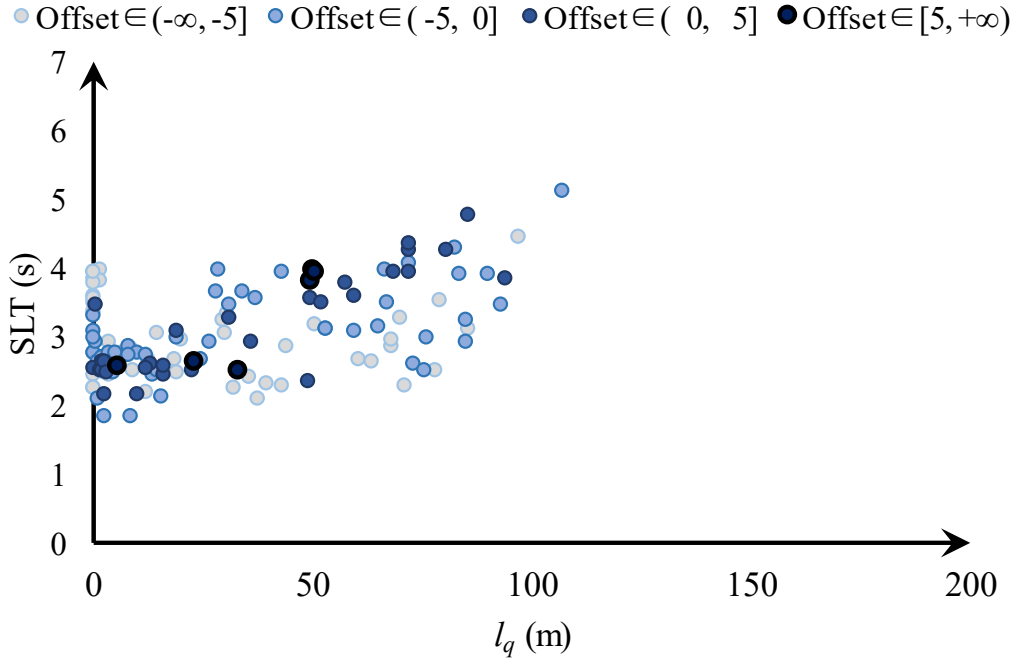

(b) SLT

Figure 3.9 SFR(a) and SLT(b) in four offset groups at approach 1

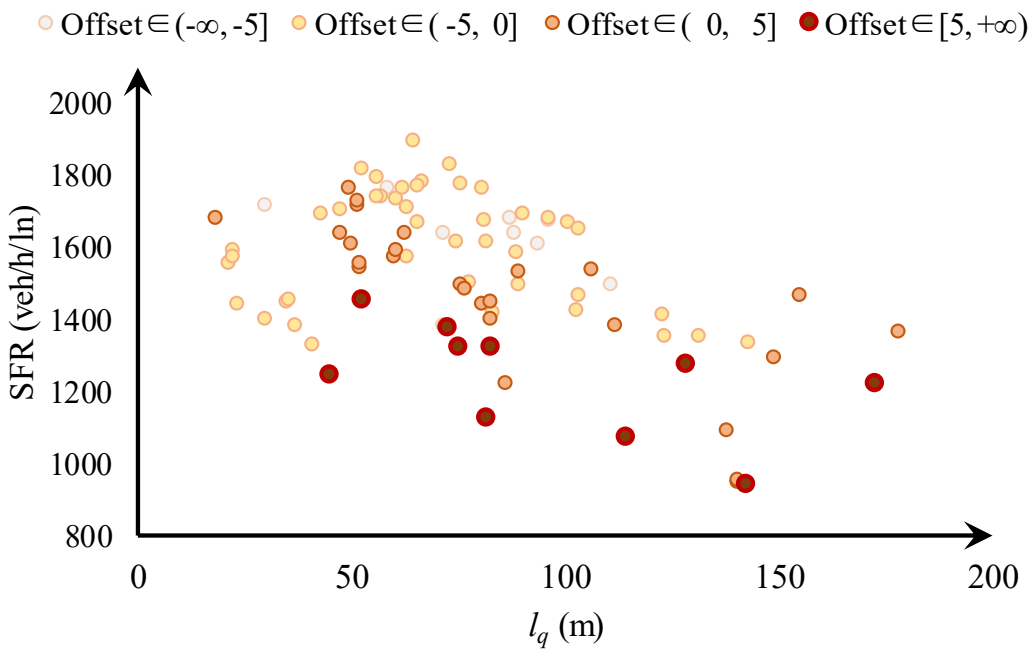

(a) SFR

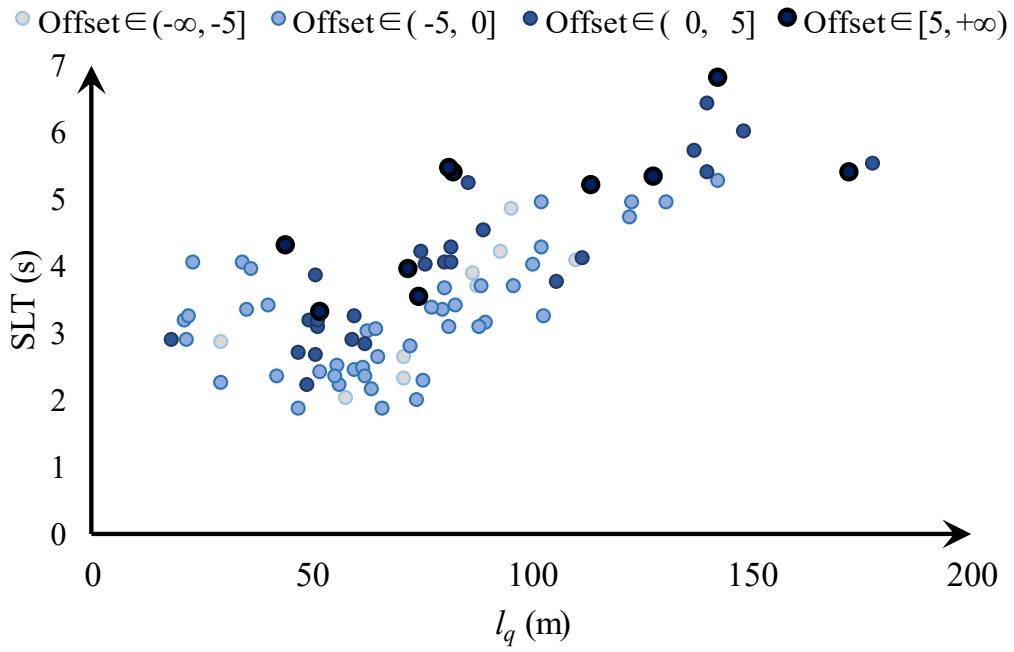

(b) SLT

Figure 3.10 SFR(a) and SLT(b) in four offset groups at approach 4

As a summary of empirical findings, it can be concluded that l_s, l_q, and offset are three main influencing factors. According to the above results, their effect mechanisms are assumed which are further introduced into the modeling designing in the next section. Long l_q in downstream results in low performance of upstream though approach. However, to some extent,

long l_s can alleviate this influence. For instance, the same queue length in links with different l_s leads to different l_{as} for upstream platoons. Also, a positive offset can extend the duration of the downstream queue while negative offset lets the downstream queue discharge soon after upstream green. So that signs of offsets are also important to be considered in the model developing.

3.2 Modeling the Influenced Discharge Behavior by Car-Following Model

3.2.1 Analysis of the Influenced Discharge Behavior

For investigating performances of existing car-following models in reproducing influenced discharge behaviors, some popular models are applied to simulate upstream vehicles' trajectories based on observed motions of last queued vehicles in the downstream link. An example of simulating results is shown in Figure 3.11. As we can observe from this figure, GM and IDM do not fit the observed trajectory accurately. Regarding the performances of existing models, they can be classified into two groups. Represented by GM, once discharged, some car-following models aim to shorten the current headway to the minimum space headway. their trajectories are approaching leading vehicles as quickly as they can. Represented by IDM, behaviors simulated these models not only aim to shorten the current headway but also constrained several limitations such desired speed. Therefore, once discharged simulated vehicles will accelerate to the desired speed instantly. However, both simulated trajectories of the two groups are faster than observed ones. It is concluded that existing models cannot produce realistic discharge behaviors because they do not consider the resistance from downstream traffic properly. In reality, drivers will adjust vehicles' movements not only based on behaviors of leading vehicles but also based on downstream information (such as queues and signals).

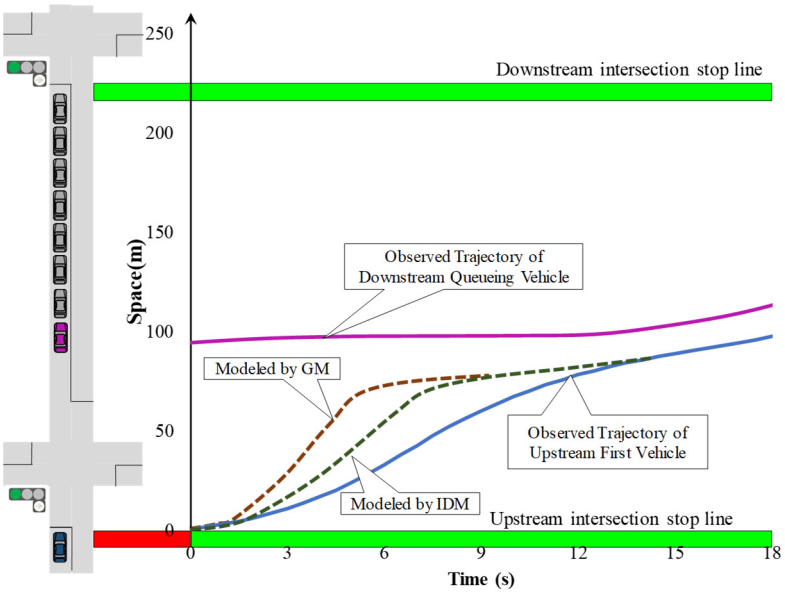

Figure 3.11 Trajectories of discharge vehicles (GM, IDM, and observation)

As early as 1959, Herman et al. (1959) introduced driver anticipation into the car-following model. While driving, drivers not only estimate the current driving conditions (speed, distance to the vehicle ahead) but also predict the future driving state in downstream. In 2012, Deng analyzed the actual driving process and claimed that drivers' anticipation can be classified into two categories (Deng, H, 2012). First is the temporal anticipation which is based on the information from the vehicle ahead and vehicle in driving including their acceleration and velocity. Second is the spatial anticipation which is spatially analyzing information from multiple downstream vehicles. In the assumed environment (short segment streets) of this study, drivers waiting in the subject approach can receive a lot of traffic information by observing downstream vehicles. In this research, upstream vehicles not only speed up reacting to the last vehicle but also adjust their driving strategies based on motions of the whole downstream platoon. It is reasonable to treat downstream influence as the result of both temporal and spatial anticipation. Therefore, in order to simulate driving behaviors in influenced discharge flow, not only the motion of the last vehicle in the downstream platoon should be included, but also the size and duration of the downstream queue should be considered in the model.

In order to understand the anticipation processes of upstream drivers in this research, two typical discharging cases at Jimbocho intersection are plotted in Figure 3.12. Grey dash lines show the discharge process of the upstream platoon without any downstream queue. Blue lines show the discharge process of upstream vehicle influenced by long queue in downstream. No

matter the acceleration rate or the cruising speed after the acceleration of blue lines is lower than grey lines. Through comparison, it can be found that without the influence from the downstream queue upstream platoon discharging achieved a higher efficiency than the one facing to long downstream queue. We further observed that blue lines join the downstream queue just at the time when the last vehicle in downstream almost starts to move. This can provide drivers with more comfortable and safer travel processes. The same phenomenon can be observed in most cases of influenced flow. It can be inferred that the assumed optimization thought for avoiding fully stops really exist in most drivers' minds.

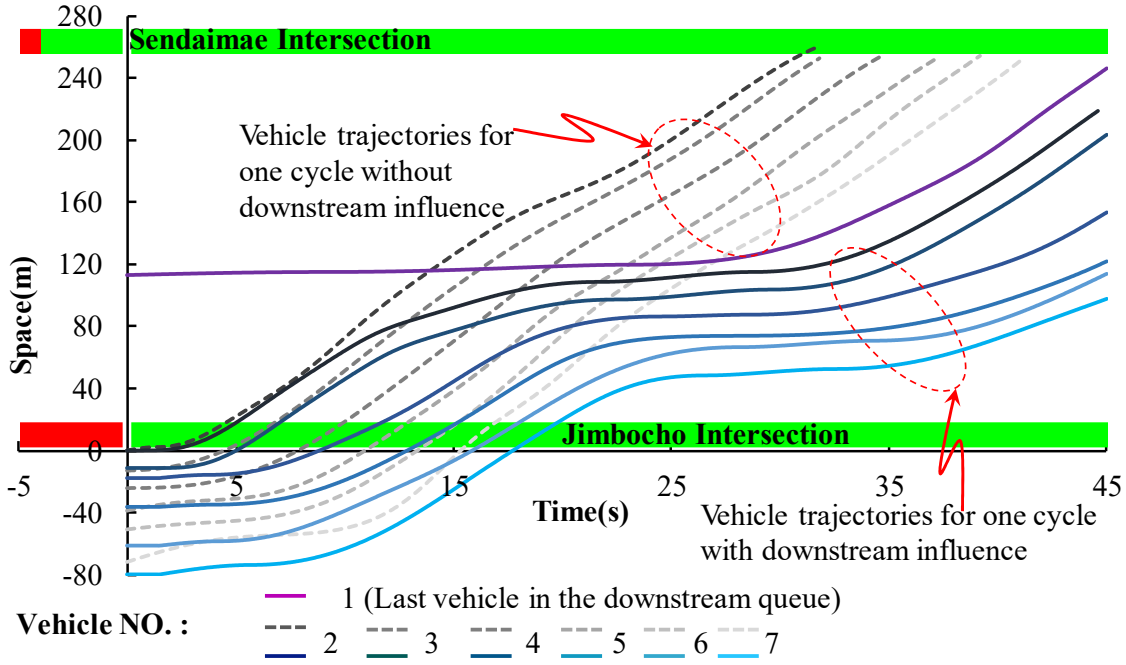

Figure 3.12 Influenced and uninfluenced discharging trajectories

3.2.2 Improved Intelligent Driver Model (IDM+)

Model development are on basis of the assumption that two signalized intersections that are spaced closely which allows vehicles in the upstream intersection to observe the situation at the downstream intersection, such as l_q, l_s, and signal indications. Considering the inference that drivers will react to not only front vehicles but also the action of the downstream platoon. Hence, in this study, the origin car-following model ($f_{car\text{-}follow}$) is improved by adding a downstream influence module ($f_{downstream}$). The basic structure of the new model is as follows.

$$\frac{dv}{dt} = f_{car-follow} + f_{downstream} \tag{3-6}$$

Seldom of the existing car-following models can properly simulate traffic propagation on signalized arterials because most of them are specially designed for simulating traffic flow on motorway sections. This point of view was also acknowledged by Cohen (2002). He claimed that the majority of the current models are specially designed for the uninterrupted flow on freeways and only a few of them can deal with the interrupted flow on urban roads. Speed changes on motorway sections are low frequency and small amplitude. While speed changes on the signalized arterial are far more dramatic than it on motorways. Among the popular car-following models, IDM is selected. Because through multiple attempts, it was found that IDM has better performance than other car following models in reproducing real discharge trajectories. The IDM (Treiber, 2000) is a time-continuous car-following model with a good robustness performance. IDM considers the acceleration, speed, and distance between the preceding vehicle IDM and current driving vehicle. It is described by two ordinary differential equations as follows (Equation (3-7) and (3-8)).

$$\begin{cases} \dfrac{dx_\alpha(t)}{dt} = v_\alpha(t) \\ \dfrac{dv_\alpha(t)}{dt} = a\left(1 - \left(\dfrac{v_\alpha(t)}{v_0}\right)^\delta - \left(\dfrac{d^*}{d_\alpha(t)}\right)^2\right) \end{cases} \tag{3-7}$$

$$d^* = d_0 + v_\alpha(t)T + \frac{v_\alpha(t)\Delta v_\alpha(t)}{2\sqrt{ab}} \tag{3-8}$$

Where, T is the minimum time headway (s), a is the maximum vehicle acceleration (m/s^2), b is the comfortable braking deceleration (m/s^2), δ is the acceleration exponent which is usually set to 4, d_α is the net distance (m), d^* is the desired minimum net distance (m). Vehicle α-1 refers to the vehicle directly in front of vehicle α in the platoon. x_α and v_α are the position and velocity, respectively, of vehicle α at time t. In addition, the velocity difference or approaching rate is $\Delta v_\alpha = v_\alpha - v_{\alpha-1}$. l_α denotes the length of vehicle α. In order to simplify the process, no heavy vehicles are considered in this study and all passenger vehicles are assumed to have equal length l. The net distance headway between vehicle α and vehicle α-1 is defined as $d_\alpha = x_{\alpha-1} - x_\alpha - l_{\alpha-1}$

For designing the downstream module, the discharging process in Figure 3.12 is deformed based on the following rules, as shown in Figure 3.13. Firstly, vehicles' trajectories are divided into three sections: acceleration, running, and deceleration. Secondly, the running process is deformed into a linear curve assuming that the cruising speed is constant. Thirdly, omitting the acceleration and deceleration in the start and stop processes are neglected. The whole trajectory is deformed into polygonal lines as shown in Figure 3.14. When upstream drivers are waiting to be discharged at the approach, they have plenty of time to observe the downstream traffic. By visual observation, they can know the size of the downstream queue and signal displays of the downstream and the subject intersection. Based on this information, they can anticipate the duration of the downstream queue (the time when the last vehicle in the downstream queue starts to move) and roughly plan the driving route. Once they cannot freely pass through the intersection and downstream link due to the hindrance of the downstream queue, drivers may not pursue their desired speed anymore. They may sacrifice driving efficiency to ensure comfort and safety. In this situation, if they can catch up the downstream platoon immediately after the last downstream queued vehicle starts to move, upstream drivers can run a safe path (small speed changes) but also keep driving efficiency (Even if they drive faster, travel time can't be shorter than this way). This path in this study is called the optimal route and Figure 3.14 shows an example of the optimal route. The cruising speed of the optimal route is named as optimal speed v_{op} accordingly which can be easily calculated as shown in Equation (3-3) and (3-4).

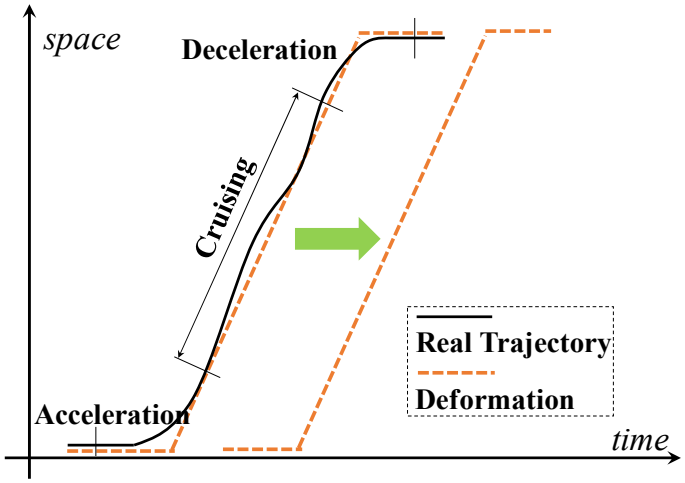

a. Assume that after acceleration, vehicles keep cruising with constant speeds until stop.
b. Neglect the acceleration and deceleration part.

Figure 3.13 Trajectory deformation

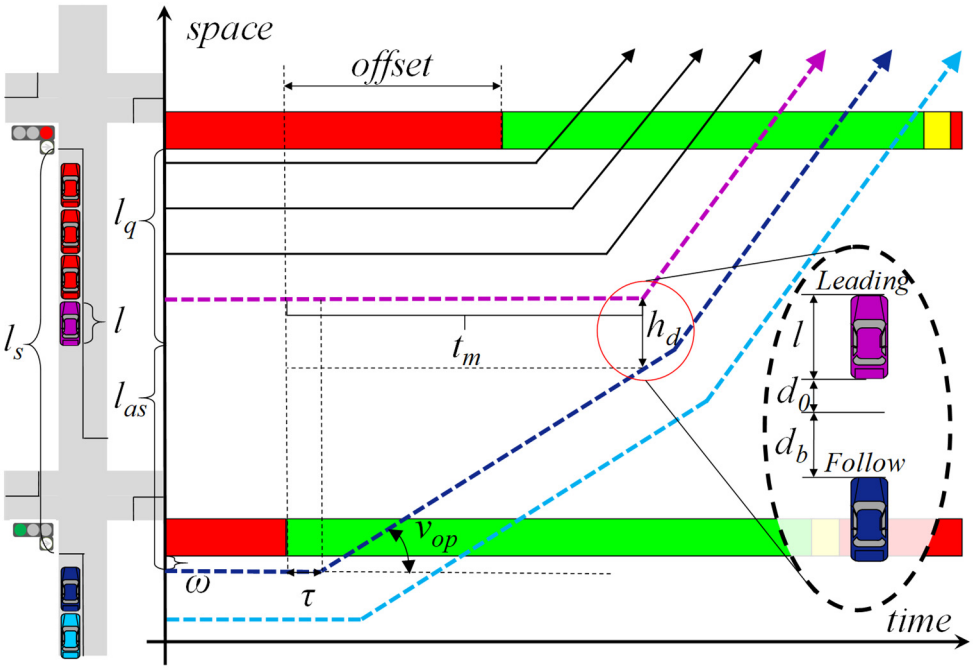

Note: h_d is the distance headway or space headway (m), l is the vehicle length (m), τ is the drivers' reaction time (s), d_b is the brake distance, the product of the reaction time and the current speed (m), ω is the distance from upstream 1st vehicle's front bumper to stop line (m), d_0 is the minimum stopping distance (m), n is the number of vehicles in the downstream queue, v_{op} defines the optimal speed (m/s), respectively, t_m defines the elapsed time from the onset of upstream green signal until the last vehicle of downstream queue starts to move (s).

Figure 3.14 Deformed discharging process

$$v_{op}=\frac{l_{as}+l-h_d}{t_m-\tau} \tag{3-9}$$

Where v_0 is the velocity the vehicle would drive at in free traffic (m/s).

Substitute h_d into Equation (3-9), then

$$v_{op}=\frac{l_{as}-d_0}{t_m} \tag{3-10}$$

Also, it can be inferred that

$$l_{as}=l_s-l_q+\omega \tag{3-11}$$

$$l_q=nl+(n-1)d_0+\omega \tag{3-12}$$

$$t_m = n\tau + offset \tag{3-13}$$

By substituting the Equations (3-11), (3-12), and (3-13) into (3-10), the relationship between *offset*, l_s, l_{as}, and v_{op} can be deduced in Equation (3-14). Theoretically, v_{op} should be larger than 0 and smaller than the drivers' desired speed v_0. Also, in some cases, queue in downstream may has been discharged before the onset of upstream green (t_m is smaller than 0), which represents good downstream situations. v_{op} for these cases equal to v_0 as well.

$$v_{op} = \begin{cases} min\left(\dfrac{l_s - l_q}{\tau \dfrac{l_q + d_0}{d_0 + l} + offset},\ v_0 \right) & \text{if} \quad \tau \dfrac{l_q + d_0}{d_0 + l} + offset > 0 \\ v_0 & \text{otherwise} \end{cases} \tag{3-14}$$

Base on the above analysis, we can know that downstream impacts are results of both temporal and spatial influence. The longer the downstream queue in a road segment becomes and the larger the offset value is, the stronger the downstream influence becomes. The v_{op} is variable which exactly meets the above statement and it introduced to measure the degree of downstream impact. Also, the downstream module is designed by taking v_{op} as a core variable. The improved model is described by the following two ordinary differential equations (Equation (3-15) and (3-16)). In this study, the improved IDM is named as IDM+.

$$\begin{cases} \dfrac{dx_\alpha(t)}{dt} = v_\alpha(t) \\ \dfrac{dv_\alpha(t)}{dt} = a\left(1 - \left(\dfrac{v_\alpha(t)}{v_0} \right)^\delta - \left(\dfrac{d^*}{d_\alpha(t)} \right)^2 \right) - \gamma c \left(\dfrac{v_0 - v_{op}}{v_0} \right)^k \end{cases} \tag{3-15}$$

$$\gamma = \begin{cases} 1 - \left(\dfrac{\rho - 1}{h} \right)^g, & \text{if} \quad 1 - \left(\dfrac{\rho - 1}{h} \right)^g \geq \mu \\ \mu, & \text{otherwise} \end{cases} \tag{3-16}$$

In order to maintain the car-following function, the first half part of the model (Equation 3-15) preserves the original formula of IDM. In the module of IDM, high deceleration rates are used and the following vehicle can react to the leading car instantly (0 reaction time). These settings can guarantee the crash-free in the collective dynamic, which prevents the newly designed model from discussing local and asymptotic stability problems. The second half of

Equation (3-9) β is the module designed to represent downstream influence. In the original formula, β works as a negative force (or deceleration) on the origin desired acceleration of the upstream driver reproducing behaviors of resistance to downstream queues. Among parameters in the downstream module, c (m/s^2) controls the amplitude of the negative force and k controls the increasing pattern of the negative force).

The core part of this β function is the comparison between v_{op} and v_0. "$v_{op}>v_0$" means that drivers cannot freely run with desired speeds. Downstream conditions have negative impacts upstream driving. "$v_{op}<v_0$ or $v_{op}=v_0$" means drivers can drive as fast as they want. They can run through the downstream link with their desired speed (v_0). There is no negative downstream influence and drivers in the subject approach are uninfluenced. Meanwhile, we observed that visions of drivers in the rear part of the platoon are partially blocked by former vehicles. Therefore, it is common sense that with the vehicle sequence in an upstream platoon moving backward, the downstream influence they received decreases. Decline patterns differ in different road geometries. This decline effect of downstream influence is called platoon attenuation and it is explained by a platoon attenuation coefficient γ as shown in Equation (3-16). Different geometric layouts may lead to different visibility conditions. For instance, in a downhill section, drivers can see more far ahead than in an uphill section. This topic requires further investigation in future research.

In the beginning, a sensitivity analysis is carried out to show features of the module (β). v_0, c, k, d_0, τ, and l are set to be 20m/s, 1.5m/s^2, 4, 2m, 1s, and 4.5m in the sensitivity analysis. Two l_s (200m and 150m) are defined to represent a shorter link and a longer link. For both two l_s, values of *offset* gradually increase from -10s to 10s with an interval of 1s and values of l_q increase from 0m until equaling to l_s. The results of the sensitivity analysis are illustrated in Figure 3.15. In Figure 3.15(a) and (b), as the l_q increases, the value of β also increases. This effect corresponds to the real-world observation that longer queue leads to greater downstream impacts. At a specific l_q, as values of *offset* increases, β becomes larger. This effect is consistent with the empirical finding that large positive offsets can aggravate the downstream influence. Furthermore, regarding the comparison between curves in Figure 3.15(a) and Figure 3.15(b), it is obvious that for points with the same l_q and *offset*, β values in Figure 3.15(b) is higher than Figure 3.15(a). This mechanism accords with the other conclusion that longer l_s can accommodate more queued vehicles and mitigate downstream impacts. The above statements

are able to confirm that the newly designed downstream module is rational and it is meaningful to continue calibrating the new model.

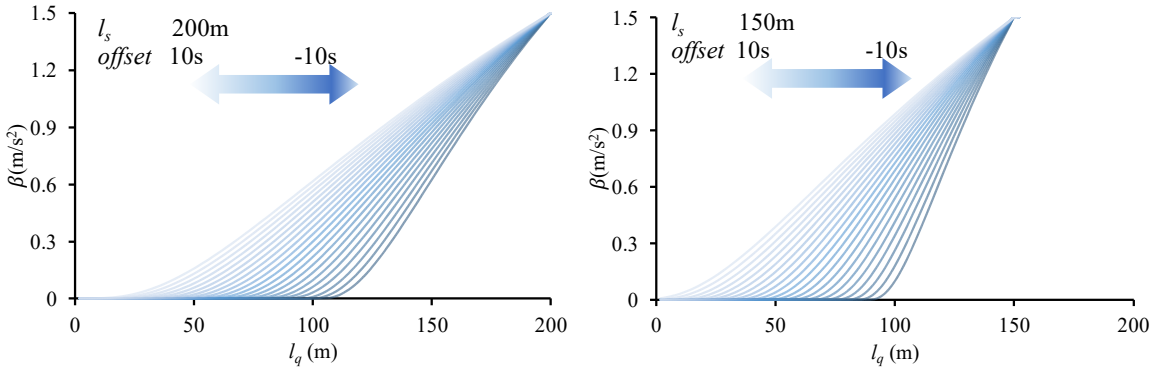

(a) Segment length (l_s) is 200m (b) Segment length (ls) is 150m

Figure 3.15 Characteristics of the downstream influence module

3.2.3 Parameters Calibration by Generic Algorithm

Vehicles involved in the discharge process are numbered. As shown in Figure 3.16, the last queued downstream vehicle numbered as 1 and the first vehicle waiting in the subject intersection is numbered as 2. Vehicles waiting after vehicle 2 are numbered in sequence. In the calibration, with the empirical trajectories of their corresponding leading vehicles serving as the input data, simulated trajectories of vehicles 2, 3, 4…… can be calculated by car-following models. The flow chart in Figure 3.17 shows the logic of generating simulated data that is used for calibration. The observed data used for calibration are from Yasukuni-Dori. For a discharge process, trajectories of the last queued vehicle in downstream and all upstream queued vehicles are recorded. Trajectories of upstream vehicles are recorded from the onset of upstream green until all upstream queued vehicles join the downstream queue. Finally, a total of 30 sets of data were collected. Figure 3.16 shows an example of collected data and explains the method of numbering vehicles in the discharging process.

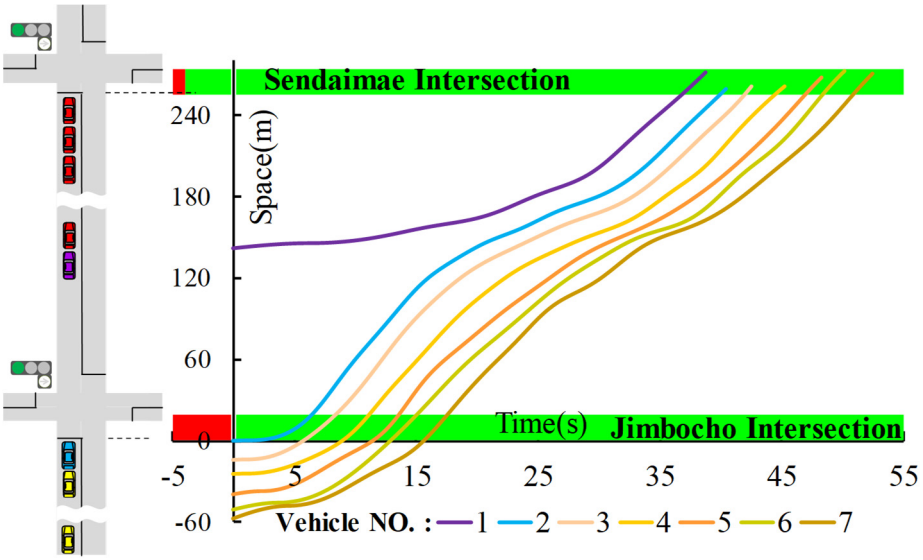

Figure 3.16 An example of trajectory data and the vehicle numbering method

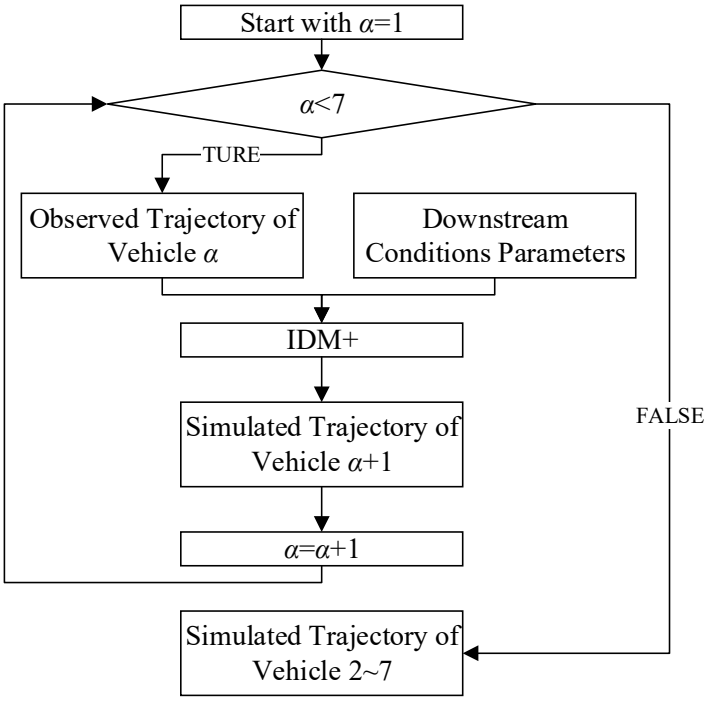

Figure 3.17 Flow chart of generating simulated vehicle trajectories.

Firstly, parameters in the proposed model should be carefully calibrated. Only after calibration, the model can be further applied to discuss its macroscopic and microscopic feature. How many mistake ratios are between observed and simulated data is the key point to judge whether the calibrated car-following model is good or not. In this research, the model will be regarded to have a good fitting performance if it can accurately reproduce observed discharge trajectories and maintain a neglectable error with the actual data. The mistake ratio is commonly measured by fitness values. In previous simulation researches, different indicators

by different fitness methods were introduced to calibrating simulators or micro models. The pros and cons of these fitness measurements have been comprehensively explained and compared in Traffic Simulation: Case for guidelines (Antoniou, C et al. 2014). Geoffrey E. Heavers (GEH) statistic is one of the most popular fitness calculation methods. It merged considerations of both relative and absolute differences into one function and it has been widely applied. For instance, Abuamer, I. M., Sadat, M. et al. (2016, 2017 and 2017) built simulation works by VISSIM for modeling ramp metering sections on Istanbul freeways. In their studies, the volume on main roads is treated as the key indicator for calibration. Fitness measurement is calculated by the GEH method. To achieve a reliable simulation performance, trajectories from the proposed model should be comparable with the whole observed data points in an acceptable mistake ratio. Kesting and Treiber (2008) used the mixed error to calibrate the IDM and proved that this fitness measurement is suitable for the IDM calibration. The fitness equation (Equation 3-17 and 3-18) of this study is designed by drawing on the mixed error measurement. Calibrated by this equation, drivers' average behaviors can be captured.

$$Fitness = \frac{1}{m}\sum_{\alpha}^{m}\sqrt{\frac{1}{\left\langle s_{\alpha}^{data}\right\rangle}\times\left\langle\frac{\left(s_{\alpha}^{sim}-s_{\alpha}^{data}\right)^{2}}{\left|s_{\alpha}^{data}\right|}\right\rangle} \tag{3-17}$$

Where s_{α}^{data} is the empirical trajectory data on time series of vehicle α, s_{α}^{sim} is the simulated trajectory data on time series of vehicle α with the observed leading vehicle serving as external input, and m is the number of vehicles for fitness calculation. Here, the expression $\langle . \rangle$ means the temporal average of time series of duration ΔT as shown in Equation (3-13)

$$\left\langle z\right\rangle = \frac{1}{\Delta T}\int_{0}^{\Delta T} z(t)\,dt \tag{3-18}$$

The calibration procedure can be transformed into an optimization problem that is finding a set of parameters aiming to let differences (*Fitness*) between simulated and observed trajectories be minimal. As shown in Figure 3.18, optimization processes for the calibration are carried out by the genetic algorithm which is performed based on the GA function of Matlab (R2017b). The GA process for the calibration issue is introduced as the following four steps.

1. A certain amount (defined by the population size) of possible solutions will be generated stochastically which are subject to the given constraints. Each possible

solution is an individual of the whole population and contains a set of parameters of the car-following model (called as the gene).

2. The solution set in one calculation iteration is named as the generation and the solution set created in the first step is the first generation. In each generation, fitness value will be calculated and assigned to each individual via Equation 3-17 and 3-18.
3. In each generation, individuals with the lowest fitness value will be kept unchanged and be inherited to the next generation. Pairs of individuals will be randomly selected and combined to generate a new individual. Individuals with lower fitness values in the last generation have a higher probability of becoming parents. Genes of new individuals are produced through inheriting, mutating, and crossover. By this step, a new generation will be created.
4. The new generation will go through the second and third steps again until average and best fitness values for generations satisfy convergence criteria as the iteration goes on. Then calculation will terminate and final parameters will be output.

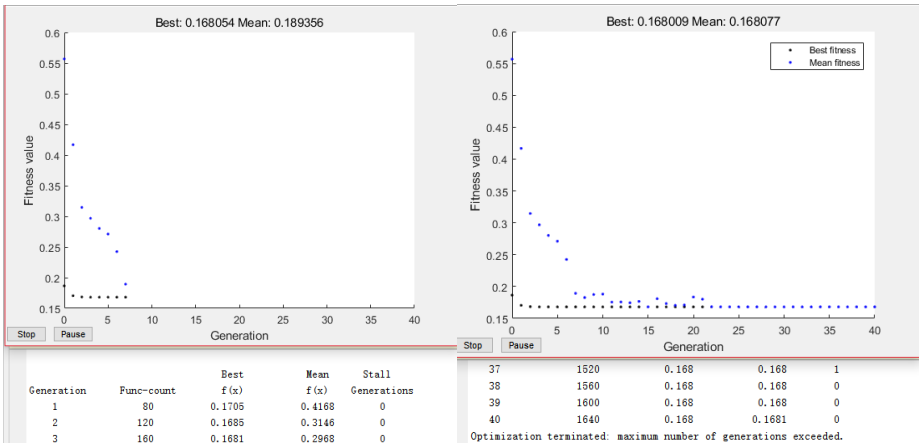

Figure 3.18 Iteration process of GA in Matlab

The reaction time for signal response in this study is determined as one second, which is the recommended value in the Institute of Transportation Engineers (1994). In addition to this, IDM has 5 parameters that need to be calibrated. While IDM+ contains 10 indicators including 5 parameters that are the same as those in IDM. Based on several attempts and study experience, we set constraints (minimum and maximum values) for all parameters to restrict them into reasonable solution space but not deleting any possible optimal solution as shown in Table 3-2. The value of parameter c reflects the extent of downstream impacts and the k parameter defines the growth rate of downstream influence. Among the parameters in platoon attenuation,

h is the vehicle sequence in the upstream queue where the platoon attenuation converges. The downstream influence becomes lower with the vehicle sequence in the upstream queue increases. Because the visual sight of vehicles in the rear part of the platoon is partially blocked by former vehicles. They received less downstream information than former vehicles. However, they can still observe the suspended signal lights (subject and downstream) and speculate the downstream situation based on the driving experience. After the h^{th} vehicle, the downstream impact received by upstream vehicles will not be changed anymore. Also, platoon sizes of collected samples are mostly equal to 6. Therefore, the constraints for h are [0.1, 6]. Both IDM and IDM+ are calibrated with the observed 30 sets of trajectory data. As shown in Table 3-2, in calibration results, the fitness value of IDM+ (16.80%) is lower than IDM (25.27%), which indicates that by considering the downstream influence IDM+ has a better ability in simulating the influenced discharging driving behavior.

Table 3-2 Parameters constraints and calibration results

Parameters	Constraints [min, max]	IDM+ Result	IDM Result
v_0 (m/s)	[1, 30]	24.23	22.82
T (s)	[0, 1.5]	1.02	1.52
a (m/s^2)	[0.1, 6]	2.05	2.05
b (m/s^2)	[0.1, 4]	3.94	3.91
s_0 (m)	[0.1, 8]	2.05	2.05
c (m/s^2)	[0.1, 6]	1.82	~
k	[0.1, 6]	1.85	~
h	[0.1, 6]	6.00	~
g	[0.1, 6]	4.00	~
μ	[0.01, 1]	0.62	~
Fitness%		16.80	25.27

3.3 Model Validation

3.3.1 Simulation by IDM+

In order to validate the improved model, we assumed a specific road system for simulating influenced discharging processes under different downstream conditions. As illustrated in Figure 3.19, the assumed road section is just two signalized intersections connected by a two-lane road. Turning movements at the major and minor streets are not considered because this

research only studies the discharge flow on through lanes. Furthermore, in theory, some vehicles that were from turning phases of the minor street may still be moving ahead of the upstream platoon (moving vehicle) after the onset of green indication. Even some of them may still be running in the intersection (clearing vehicle) and did not join into downstream queues. Their presence will deteriorate the upstream discharge performance. However, they are excluded from experiment designing as well. Because segment links at both observed and simulated road sections are short. In addition, inter-green intervals of the observed intersections are long enough (larger than 7s) so that it can avoid this phenomenon. In most cases, no moving vehicle or clearing vehicle can be observed. Therefore, this event is regarded as a small probability issue so that it will not be specially considered.

Meanwhile, corresponding to screening rules of the empirical study, no heavy vehicle is included and all vehicles are set to be the same length (4.5m) which is the observed average value of passenger vehicles on Yasukuni road. Also, no secondary downstream intersection is simulated because experiments assume that downstream conditions of the second intersection are good so that the traffic flowing out from the system is uninfluenced. In principle, every intersection may be affected by its downstream traffic. However, it is difficult to properly consider the traffic condition at the secondary downstream intersection. Because the second intersection may further be influenced by its downstream. It will be an endless discussion to consider the link lengths, offsets, and queue lengths of multiple downstream intersections. More importantly, only parameter t_m describes the situation of downstream discharge in the IDM+. When demand is lower than the capacity, the t_m is only governed by the number of queued vehicles in downstream links (n), reaction time (τ), and offset as shown in Equation (3-12). It is irrelevant to the traffic of secondary downstream intersection. When traffic at intersections is oversaturated, spillbacks will occur, which shall be out of range of this study. Therefore, this simplification and assumption are justified and acceptable.

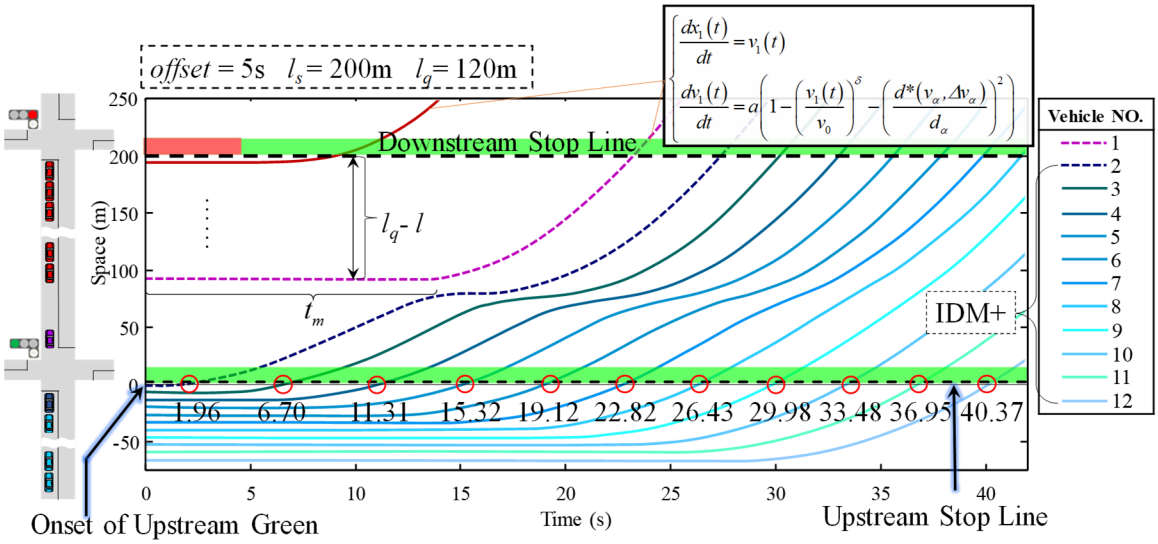

Figure 3.19 IDM+ based simulation platform

Simulation experiments are also performed in MATLAB (R2017b). Unlike the simulation experiments established in other simulation studies (such as Akyol, G., Silgu, M. A., and Celikoglu, H. B., 2019 or Erdağı, İ. G., Silgu, M. A., and Çelikoğlu, H. B., 2019), this simulation work does not plan to investigate the performance of long-time traffic at the assumed intersections. Instead, we only pay close attention to a small but important process such as one discharge process on the through lane in this study. In one case, the simulation period starts from the onset of upstream green until all upstream queued vehicles pass the upstream stop line. Hence, each simulation round only lasts for 30~50 seconds. Before discharging, link length (l_s) between two intersections will be defined and a certain number of queued vehicles will be assigned to the downstream link to demonstrate values of l_q. The green starting time of upstream and downstream signals will be given to simulate *offset* values. As shown in Figure 3.19, the l_s, l_q, and *offset* are input variables of the experiment. These three parameters will determine and generate the trajectory of vehicle 1. Successively, trajectories of other vehicles will be calculated and generated by IDM+ based on the trajectory of vehicle 1.

Two scenarios (Scenario 1: l_s=300m and Scenario 2: l_s=200m) are assumed to represent the shorter downstream link and the longer downstream link. For both two scenarios, values of l_q increase from 0m to until spillback issues are detected and values of *offset* gradually increase from -9s to 9s with an interval of 2s. For each case, the passing time of each vehicle at the upstream stop line is recorded. The SFR and SLT of the discharging process will be measured by the method introduced in ***Chapter 3.1.3***. As we introduced before, calibrated IDM+ is able

to capture average driving behaviors. Correspondingly, simulated SFRs and SLTs represent the average values of the upstream discharge flow. Figure 3.19 shows the result of one simulation experiment. Departure headways at the stop line gradually decrease to a stable value (saturation headway) with the increase of vehicle sequence. Therefore, SFRs and SLTs are measurable from the recorded passing time. They are calculated through the method introduced in ***Chapter 3.1.3***. The results of simulated SFRs are shown in Figure 3.20, Figure 3.21, and Figure 3.22. The results of simulated SLTs are shown in Figure 3.23, Figure 3.24, and Figure 3.25.

From graph shapes in Figure 3.20(a) and (b), it is found that with values l_q decrease to 0m and values of *offset* decrease from 9 s to 9s, SFRs in both two scenarios increase gradually and converge to the same value (approximately 1700pch/h/ln). In this stage, downstream impacts are zero and SFRs are uninfluenced. SFRs in both two scenarios deteriorate to 1200 pch/h/ln with growths of l_q and *offset*. In the comparison of the graph shapes in Figure 3.20(a) and (b), it is obvious that the decrease rate of SFRs on these directions (growths of l_q and *offset*) in Figure 3.20(a) is higher than Figure 3.20(b). This trend accords with the empirical finding that drivers are more sensitive to the downstream queue that is in a shorter segment.

Figure 3.21 is the right elevation of Figure 3.20 which shows the relationship between *offset* and SFR on three specific queue length (40m, 80m, and 120m). In general, as the *offset* increases, the SFR decreases. As shown in Figure 3.21(a), when l_q is equal to 40 meters, values of SFR keep stable for all *offset* values. However, for the same l_q in a shorter segment (200m), SFR curve just keeps constant between -9s and 3s. In the interval [3s, 9s], SFRs decrease from 1700 veh/h/ln to 1450veh/h/ln. Trends of curves in Figure 3.21(b) (l_s=200m) are similar to those in Figure 3.21(a). However, decreasing rates of SFR is more intense in Figure 3.21(b) due to the influence of short l_s. With the l_q increases (80m and 120m), ranges of *offset* values under which SFR reduces becomes wider. This is a rational result since drivers facing short queues may not worry about signal display too much.

Figure 3.22 is the front elevation of Figure 3.20 which shows the relationship between queue length and SFR on 10 specific offsets (from -9s to 9s with an interval of 2s). Trends in Figure 3.22 (a) and (b) highlighted the relationship between downstream impacts and values of *offset*. Under negative values of *offset*, the downstream queue will start discharging earlier than the upstream platoon, which reduces the duration of downstream queues. The downstream impacts received by upstream drivers is small. On the contrary, under the positive values of

offset, upstream drivers can observe the red signal at the downstream intersection and understand the situation. Downstream queues will start to discharge late than upstream platoons and durations of downstream queues become long. Therefore, SFRs under negative *offset* values are higher than SFRs under positive *offset* values. Also, sections, where SFRs are uninfluenced under positive *offset* values, are shorter than those under negative *offset* values. This indicates that upstream SFRs are more easily affected by downstream queues with large positive values.

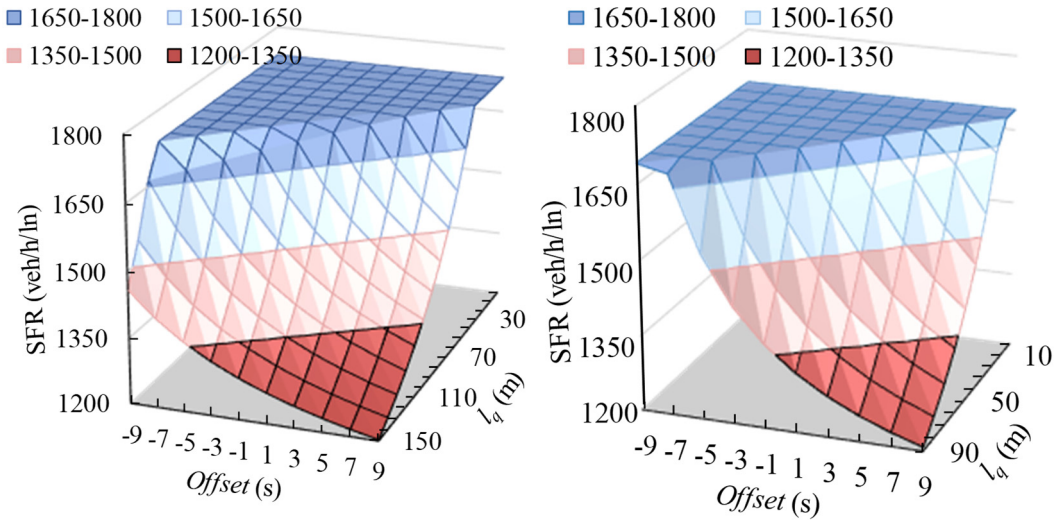

(a) Scenario 1: l_s=300m (b) Scenario 2: l_s=200m

Figure 3.20 The relationship between SFR, l_q, and *offset*

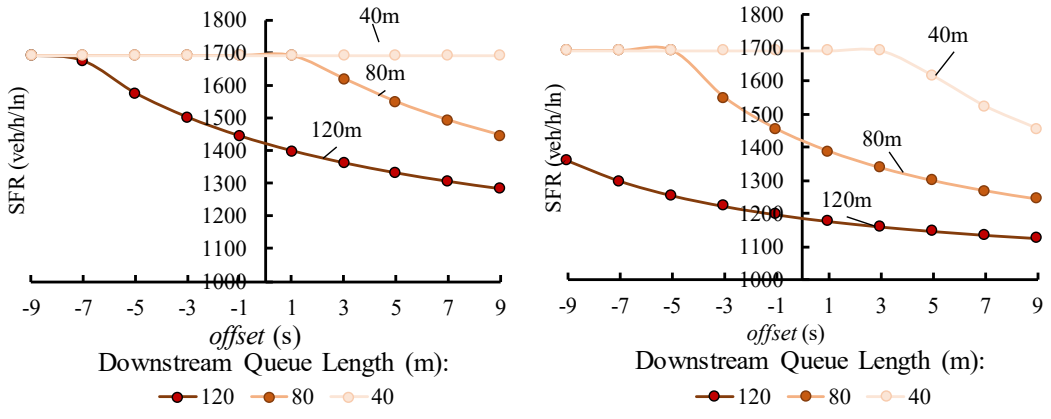

(a) Scenario 1: l_s=300m (b) Scenario 2: l_s=200m

Figure 3.21 Front view: the relationship between SFR and *offset*

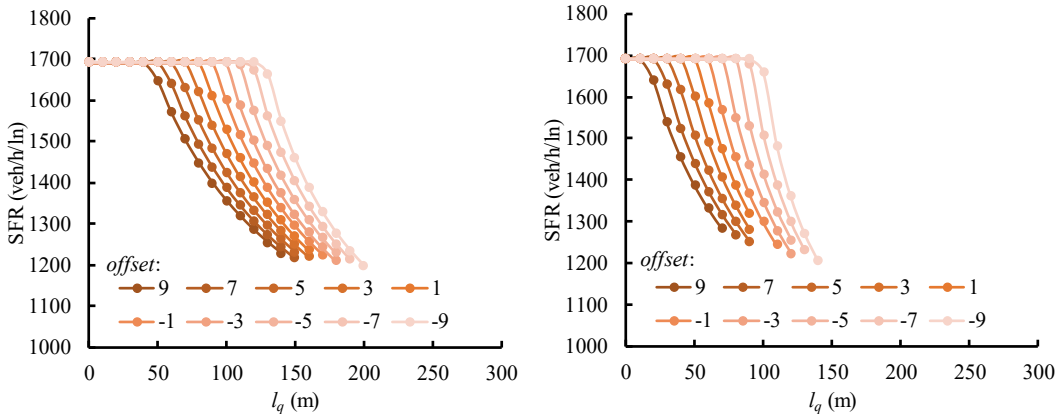

(a) Scenario 1: l_s=300m (b) Scenario 2: l_s=200m

Figure 3.22 Side view: the relationship between SFR and l_q

Exactly, the opposite trend can be observed from SLTs figures. Figure 3.23 shows that with the increase of downstream queue length (l_q) and *offset*, SLTs increase significantly. On the contrary, as l_q and *offset* decrease, SLTs gradually reduce and reach a stable limit (approximately 2.5s), where the downstream influence is almost zero. In addition, it is obvious that the growth rate of SLT on l_q and *offse*t in Figure 3.23 (a) is more intense than that in Figure 3.23 (b). This is because the shorter segment length with a long downstream queue (Figure 3.23 (a)) can result in stronger space-time pressure from downstream.

Figure 3.24 is the right elevation of Figure 3.23 which shows the relationship between *offset* and SLT on three specific queue length (40m, 80m, and 120m). In general, as the *offset* increases, the SLT increases. As shown in Figure 3.24 (a), when l_q is equal to 40 meters, values of SLT keep stable for from -9s until 7s. Whereas, for the same l_q in a shorter segment (200m), the SLT curve only keeps stable between -9s and -3s. In the interval [-3s, 9s], SLTs increase from 2.5s to 4s. However, growth rates of SLT in Figure 3.24(b) is faster due to the short l_s. With values of l_q increases (80m and 120m), ranges of *offset* values under which SFR reduces becomes wider. Trends of curves in Figure 3.24 (b) (l_s=200m) are similar to those in Figure 3.24(a).

Figure 3.25 is the front elevation of Figure 3.23 which shows the relationship between queue length and SLT on 10 specific offsets (from -9s to 9s with an interval of 2s). Same as findings in figures of SFR, the impact of downstream queue length is strongly related to the value of *offset*. With offset increases, stable parts of curves become longer. Comparing with Figure 3.25(a) and (b), it is found that growth speeds of SLTs in shorter segment cases are more

intense. At negative *offset* values, the downstream platoon will start discharging before the onset of upstream green indication. Therefore, the duration of the downstream queue is shorter. This reduces the risk that upstream routes are hindered by the downstream queue. Therefore, the upstream platoon receives less downstream impacts and quick start-ups. On the contrary, if the *offset* is positive, discharging drivers will hesitate to fully accelerate while observing that the downstream segment is occupied with a lot of queuing vehicles that are still waiting for the green signal indication in the downstream intersection. The positive offset will magnify the impact of the downstream queue leading to a significant increasing of SLT. Meanwhile, the same as curves of SFR, data points of SLTs with l_q more than 150m (for 300m segment length) or 90m (for 200m segment length) in which spillbacks occur are removed.

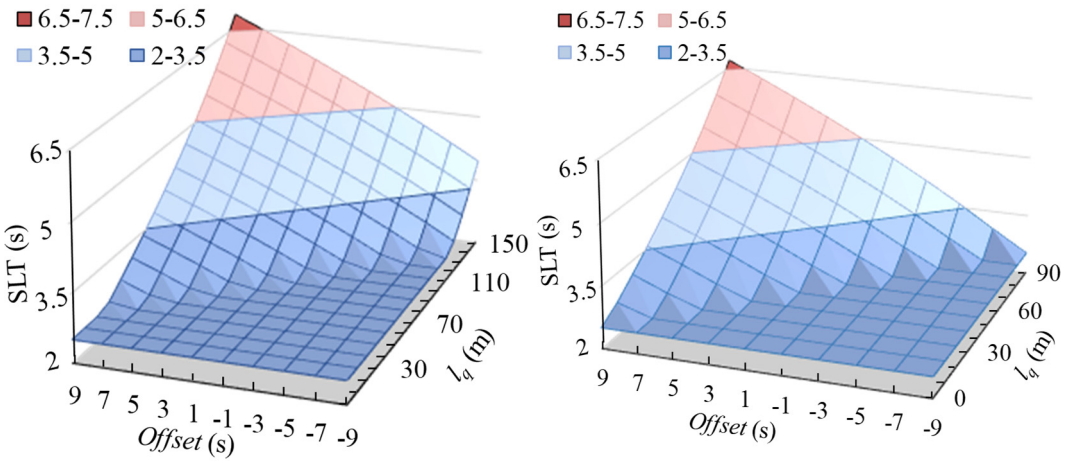

(a) Scenario 1: l_s=300m (b) Scenario 2: l_s=200m

Figure 3.23 The relationship between SLT, l_q, and *offset*

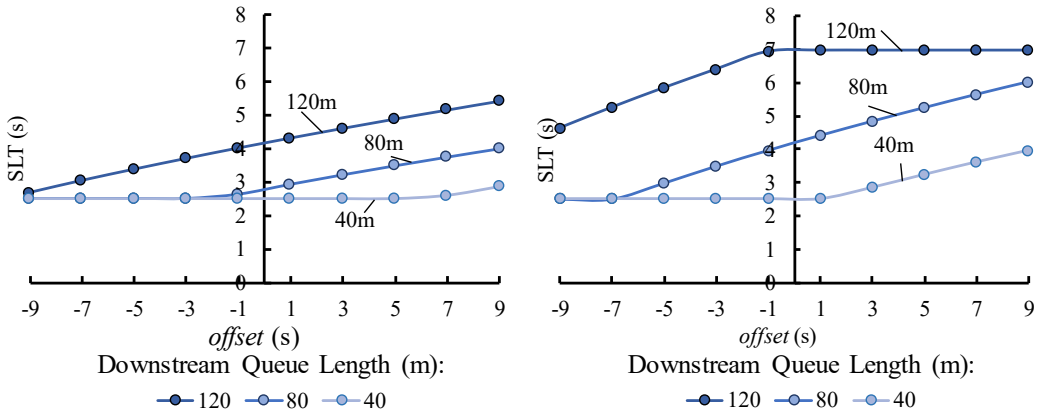

(a) Scenario 1: l_s=300m (b) Scenario 2: l_s=200m

Figure 3.24 Front view: the relationship between SLT and *offset*

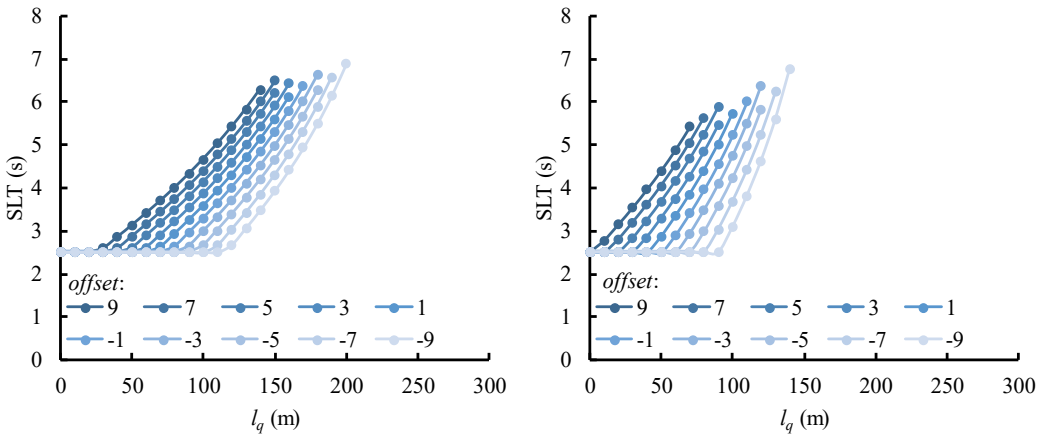

(a) Scenario 1: l_s=300m (b) Scenario 2: l_s=200m

Figure 3.25 Side view: the relationship between SLT and l_q

3.3.2 Simulation in VISSIM

VISSIM is an advanced simulator that can realize various simulation functions. It can not only handle modeling for uninterrupted or interrupted traffic flow but also deal with simulations for pedestrian and bike flow. Therefore, it has been widely applied in practice and researches in recent years. Also, VISSIM is a flexible software, many researchers developed secondary programs for VISSIM to achieve more functions, such as estimation of vehicles' energy consumption and pollutant emission (Silgu, M. A., et al., 2018).

The hypothetical road section is also simulated in the VISSIM (PTV, 2015), as shown in Figure 3.26. Longitudinal movements of vehicles in VISSIM are calculated based on car-following models (Wiedemann 74 and Wiedemann 99) and all vehicles' behaviors in VISSIM have been set with default values. The platform consists of two roads (minor and main road) and different traffic volume (red vehicle) has been set for the minor road. Before the upstream green, queue in downstream links with different lengths can be generated by the flow from the minor street for different cases. Also, the downstream signal is set to turn green at different times for simulating various offset values. At the onset of green indication, upstream queued vehicles (blue) discharge into the downstream segment reacting to different downstream conditions.

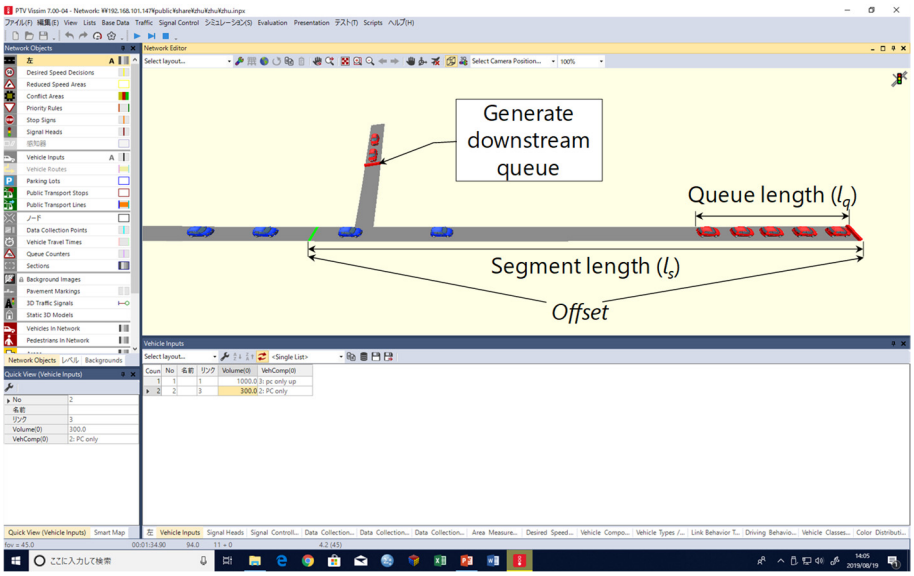

Figure 3.26 Simulation platform in PTV VISSIM

3.3.3 Comparison with Empirical Data

There is only one offset type on Hirokoji-tori, Nagoya for all surveyed periods, which is not significant for data comparison. As for the Yasukuni-tori in Tokyo, sample sizes of approaches 3 (12 samples) and 5 (4 samples) are not big enough for validation. Also, surveyed samples of approach 2 are all cases with small or even zero downstream influence due to the negative offset settings (-15s~-2s). Finally, only observed data from approaches 1 and 4 have been selected for the validation. The downstream lengths of approach 1 and approach 4 are both 250m. Therefore, samples from the two approaches can be integrated and analyzed together. Among the data, cases of *offset*=1s, 5s, and 9s have even offset spans and are with sufficient samples. Hence, they are selected for data plotting. As for the simulated data by IDM+, an IDM+ simulation platform (250m downstream segment length which is the same as approaches 1 and 4) is created on the basis of the idea mentioned in ***Chapter 3.3.1***. Also, the same simulation platform (250m spaced two signalized intersections) is built by PTV VISSIM. For both IDM+ based simulation and VISSIM based simulation, simulation operates only one discharge process for each case (less than 60s) then the performance of the upstream platoon is measured. Three offset values (1s, 5s, and 9s) are set and the queue length in downstream increases from 0 until spillback occurs.

Figure 3.27 shows results of observed SFRs and simulated SFRs (IDM+ and VISSIM) under 1s, 5s, and 9s *offset*. IDM+ curves show a good correspondence with empirical data (Data

points of observed SFRs are evenly distributed around curves that were simulated by IDM+). The mean absolute percentage error (MAPE) for IDM+ is 3.39% (0.09% ~10.29%) and the root mean square error (RMSE) is 71.02pcu/h/ln. These values indicate that the proposed model (IDM+) is reliable for reproducing observed SFR. SFRs simulated by the proposed model decrease sharply with the increase in queue length, in a very similar trend as the observed SFRs for all 1s, 5s, and 9s offsets. When the *offset* decreases (from 9s to 1s), decreasing trends of SFRs becomes milder and the stable part becomes longer, which indicates that downstream impacts on SFR are weakened for small offset values.

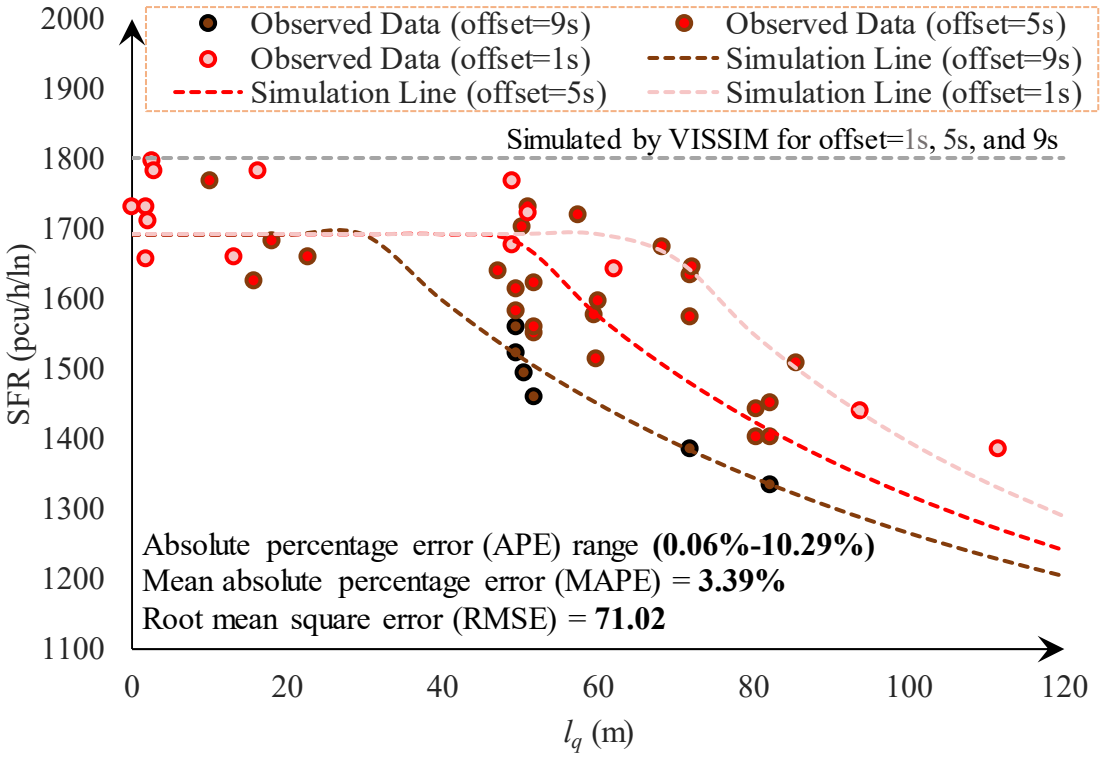

Figure 3.27 Validation result of SFR (IDM+, VISSIM, observed data)

Figure 3.28 shows results of observed SLTs and simulated SLTs (IDM+ and VISSIM) under 1s, 5s, and 9s *offset*. IDM+ curves show the same trend with the empirical SLT (Data points of observed SLTs are evenly distributed on both sides of IDM+ curves). The mean absolute percentage error (MAPE) for IDM+ is 7.59% (0.15% ~23.13%) and the root mean square error (RMSE) is 0.35s. These values indicate that the IDM+ fits observed SLT well. As values of offset decrease (from 9s to 1s), growth trends of SLTs become milder and the flat parts are longer. These trends are similar to what is shown in empirical data, which indicates the fact that downstream impacts on SLT become smaller as offset values decrease. In addition,

the result of VISSIM shows that SFRs simulated by VISSIM do not change at all for all downstream conditions. Also, even though SLTs from the VISSIM for offset=5s and 9s increases in rear parts of curves with l_q increases, SLTs simulated by VISSIM are obviously smaller than empirical data and ones modeled by simulation. VISSIM can explain the downstream influence caused by the upstream platoon reacting to the last vehicle in the downstream queue. Hence, SLTs from the VISSIM for offset=5s and 9s increase in rear parts. However, VISSIM neglects considering the time-space pressure on upstream vehicles which is caused by the size and duration of the downstream queue. This is also the reason the SLTs in VISSIM is extremely smaller than empirical data. This finding confirms the shortcoming of current simulators which we mentioned in ***Chapter 2***.

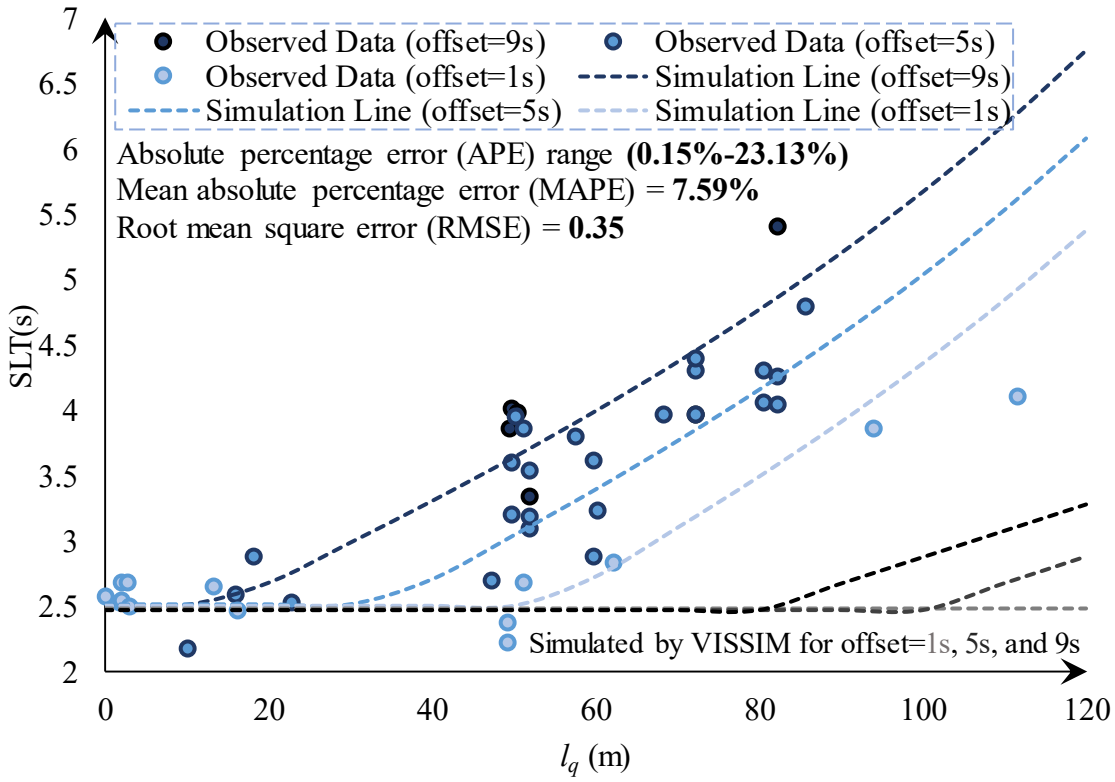

Figure 3.28 Validation result of SLT (IDM+, VISSIM, observed data)

3.4 Modeling the Influenced SFR and SLT

3.4.1 Simulation Experiment

On the basis of the proposed car-following model (IDM+), more simulation scenarios are designed to generate enough data for modeling the relationship between downstream and influenced SFR and SLT. 6 options of downstream segment lengths (increase from 100m to 350m with an interval of 50m) combined with 10 offset options (-9s, 7s, -5s, -3s, -1s, 1s, 3s, 5s, 7s, 9s), a total of 60 experiments are created. Like the experiment designed in ***Chapter 3.3.1***, each of these 50 simulation experiments only runs for one discharge. In one discharge process, queued vehicles (enough for the platoon to reach the saturated flow) discharge from the upstream approach until joining the downstream queue or passing through the downstream stop-line. Trajectories of last vehicles in the downstream shift regarding the value of queue length increasing from 0m to the segment length. After screening out the data in which spillback happened, 620 valid data were generated for regressing finally.

3.4.2 Regression Analysis

After obtaining the above experiment data, they are plotted for analyzing trends of SFR and SLT on downstream impacts. Several parameters have been examined such as l_q, l_s, *offset,* and so on. Finally, we find that data points of SLTs and SFRs converge into regular curves on values of optimal speed (v_{op}) as shown in Figure 3.29, which are easy to formulate.

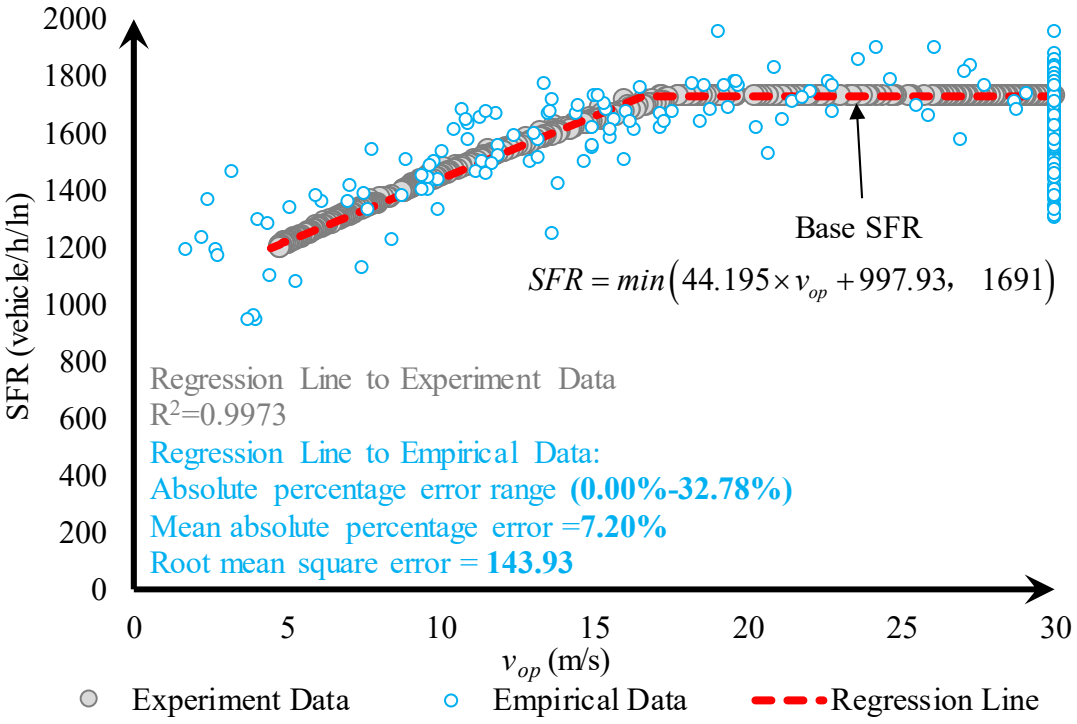

(a) SFR

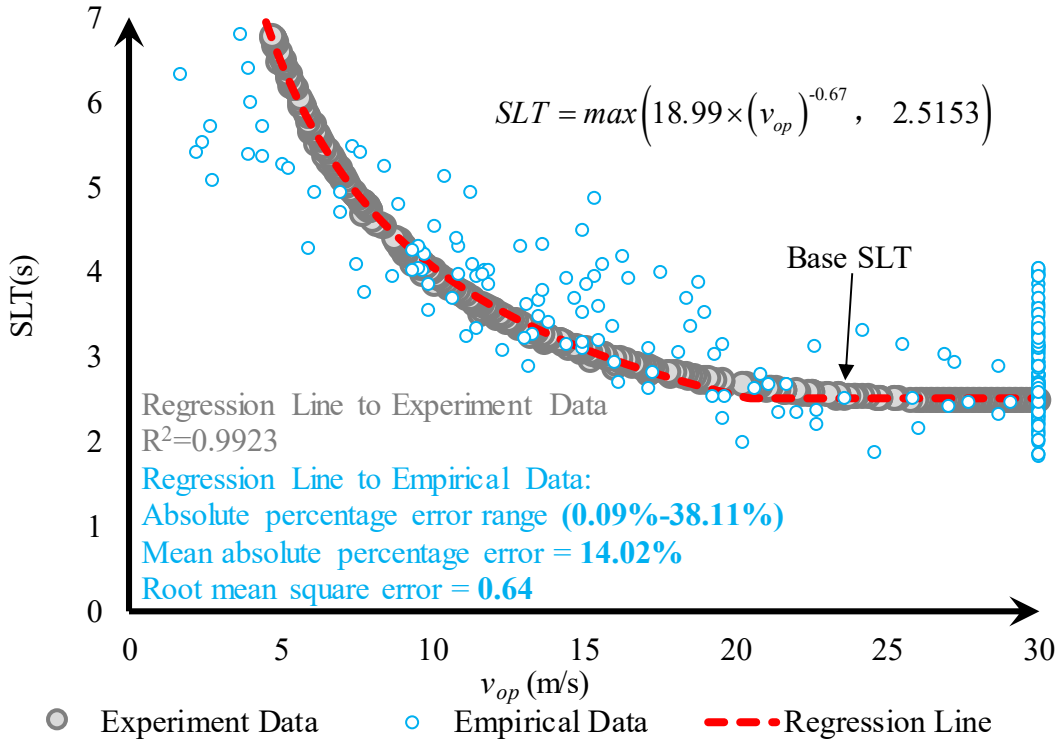

(b) SLT

Figure 3.29 Models of influenced SFR and SLT

For showing results clearly, data points with v_{op} values exceeding 30m/s are classified as data with v_{op} equal to 30m/s. Because when v_{op} is larger than 30m/s, both SFR and SLT have reached stable stages. In these parts, downstream impacts are minimal. SFRs no longer increase significantly with the growth of v_{op}, and SLTs decrease significantly with the increasement of v_{op}. Therefore, this deformation will not influence the accuracy of models. Values where SFRs and SLTs become stable are called base SFR (SFR_{base}=1691veh/h/ln) and base SLT (SLT_{base}=2.5153s). Regression models for estimating SFR and SLT are shown by Equations (3-19) and (3-20), respectively.

$$SFR = min\left(44.195 \times v_{op} + 997.93,\ \ 1691\right) \tag{3-19}$$

$$SLT = max\left(18.99 \times \left(v_{op}\right)^{-0.67},\ \ 2.5153\right) \tag{3-20}$$

The regression model for the influenced SFR is shown in Figure 3.29(a). The relationship between SFR and v_{op} is formulated into a piecewise model which consists of a flat section and a linear increasing part. The regression line of influenced SFR fully coincides with SFR data points from experiments. Also, the value of R^2 (Regression Line to Experiment Data) is 0.9973, which further indicates that the result predicted by IDM+ can be perfectly replaced by the newly proposed piecewise formula. On the other hand, the regression model for the influenced SLT is shown in Figure 3.29(b), the relationship between SLT and v_{op} is formulated into a piecewise model which consists of constant part and increasing part. The regression line fully coincides with data points from experiments. R^2 (Regression Line to Experiment Data) is 0.9923, which further indicates that the result predicted by IDM+ can be totally replaced by the newly proposed piecewise formula.

While comparing with empirical data, it is found that regression lines of SFR and SLT also show good fit results. Observed data points show the same trend as regression curves. Statistically, for SFRs, the absolute percentage error range is between 0.00% and 32.78%. The mean absolute percentage error is 7.20% and root mean square error is 143.93 veh/h/ln. For SLTs, the absolute percentage error range is between 0.00% and 38.11%. The mean absolute percentage error is 14.02% and root mean square error is 0.64s. In addition, it can be observed that there is no experiment data when v_{op} is less than 4.5m/s. Because in this interval, the downstream traffic is congested and upstream discharge platoons are stopped by the downstream queue. These cases are treated as spillback and excluded.

3.5 Summary

One of the most important contributions of this chapter is creating a new car-following model that can capture the driving behavior under different downstream conditions. The proposed car-following model (IDM+) pointed out the flaws of existing micro-simulators. The downstream module of IDM+ can provide a good idea or hint for existing micro-simulators to improve their core models. So that they can simulate the discharge flow more accurately. Another important contribution is proposing generalized models of influenced SFR and SLT. By these models, the capacity drop can be estimated with micro indicators of downstream situations. Also, the research process is summarized as follows.

A typical Japanese arterial, Yasukuni-tori in Tokyo was observed and studied in this chapter. Based on empirical analysis, it was found that the queue length in the downstream link, offset, and segment length could influence the SFR and SLT at upstream intersections. Longer queue in shorter downstream links with large offset signals leads to a lower SFR and a higher SLT. An improved car-following model, IDM+ was created by incorporating the above-mentioned downstream parameters into an existing car-following model, IDM. Parameters in this model were calibrated by using the Generic Algorithm. On the basis of a micro-simulation platform (a one-lane road with two consecutive signalized intersections), the effectiveness and characteristic of the newly proposed car-following model were validated and tested comparing with surveyed SFR and SLT. It has been proved that the IDM+ is able to explain the influenced driving behavior and the result from the designed simulation platform can reproduce the influenced SFR and SLT considering different downstream conditions. Furthermore, based on the simulation platform, relationships between influenced SFR, SLT, and downstream conditions (v_{op}) were further simplified into two piecewise regression models. These two models can not only show the same varying trends from IDM+ but also have a good fit with empirical data. Therefore, they are reliable and will be further applied in the next Chapter.

CHAPTER 4 MODELING DOWNSTREAM IMPACTS ON SIGNALIZED ARTERIALS

Accurately modeling the traffic propagation along signalized arterials has been an important topic of traffic engineering for decades. It is the basis for optimizing signal timings of signalized arterials. Several simulators such as VISSIM, AIMSUM, and TRANSYT are undertaking this job. They work based on different basic traffic models such as CTM, car-following model, and cellar automata. By adding consideration of new influencing factors can improve their estimation accuracies. Downstream influence is one of the important issues that have been neglected for now. ***Chapter 3*** studied the downstream influence of an isolated intersection. The relationship between downstream conditions and the SFR&SLT at the upstream intersection is revealed. In ***Chapter 4***, research will mainly focus on the downstream influence at an arterial level and provide the model basis for solving the relationship between downstream situations and traffic conditions.

There are a lot of existing traffic models that can simulate the interrupted traffic flow along signalized arterials. However, none of them have properly considered the downstream influence over the upstream intersection which has been analyzed in the last chapter. Traffic propagation along signalized arterials considering downstream impacts is a complicated issue and an iterative process. Upstream traffic flows into the downstream link and forms the queue in downstream. However, the size and the duration of the queue in the downstream link will influence the traffic flow from the upstream in turn. Through this work, a reliable model for simulating the traffic on signalized corridors considering influenced SFR and SLT will be built based on the modified CTM. This model will be validated on a Japanese corridor, Hirokoji-tori. Meanwhile, how the downstream influence performs on the signalized corridor will be analyzed by a sensitivity analysis.

4.1 Traffic Model on Signalized Arterials Considering Downstream Impacts

4.1.1 From IDM+ to CTM

This chapter will mainly discuss the downstream influence on signalized arterials. It is a possible way to further built a simulation platform for multiple intersections based on IDM+. Several detailed driving behaviors such as overtaking, cutting in effect need to be considered. These behaviors are beyond the scope of this study, but they are necessary for the car-following model-based simulation platform. Several scenarios need to be designed if these behaviors are properly set. This will make the research deviate from the main study target. Meanwhile, as an extension of this study, signal control optimization considering the current downstream condition will be achieved not only for a single signalized intersection but also for a signalized corridor or network in future studies. At those research stages, applying the car-following model will be a complicated and unwise approach. Accordingly, we resort to solutions of this chapter to meso or macro models. The macro-level models such LWR model are a hydrodynamic model that simply solves the relationship between flow, density, and speed. It cannot integrate well with the SFR and SLT models. Therefore, the final answer exists in meso level model.

Cellar automata (CA) and the cell transmission model (CTM) are two main mesoscopic traffic models currently. As a meso-level model, CTM and CA is a connection between macro and micro traffic models. They can not only reproduce the detailed micro phenomena such as lane group blockage or queue storage but also reflect the kinematic theory which can be addressed by macro-level models. In a CA, space and time are divided into discrete cells and steps. Each cell is either empty or contains a single car. A car has a discrete speed. The model structure of CA is not appropriate for combining with models of SFR and SLT. In a CTM, space and time are divided into discrete cells and steps. Each cell defines a certain length of the road section and the boundary flux between cell are determined in CTM. The boundary flux is a good entry point for models' combination. In CTM, overtaking and cutting in effect can be explained or covered by the fundamental diagram. CTM balances the accuracy degree and computational complexity very well.

As early as the end of the last century, Daganzo (1994) proposed the basic Cell

Transmission Model (CTM), to solve the kinematic wave equation on homogeneous highway sections. In the same year, he also proposed a generalized CTM theory for complex urban networks. The generalized CTM is flexible for modeling urban traffic and optimizing signal arrangements. For example, Lo (2001) modeled traffic propagations on urban arterials in Hongkong based on generalized CTM. Based on this work, the optimal signal timing plan is solved by GA. A lot of secondary extensions and modifications have been developed for CTM in order to make the theory more applicable to urban traffic. For example, some researchers contributed to improving CTM in the field of simulating detailed traffic maneuvers. Liu (2008) proposed an improved procedure based on CTM to simulate detailed platoon accumulations and dissipations at different lane-group types in a detailed way by CTM. By this model, even some detailed phenomena can be reproduced such as through vehicles may be blocked by queued left-turn vehicles at shared-left turn lanes. Recently, some researchers made some modification on the CTM basic theory, in order to correct the drawbacks of CTM in simulating micro driving behaviors. For instance, traditional CTM cannot reproduce discharge processes at intersections. Srivastava et al. (2015) modified the sending function so that CTM can capture realistic platoon discharge features (SFR and SLT).

As can be seen from the above researches, CTM is an extremely flexible model. Extension researches made it can be well applied in different situations, no matter for highways or urban roads. Therefore, for modeling the SFR and SLT influenced by micro parameters along corridors, the modified CTM should be the best option and selected for this research. In this section, the basic and generalized equations of CTM and modified CTM are referred firstly. Based on these pieces of knowledge, the way how the modified CTM is improved is introduced as well. At last, the effect equivalence of CTM and micro model (IDM+) based simulation is further proved.

4.1.2 Basic CTM and Generalized CTM

CTM (Daganzo, 1994) is a discretized framework, which has become one of the most popular and accepted tools used for traffic modeling. Originally CTM is designed for solving the LWR model and the basic definition of CTM is applied for long homogeneous freeway sections. In the homogeneous definition, roadway space is discretized into cells with even length L, while time is discretized into time steps (length Δt). Meanwhile, it is required that

each cell has the same traffic capacity. The length of each cell is equal to the distance that a single vehicle travels in one-time step at the free-flow speed. Therefore, when there is no congestion, one expects that a vehicle would move from one cell to another at each time step. Then, CTM predicts macroscopic traffic behavior by evaluating the flow (Φ_j) and density (k_j) at a finite number of intermediate points at different time steps. This is done by defining the sending flow (S_j) and the receiving flow (R_j) of each cell as a function of traffic density and then calculating boundary fluxes according to upstream sending and downstream receiving.

CTM introduces the concept of demand (or sending flow), and supply (or receiving flow) as functions of the densities in each cell. The boundary flux (flowrate across the shared boundary of any two cells) is determined as the minimum of the demand in the upstream cell and supply in the downstream cell. The conceptual framework of the basic CTM is illustrated in Figure 4.1. Figure 4.1 (a) shows the discretization of a link into cells and the computation of boundary fluxes. Figure 4.1 (b) shows the sending and receiving curves which are most commonly used in macroscopic models, corresponding to the triangular fundamental diagram. Formula (4-1)-(4-4) are basic transmission equations of CTM.

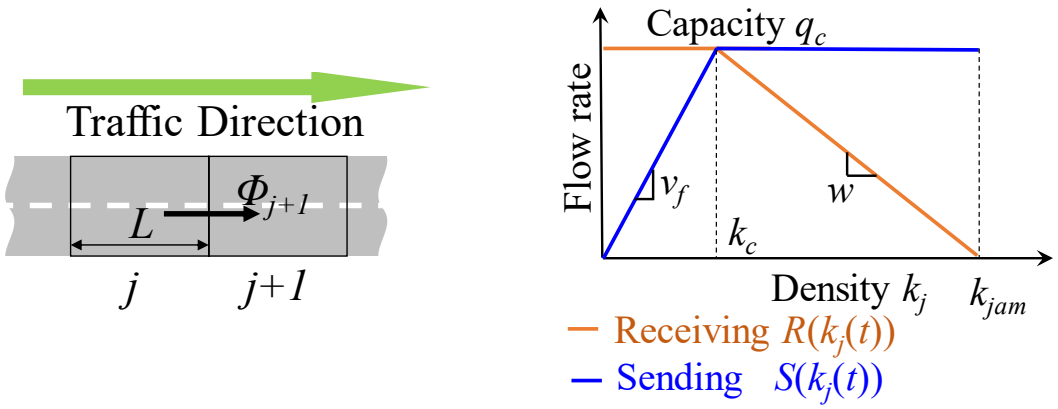

(a) Homogeneous cells and boundary fluxes (b) Sending and receiving curves

Figure 4.1 Conceptual framework of the basic CTM

$$k_j(t+\Delta t)=k_j(t)+\frac{\Delta t}{L}\left(\Phi_j(t)-\Phi_{j+1}(t)\right) \tag{4-1}$$

$$\Phi_j(t)=min\left\{S_{j-1}(t),R_j(t)\right\} \tag{4-2}$$

$$S_j(t)=S\left(k_j(t)\right)=min\left\{v_f k_j(t), q_c\right\} \tag{4-3}$$

$$R_j(t)=R\left(k_j(t)\right)=min\left\{q_c, w\left(k_{jam}-k_j(t)\right)\right\} \tag{4-4}$$

Where j is the cell number, $k_j(t)$ is the density of cell j at time t (veh/m), Δt is the time step, $\Phi_j(t)$ is the flux from cell j-1 to cell j (veh/h), v_f is the free speed (m/s), $S_j(t)$ is the sending value of cell j at time t (veh/h), $R_j(t)$ is the receiving value of cell j at time t (veh/h), $S'_j(t)$ is the modified sending value of cell j at time t (veh/h), q_c is the cell capacity (veh/h), w is the shockwave speed (m/s), k_c is the critical density, respectively, k_{jam} defines the jam density (veh/m).

However, homogeneous settings are not available for all study cases, especially when simulating the urban road network. The generalized CTM (Daganzo, 1995) is an extensive theory of the basic CTM to predict the evolution of traffic flows for complex networks over time under all traffic conditions. The generalized CTM can be logically transformed from basic CTM. It can properly solve the above-mentioned problem, which facilitated the calculation among cells with varying traffic capacities, such as the road section described in Figure 4.2 (a).

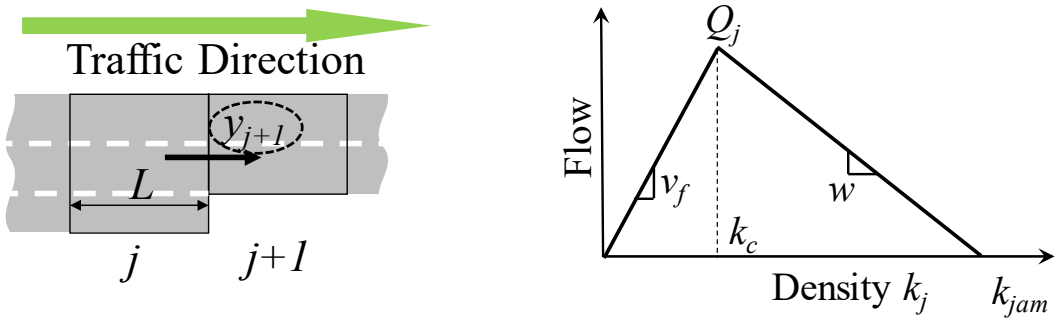

(a) Inhomogeneous cells and fluxes (b) Sending and receiving curves

Figure 4.2 Conceptual framework of the generalized CTM

In the generalized CTM theory, roadway space is also discretized into cells with even length L and time is discretized into time steps (Δt). The generalized CTM predicts macroscopic traffic behavior by evaluating the traverse vehicles (y_j) and vehicle holding number (n_j) at a finite number of intermediate points at different time steps. For achieving this, two constants associated with each cell are defined, they are: (1) N_j is the vehicle holding capacity, which is

the maximum number of vehicles that can be present in cell j at time t. N_j is the product of the cell's length, its jam density, and lane number. (2) Q_j is the capacity of cell j which is the maximum number of vehicles that can flow into cell j when the time step goes from t to $t+\Delta t$. These constants vary with time so that it is able to model transient traffic incidents.

The flow propagation equation can be written as the cell occupancy at time $t+\Delta t$ equals its occupancy at time t plus the inflow and minus the outflow. Meanwhile, the inflow into cell $j+1$ (the outflow of the preceding cell) at time t is governed by the vehicle holding number (n_j) which means the number of vehicles in the upstream cell waiting to enter cell $j+1$, the available space in cell $j+1$ (N_{j+1}-n_{j+1} (t)), the capacity of cell j (Q_j), and hydrodynamic approximation factor which is equal to w/v_f. Formula (4-5)-(4-9) show transmission equations of the generalized CTM.

$$N_j = k_{jam} n_l L \tag{4-5}$$

$$n_j = k_j(t) n_l L \tag{4-6}$$

$$Q_j = q_c / 3600 \tag{4-7}$$

$$y_{j+1}(t) = min\left\{ n_j(t),\ \ Q_{j+1},\ \ w/v_f \left[N_{j+1} - n_{j+1}(t) \right] \right\} \tag{4-8}$$

$$n_{j+1}(t+\Delta t) = n_j(t) + y_j(t) - y_{j+1}(t) \tag{4-9}$$

Where n_l is the number of lanes.

4.1.3 Modified CTM

In 2015, Srivastava et al. (2015) modified and improved the demand function of the basic CTM letting the model be able to reproduce realistic queue discharge features at an intersection for vehicle platoon accelerating far distant from an initial standing queue. The new model can simulate observed parameters of the discharge flow, such as headway, SLT, and SFR. The new demand function is defined through a combination of conventional macroscopic parameters, including critical density (k_c), free-flow speed (v_f), jam density (k_{jam}), and an additional

parameter, projected jam density (k_{jam}^*). The conceptual framework of the modified CTM is shown in Figure 4.3 and formula (4-10)-(4-13) are showing basic transmission equations of the modified CTM.

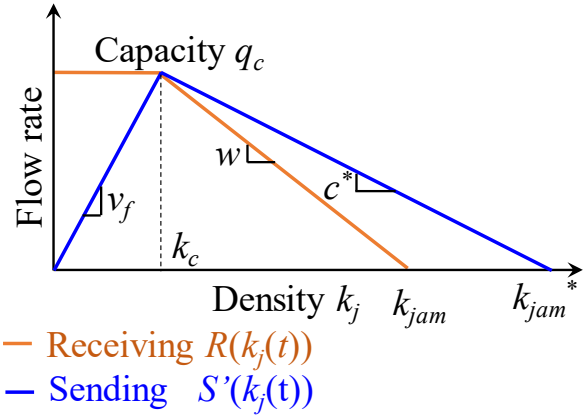

Figure 4.3 Conceptual framework of the modified CTM

$$k_j(t+\Delta t)=k_j(t)+\frac{\Delta t}{L}\left(\Phi_j(t)-\Phi_{j+1}(t)\right) \tag{4-10}$$

$$\Phi_j(t)=min\left\{S'_{j-1}(t),\ \ R_j(t)\right\} \tag{4-11}$$

$$S'_j(t)=S'\left(k_j(t)\right)=min\left\{v_f k_j(t),\ \ c^*\left(k_{jam}^*-k_j(t)\right)\right\} \tag{4-12}$$

$$R_j(t)=R\left(k_j(t)\right)=min\left\{q_c,\ \ w\left(k_{jam}-k_j(t)\right)\right\} \tag{4-13}$$

Where, c^* is the slope of the modified sending curve (m/s), k_{jam}^* is the projected jam density for the modified sending curve (veh/m).

In the modified CTM, discharge features such as SFR and SLT can be derived by parameters (q_c, w, c^*), as shown in Equation (4-14) and (4-15).

$$SFR=q_c \tag{4-14}$$

$$SLT=\frac{Lc^*}{\left(w-c^*\right)w} \tag{4-15}$$

Moreover, what is important but missing in Srivastava's paper of the modified CTM are

derivation formulas from the basic CTM form to the generalized CTM form, which is necessary for this study. According to the relationship between generalized CTM and basic CTM, generalized formulas for the modified CTM are derived. The conceptual framework of the modified CTM in the generalized form is shown in Figure 4.4 and equations are shown in (4-16)-(4-18).

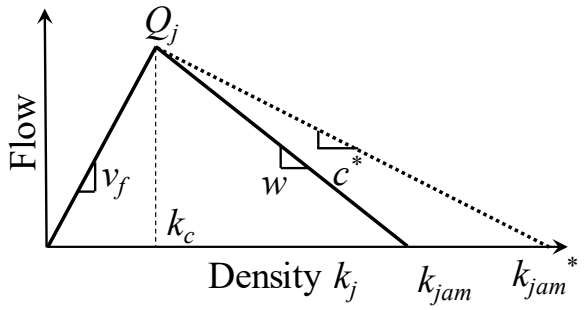

Figure 4.4 Generalized form: a conceptual framework of the modified CTM

$$N_j^* = k_{jam}^* n_l L \tag{4-16}$$

$$y_{j+1}(t) = min\left\{n_j(t),\ \ Q_{j+1},\ \ w/v_f\left[N_{j+1} - n_{j+1}(t)\right],\ \ c^*/v_f\left[N_{j+1}^* - n_{j+1}(t)\right]\right\} \tag{4-17}$$

$$n_{j+1}(t+\Delta t) = n_j(t) + y_j(t) - y_{j+1}(t) \tag{4-18}$$

4.1.4 Combination between Modified CTM and Regression Models

So far, existing CTM models and extension do not consider the impact of downstream conditions over intersection discharge features. In this study, the modified CTM is improved by letting parameters in the model determined by the influenced SFR and SLT (functions by downstream parameters) which are calculated from formula (3-14) and (3-15). Accordingly, parameters (q_c, k_c, w, and c^*) can be calculated by the following Equations (4-19)-(4-22).

$$q_c = Q_j \times 3600 = SFR \tag{4-19}$$

$$k_c = \frac{SFR}{v_f} \tag{4-20}$$

$$w=\frac{v_f SFR}{v_f k_{jam}-SFR} \tag{4-21}$$

$$c^*=\frac{SLT\times w^2}{SLT\times w+L} \tag{4-22}$$

Figure 4.5 (a) and (b) show the original and influenced triangular fundamental diagram. From these figures, the transformation process of influenced cells can be clearly understood. Once the SFR and SLT of one cell are influenced by downstream, values of parameters v_f, k_{jam} (N_j) will keep unchanged firstly. Then, the value of q_c ($3600Q_j$) will be shifted downward until equaling the new value of influenced SFR. The k_c and w are changed according to the influenced SFR by formula (4-20) and (4-21). At last, the value of c^* can be calculated by the formula () with influenced SLT value and newly calculated w.

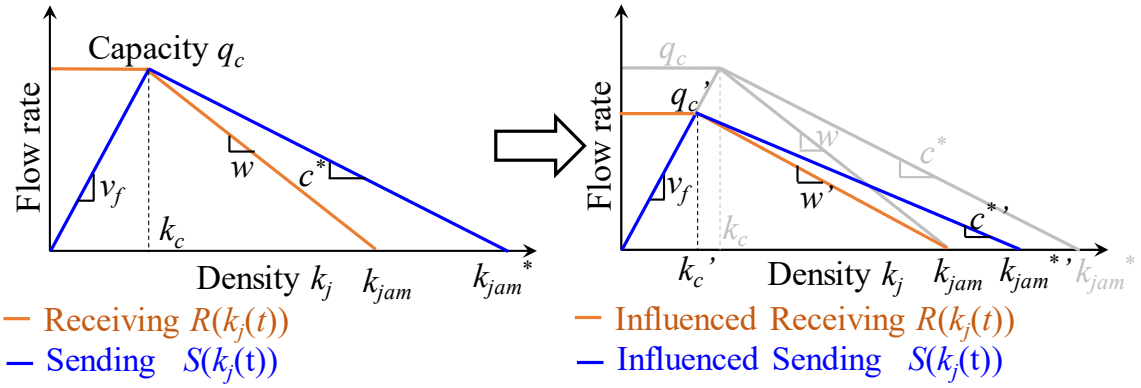

(a) Basic CTM form

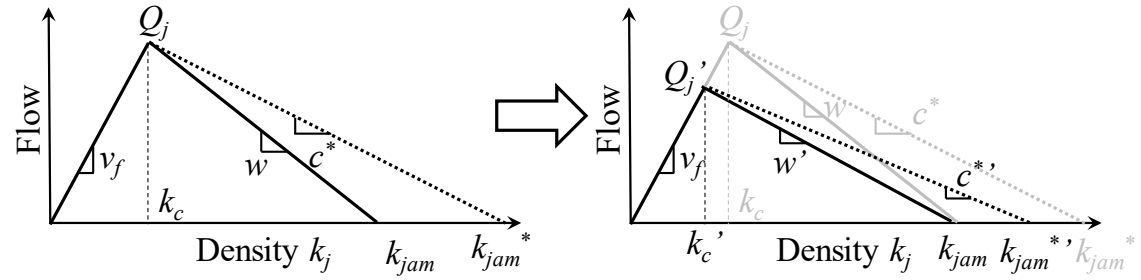

(b) Generalized CTM form

Figure 4.5 Original and influenced triangular fundamental diagrams

4.1.5 Comparison between Proposed CTM and IDM+

To facilitate narration and distinction, transmission cell defined by each CTM theory is

named with abbreviation name including traditional CTM proposed by Daganzo in 1995, modified CTM proposed by Srivastava in 2015, and modified CTM considering downstream influence proposed in this research as shown in Table 4-1. Also, another three types of functional cells are indispensable for the model establishing, as shown in Table 4-2.

Table 4-1 Abbreviation names and features of different CTM theories

Abbreviation	CTM Theory	Discharge Features
Normal cell	Traditional CTM (Daganzo in 1995)	If downstream space and signal allow, traffic flow into the next cell immediately by a constant flow rate.
Modified cell	Modified CTM (Srivastava in 2015)	The cell can reproduce realistic discharge features. The SLT and SFR are both constant values.
Influenced cell	Modified CTM with downstream impacts (Proposed CTM)	The cell can reproduce real discharge features. Also, the SLT and SFR of each cycle will be changed according to the downstream traffic conditions. Before the green time of each cycle, a new set of parameters based on the influenced SLT and SFR will be assigned to the influenced cell until the green light ends.

Table 4-2 Abbreviation names and functions of different functional cells

Abbreviation	Functions
Source cell	The cell with infinite capacity does not stand for any real distance and can always output traffic flow into the next cell with a certain flow rate.
Ending cell	The cell with infinite capacity does not stand for any real distance and can always absorb traffic flow from the previous cell.
Signal cell	The cell does not stand for any real distance and implements the rule of signal timing. It releases the traffic flow from certain movements at a given time interval.

Before further conducting any experiment by using various CTM definitions, comparing the simulation performance between the CTM and IDM+ based platform for the discharge process is quite necessary. By the technique introduced above, a similar simulation platform as ***Chapter 3.3.1*** is built as shown in Figure 4.6. For both two platforms, the downstream intersection is assumed not to be influenced by the secondary downstream intersection.

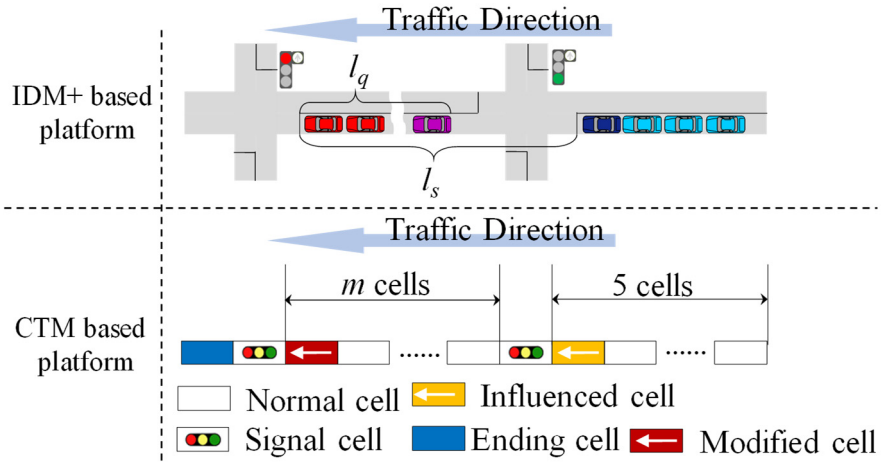

Figure 4.6 IDM+ and CTM based simulation platforms

For comparison, two scenarios that are the same as ones mentioned in ***Chapter 3.3.1*** are assumed. The first scenario has 200m downstream segment length (l_s) with 200m while the downstream length of the other scenario is 300m. For both two scenarios the offset increases from -5s to 5s. Queue length l_q increases from 0m to 200m in the first scenario (l_s=200) and from 0m to 300m in the second scenario (l_s=300m). For the IDM+ based platform, through placing a varying number of queueing vehicles in the downstream link, queues with different lengths can be generated. Meanwhile, parameters of the car-following model are set the same as ***Chapter 3***. The passing time of each vehicle at the upstream stop line is recorded.

The parameter m in this platform determines the downstream segment length (l_s), occupancies of cells define the downstream queue (l_q) (detailed l_q measurement method in the CTM platform is introduced in ***Chapter 4.2.3***). By giving different values to m, cell occupancies in downstream links, and phase settings in two signal cells, different cases can be generated for the CTM based platform. While regarding CTM parameters of this simulation, each transmission cell is defined based on the surveyed data from the Yasukuni-Dori. The time interval for each calculation step is determined to be 1s. The k_{jam} is 137 veh/km/ln and the v_f is 58.5km/h. Accordingly, the cell length of each transmission cell is 16.063m. For normal cells, q_c is equal to the base SFR value (1691veh/h/ln). For modified and influenced cells, the q_c, w, and c^* are calculated on the base SLT value (2.5153s) and the base SFR value. In addition, parameters (q_c, w, and c^*) of influenced cells are governed by functions of influenced SFR and SLT. Same as the IDM+ based platform, only one discharge process of the upstream intersection is simulated for one simulation round. Before the upstream green indication, 5 cells

in the upstream link are fully occupied which is equivalent to the setting of enough queued vehicles in the IDM+ based platform. Therefore, the upstream queue length is long enough for the platoon to reach saturated conditions in one simulation. In addition, for results from both the IDM+ and the CTM based platform, cycles in which spillback phenomena happen during the simulation will be excluded.

Figure 4.7 (a) and (b) show comparison results of SFR and SLT from these two platforms. For SFRs, the value of R^2 is 0.9973, the mean absolute percentage error is 0.51% (0~2.73%), and the root mean square error is 10.59. For SLTs, the value of R^2 is 0.9923, the mean absolute percentage error is 1.53% (0~6.31%), and the root mean square error is 0.07. The above-mentioned statistic measurements prove that simulation results from CTM based platform fit data points from IDM+ based platform very well. It further indicates that when simulating signalized arterials, the CTM and IDM+ based platforms have equivalent functions of reproducing downstream influence. The CTM based platform can be completely replaced by the IDM+ based platform.

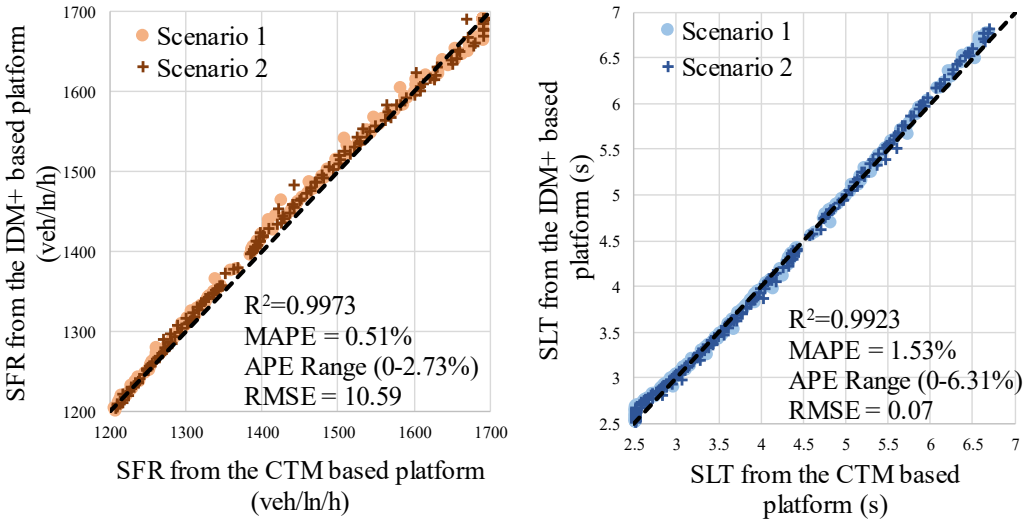

(a) SFR (b) SLT

Figure 4.7 Comparison between these IDM+ and CTM based platforms

4.2 Simulation Test on a Real-world Arterial

4.2.1 Sites Selection, Data Collection, and Data Processing

For testing the improved CTM definition on the real-world road and analyzing the accumulative effect of downstream impacts, the Hirokoji-tori is chosen to be the testbed to achieve objectives. Especially during peak hours along this arterial, it has been observed that heavy congestions happened after the intersection whose capacity is higher than input volume while the platoon at the downstream intersection can be freely discharged without any congestion. Whereas, it should be attributed to interaction effects between multiple consecutive intersections. Figure 4.8 shows the plane figure of the observed target, Hirokoji-tori. Five intersections (a) Motoyama-mae intersection (b) Motoyama intersection (c) Suemoridori-4 intersection (d) Suemoridori-3 intersection (e) Suemoridori-2 intersection on this road are closely spaced. These five intersections located on a street with a length of 831m. The longest segment between two intersections is 237m and the shortest segment is 154m. 9 observed approaches are located on these five intersections. They are the westbound (WB, hereinafter) approach of Motoyama-mae intersection, WB and eastbound (EB, hereinafter) approaches of Motoyama intersection, WB and EB approaches of Suemoridori-4 Intersection, WB and EB approaches of Suemoridori-3 intersection, WB and EB approaches of Suemoridori-2 intersection. Lane group arrangement of each approach is shown in the plane figure as well. Cycle lengths of these five intersections are all 160s with fixed offset settings. Figure 4.9 shows phase plans and offset settings of these five intersections.

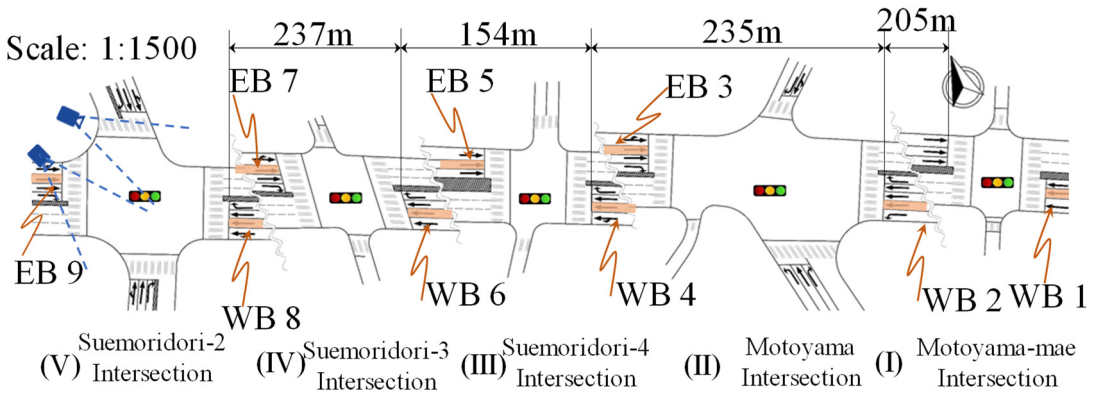

Figure 4.8 Plane figure of Hirokoji road

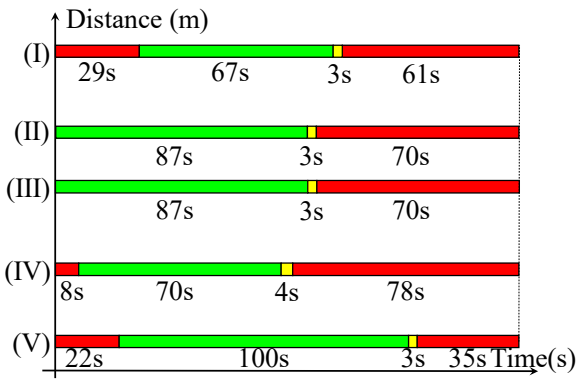

Figure 4.9 Phase settings of intersections on Hirokoji road

A video survey was conducted on Monday, May 8, 2017. 5 video recorders were placed on the roof of the building of Aichi Gakuin University (school of dentistry hospital) which is located at the northwest corner of the Suemoridori-2 intersection. They were respectively observing the Motoyama intersection, Suemoridori-4 intersection, Suemoridori-2 intersection, the road section after Suemoridori-2 intersection, and covering the whole street separately, as shown in Figure 4.10. Therefore, the traffic operating of each approach can be clearly recorded. The survey time starts from 8:00 am to 12:00 am and from 1:00 pm to 6:00 pm covering the off-peak hour and peak hour. At last, a total of 198 cycles were recorded. Only the 2nd (through) lane of each approach was selected for the data extraction, and the data processing method is the same as the method performed for Yasukuni-tori (***Chapter 3.1.3***).

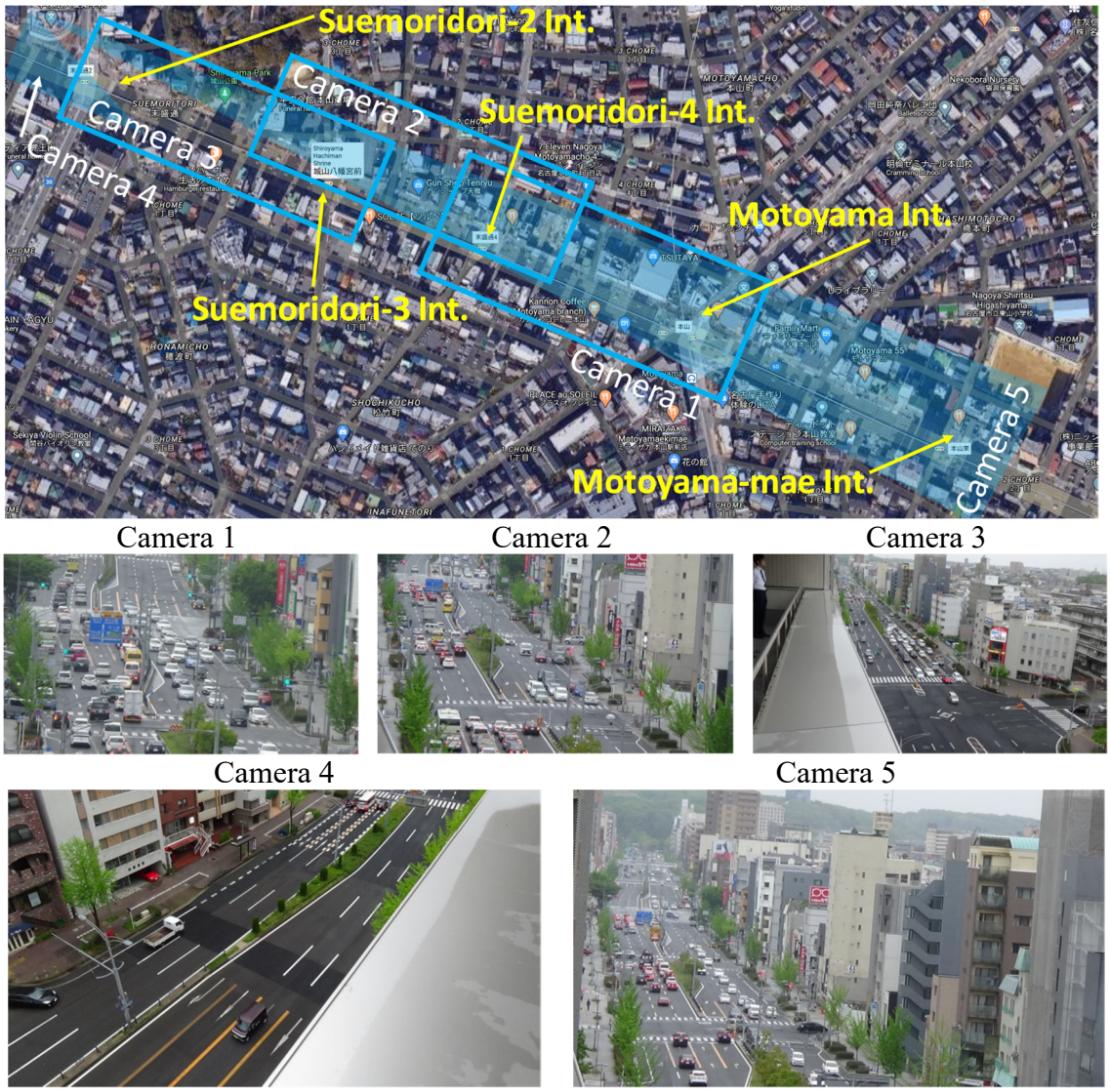

Figure 4.10 Camera positions of the field survey on Hirokoji-tori

4.2.2 Simulation Model for Real-World Arterial

As shown in Figure 4.11, the simulation platform is built for the traffic flow on the section from the stop line of Motoyama-mae EB to the stop line of Suemoridori-2 WB which is the direction of the morning peak flow. Two time periods on this road are chosen to be simulated. The first period is morning peak hour which is from 8:34:20 am to 8:47:40 am (5 signal cycles, 800s). The second period is an off-peak hour which is from 10:34:20 am to 10:47:40 am (5 signal cycles, 800s). During the selected periods, we observed that discharge flows from the WB approach of Suemoridori-2 are freely discharged without any downstream influence. Hence, downstream conditions of Suemoridori-2 intersection are not considered for the simulation. The whole selected section is 880 meters long and it is represented by 54

transmission cells and 27 functional cells (5 signal cells, 11 source cells, 11 ending cells). Each transmission cell is around 16 meters long and some segment lengths cannot be divisible by 16m. Hence, segments simulated by the CTM are not perfectly equal to actual links. There is only a 1m~8m error for each link. Regarding the objective of this simulation test we, believe that these errors will not have fatal effects on experimental results and they can be neglected.

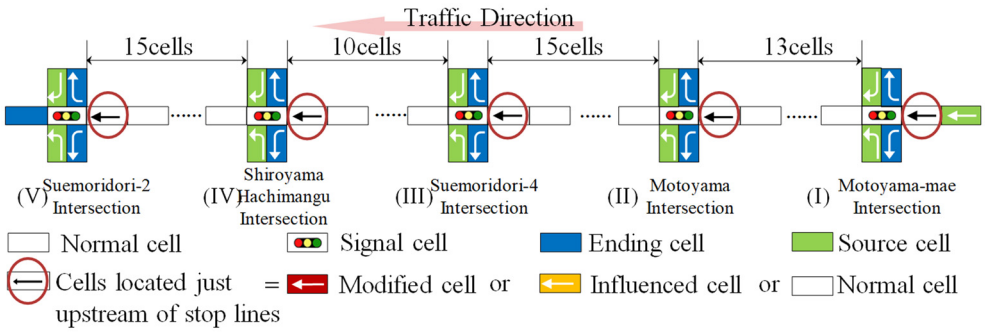

Figure 4.11 Structure of the CTM based simulation platform

Firstly, for determining parameters of cells, the same process introduced in ***Chapter 3*** is implemented for the Hirokoji-tori as well. Models for the influenced SLT and SFR have been generated as shown in Equations (4-23) and (4-24). The final results of SFR and SLT model regression are shown in Figure 4.12 (a) and (b). The time interval for each calculation step is determined to be 1s. The k_{jam} is 137 veh/km/ln and the v_f is 57.6km/h. Accordingly, the cell length of each transmission cell is 16.063m. For normal cells, q_c is equal to the base SFR value (1631 veh/h/ln). For modified and influenced cells, the q_c, w, and c^* are calculated with the base SLT value (2.9513s) and the base SFR value. In addition, parameters (q_c, w, and c^*) of influenced cells are governed by functions of influenced SFR and SLT.

$$SFR = min\left(47.224 \times v_{op} + 972.93,\ \ 1631\right) \tag{4-23}$$

$$SLT = max\left(17.99 \times \left(v_{op}\right)^{-0.75},\ \ 2.9513\right) \tag{4-24}$$

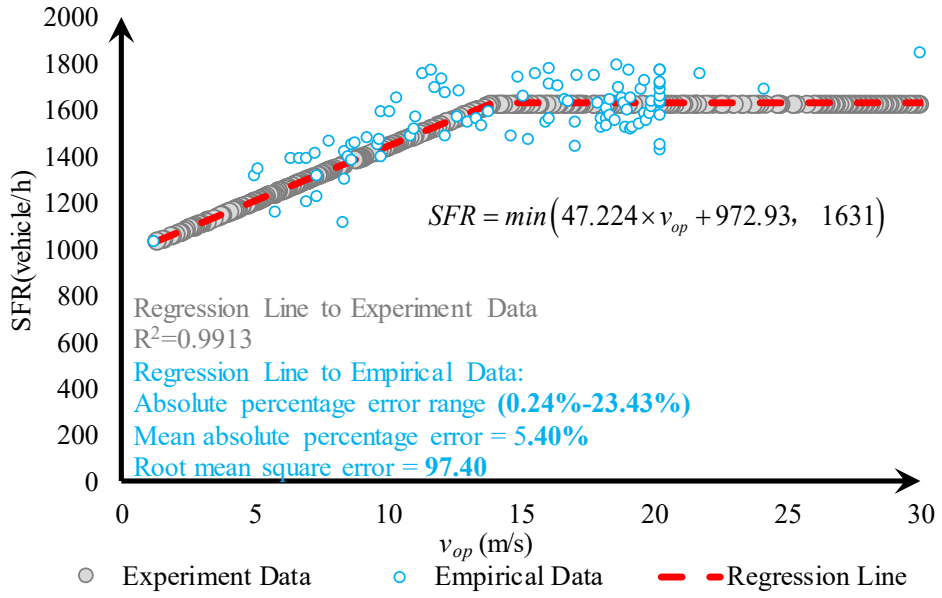

(a) SFR

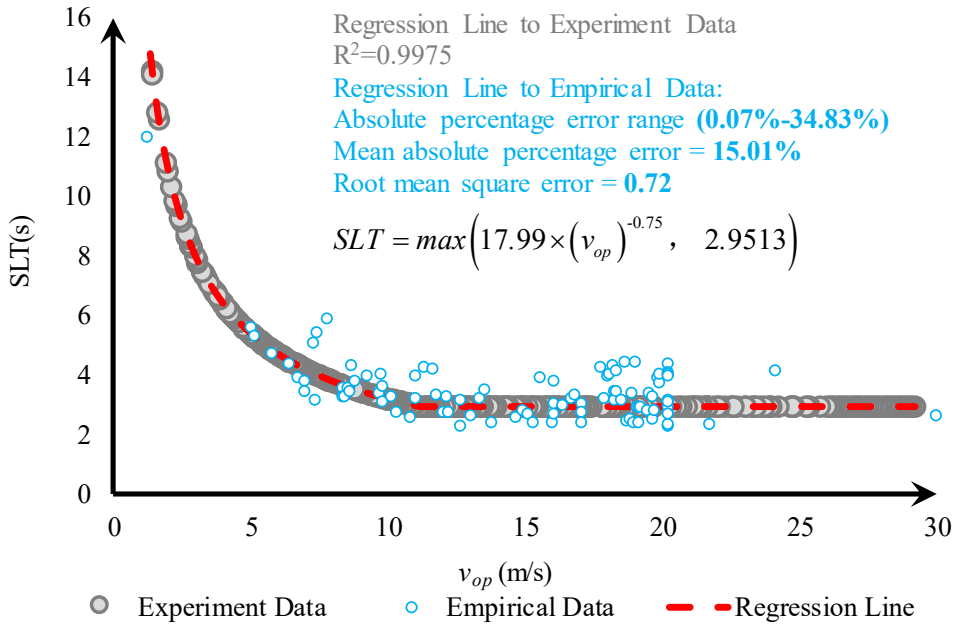

(b) SLT

Figure 4.12 Models of influenced SFR and SLT in Hirokoji-tori

In Figure 4.11, cells in red circles represent the cells that are located just upstream of stop lines. These cells define discharge features of corresponding intersections. In three simulation models (Model 1, Model 2, and Model 3), cells in red circles are set as normal cells, modified cells or influenced cells respectively.

(1) Model 1

The cells in red circles are normal cells (Daganzo, 1994 and 1995). As the signal turns green, if downstream space allows, the queued platoon discharge into downstream instantly in a constant flow rate (1631 veh/h in this study) without going through the start-up lost time.

(2) Model 2

The cells in red circles are modified cells (Srivastava, 2015). After signals turn green, discharge flow from these cells goes through the period of SLT firstly and during this time the flow rate gradually increased to the SFR. The SLT and SFR are both constant values, which are 1631veh/h and 2.9513s in this study.

(3) Model 3

The cells in red circles are influenced cells (proposed CTM in this research). Firstly, real discharge features (SFR and SLT) at signalized intersections can be reproduced. At every cycle, SLT and SFR at each intersection are adjusted regarding current downstream conditions. Before green time, these cells will receive information from the downstream link and calculate the influenced SLT and SFR (Equation (4-24) and (4-24)).

4.2.3 Model Validation

For the above two time periods, the entry flow, exit flow, and initial occupancy of the considered road segment were observed and recorded. Serving as demand profiles and initial occupancies, the above data will be input to simulation models. All 3 simulation models worked for the two selected periods and the density of each cell was recorded at each time step. The simulation result of the off-peak hour period is shown in Figure 4.13. Model 1, 2, and 3 got similar results. In particular, the traffic density distribution on time of model 2 and model 3 are exactly the same. Also, by visual comparison with the observed video, the results of all the three models are consistent with what we observed from the real-world video. It also proves that CTM theory is able to reproduce the traffic propagation and there is no significant difference between 3 models under low flow conditions.

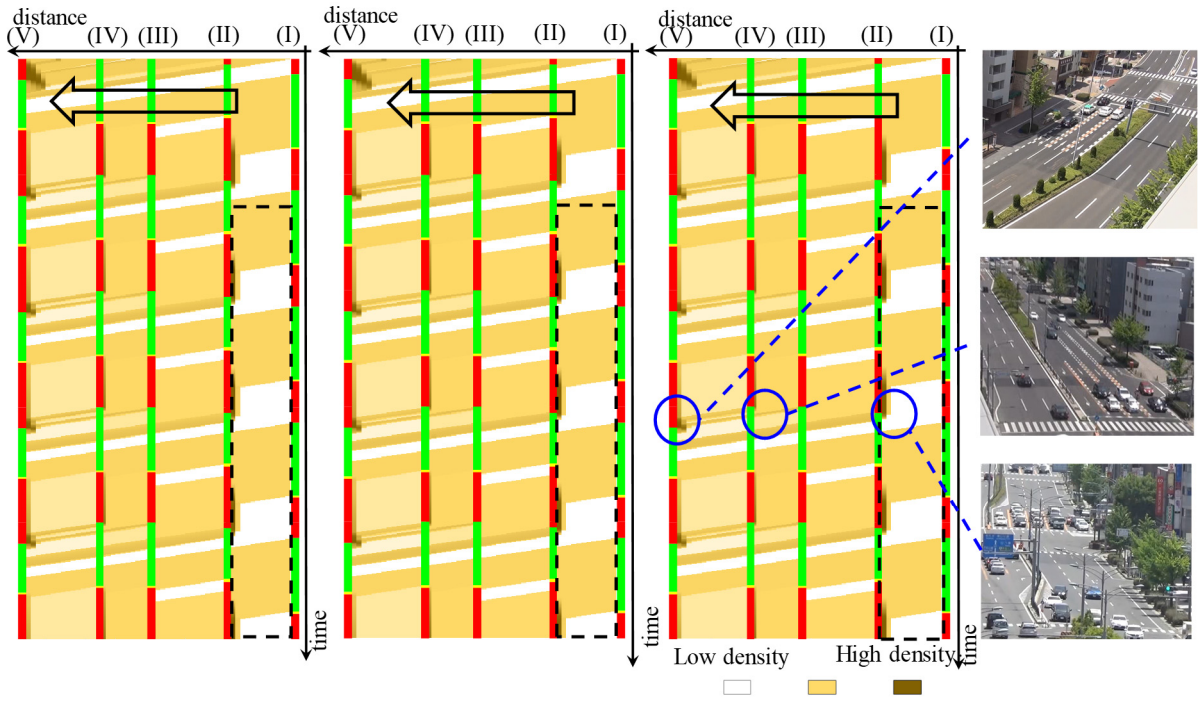

(a) Model 1 (b) Model 2 (c) Model 3 (d) Observed video

Figure 4.13 Simulation results of model 1, 2, 3 and observed video (off-peak time)

Simulation results of three models and screenshots of the observed video during the peak hour period are shown in Figure 4.14. In the result of model 1, the traffic congestion mainly occurs in the middle part of the simulated arterial (sections after intersection (III) and intersection (IV)). At sections after intersections (V), (IV), and (III), queue lengths simulated by model 2 and model 3 show great consistency in changing trends. In the road section that is circled by black dash lines (the section after the intersection (II)), it is observed that the simulated queue only occupied around 50% of this section. However, the platoon simulated by model 3 takes 80% of this section. Meanwhile, based on visual observations, traffic in the video is compared with simulation results and three typical screenshots at intersections (V), (VI), (II) are provided as well in Figure 4.14 (d). Firstly, in the video, short platoons accumulated in the section after intersection (V) and all queued vehicles during one red time can be discharged in one green phase. This finding is the same as the results simulated by all 3 models. Secondly, in the road section after the intersection (IV), no severe congestion is observed and nearly 100% waiting vehicles in one cycle can be discharged during the given green signal. At the time when the queue length is longest in a cycle, around 50% of the section is occupied by queued vehicles. Queue lengths of three models in that section match this observed phenomenon except model 1 whose result is significantly longer than the observation. Thirdly, during all observed cycles,

queue length at the section in the black dash line circle is extremely long. Even in some time, the queue extended to the intersection (I) leading to the occurrence of spillback of upstream. Only model 3 can capture this heavy congestion in this section. Both queue lengths simulated by model 1 (40% occupied) and model 2 (60% occupied) are too short than the actual value. Hence, when simulating traffic propagations on signalized arterials, model 3 (proposed model) has a better ability than model 1 (normal CTM) and model 2 (modified CTM) especially in reproducing traffic space-time distributions and predicting congestion positions. These findings emphasize the importance of considering the downstream influence in urban traffic simulations. They proved our assumption that downstream impacts can be accumulated and amplified towards the upstream direction. This mechanism may lead to traffic jams in upstream sections which are heavier than expected.

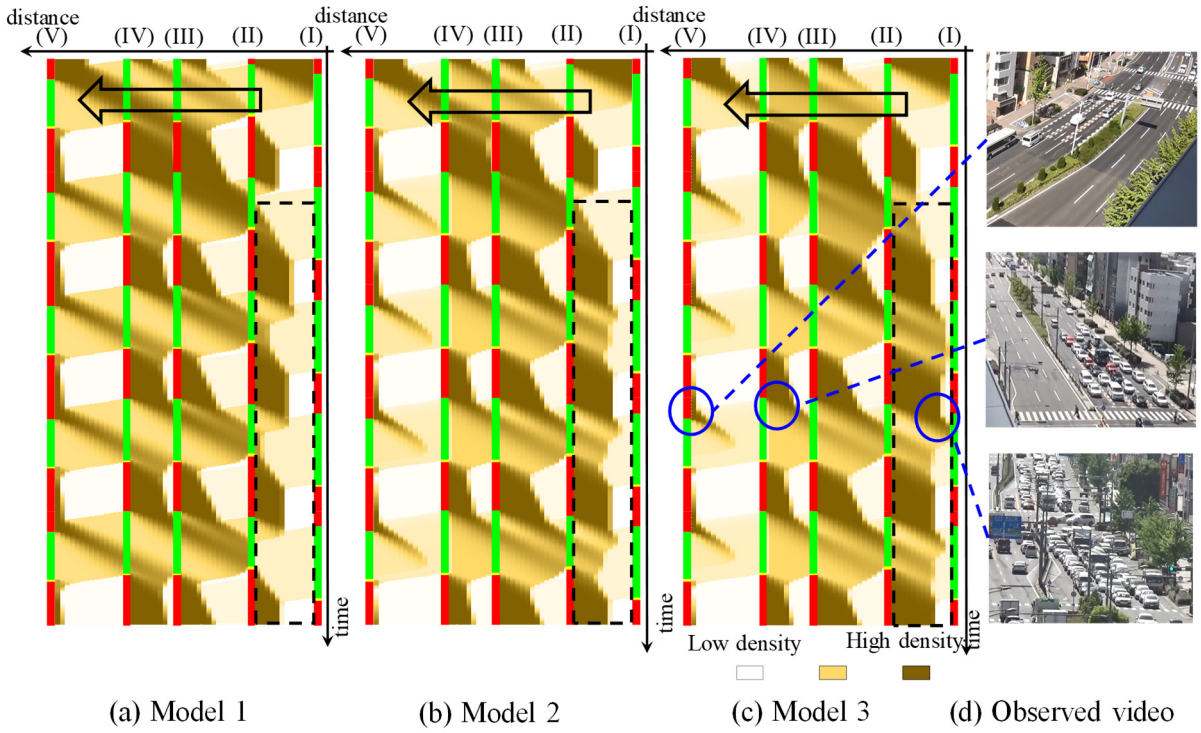

Figure 4.14 Simulation results of model 1, 2, 3 and observed video (peak hour)

For validations, time-based queue lengths (l_q) at all intersections measured from three simulation models are compared with the time-based l_q measured from the real-world video. For the observed video and simulation results, periods for measuring queue lengths are from the onset of the red signal until one platoon is completely discharged. Figure 4.15 shows the measurement method of queue lengths (l_q) for the CTM based simulation and real-world videos. For the observed video, only queues on through lanes are selected and measured. For one

measurement, l_q is equal to the distance from the stop line to the rear bumper of the last queueing vehicle. If there are more than one through lane in the road section, the l_q is equal to the average l_q of all through lanes. Regarding the l_q in CTM simulations, for one measurement, the l_q is equal to the sum distance of two parts. The first part is the distance from the stop line to the endpoint of the last jam density cell. The second part is equal to the length of one cell length multiplied by the occupancy (cell density/jam density) of the cell located just upstream of the last jam density cell. The variation of l_q during the off-peak hour is quite small and it is no sense to compare values of l_q with negligible fluctuations for field data and simulation models. Therefore, only comparison results of queue lengths during the peak-hour period are illustrated as shown in Figure 4.16.

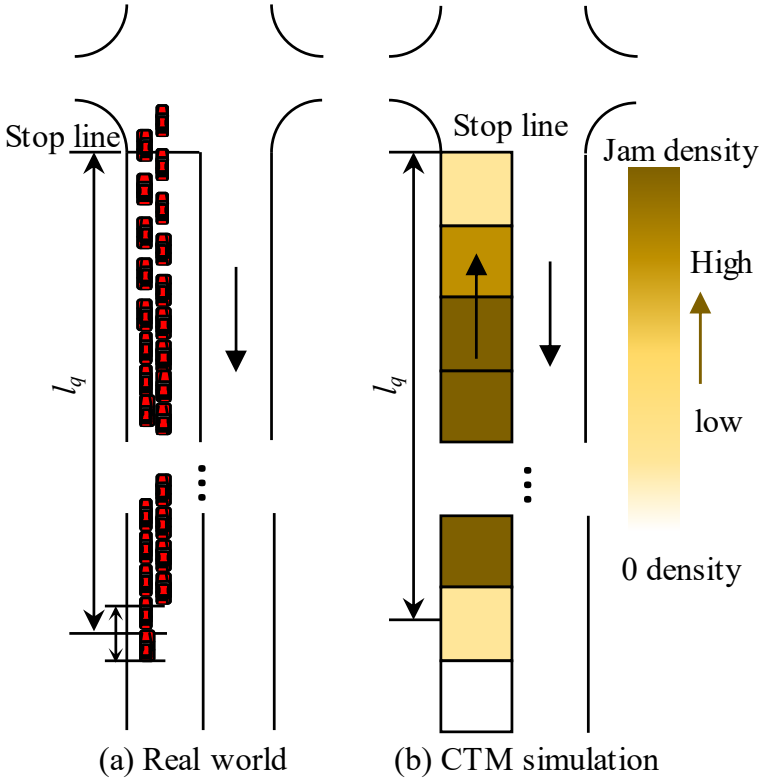

Figure 4.15 Queue length measurement method

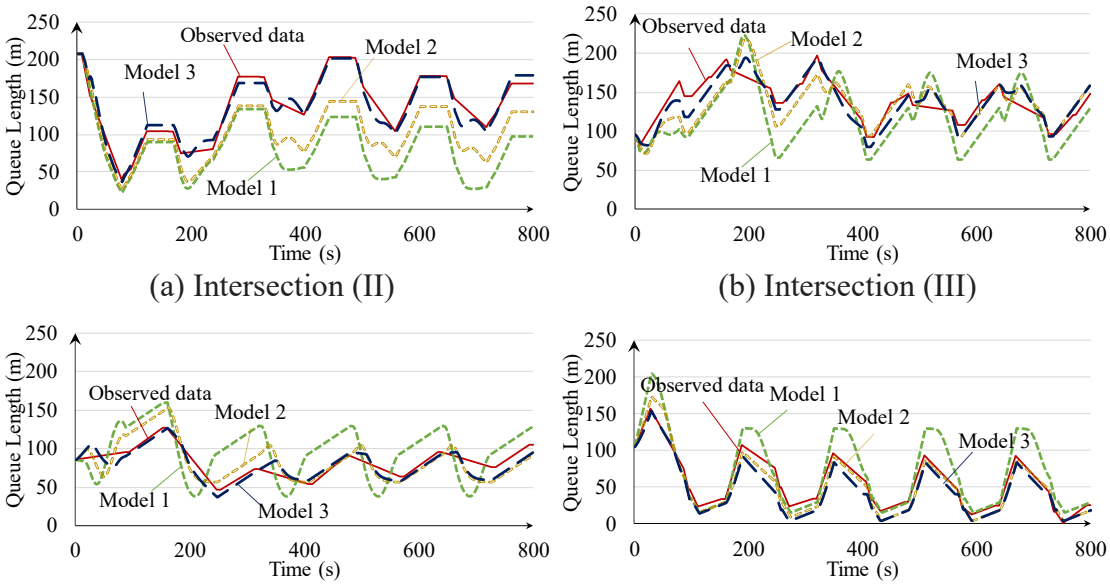

(a) Intersection (II) (b) Intersection (III)

(c) Intersection (IV) (d) Intersection (V)

Figure 4.16 Time-based queue lengths at each intersection

Changing trends of queue length which is simulated by model 1 are completely different from observed trends at four intersections during the selected five cycles. As for queue lengths generated by model 2 and model 3, they are similar to the empirical data at the intersections (III), (IV) and (V), as shown in Figure 4.16 (b), (c), and (d). At the intersection (II), the queue length curve simulated by model 2 is quite different from the observed one as shown in Figure 4.16 (a). Whereas, the queue length curve of model 3 fits the queue length very well no matter for the changing trend or the value magnitude. It can be concluded that the proposed model has a better ability in reproducing queue length distribution and traffic propagation on signalized arterials than model 1 (normal CTM) and model 2 (modified CTM).

Total delay (TD, hereinafter) is measured for the given period and defines the overall running slowly and stopping time of all vehicles when they were passing the road section (s). In further comparison, TDs at four intersections ((II), (III), (IV), and (V)) are measured from the surveyed site and three CTM based simulation models. Calculation methods for empirical data and simulation models are different as follows.

(1) TD of empirical data (TD_{emp})

Total delays of the empirical data are calculated considering the integral difference between time-based arrival flow ($n_{arrived}(t)$) and time-based discharged flow ($n_{discharged}(t)$). Therefore, TD_{emp} equals the cumulative number of arrived vehicles minus the cumulative

number of discharged vehicles as shown in Equations (4-25).

$$TD_{emp}=\sum_{t}\left(\left(n_{arrived}(t)-n_{discharged}(t)\right)\times\Delta t\right) \quad (4\text{-}25)$$

(2) TD of the simulation model (TD_{sim})

In CTM based platform, under low traffic levels, all traffic in one cell should flow into the downstream cell during the next time step theoretically (Lo, 2001). With raisings of cell densities, portions of vehicles must stay in original cells during the next iteration and delays are incurred by this part of traffic for this time interval. Considering this principle, delays of CTM based platform are calculated by following two equations (Equation (4-26) and (4-27)).

$$n_j(t)=k_j(t)\times n_l\times L \quad (4\text{-}26)$$

$$TD_{sim}=\sum_{t}\sum_{j}\left(\left(n_j(t)-\Phi_{j+1}(t)\times\Delta t\right)\times\Delta t\right) \quad (4\text{-}27)$$

Where $n_j(t)$ is the number of vehicles in cell j at time t waiting into cell $j+1$ and n_l defines the number of lanes in one cell.

Results of TDs are compared in Histogram as shown in Figure 4.17. At each intersection, the TD_{sim} of model 1 is obviously different from the TD_{emp}, especially at intersections (V) and (II). Regarding the model 2 and model 3, their TD_{sim} of model 3 at intersections (V), (VI) and (III) are similar to the observed data. At these three intersections, the difference between empirical data and model 3 is almost the same as the difference between empirical data and model 2. At intersection (II), an extremely large error which is 8052s (21.7% of the observed data) between observed data and the result of model 2 can be observed. In contrast, the error between model 3 and empirical data, which is only 1274s, is negligible (3.4% of the actual value). It indicates that model 3 can estimate the delay that occurred on this signalized arterial more accurately than model 1 and model 2. These findings also emphasized that considering downstream impacts is necessary for simulating arterials.

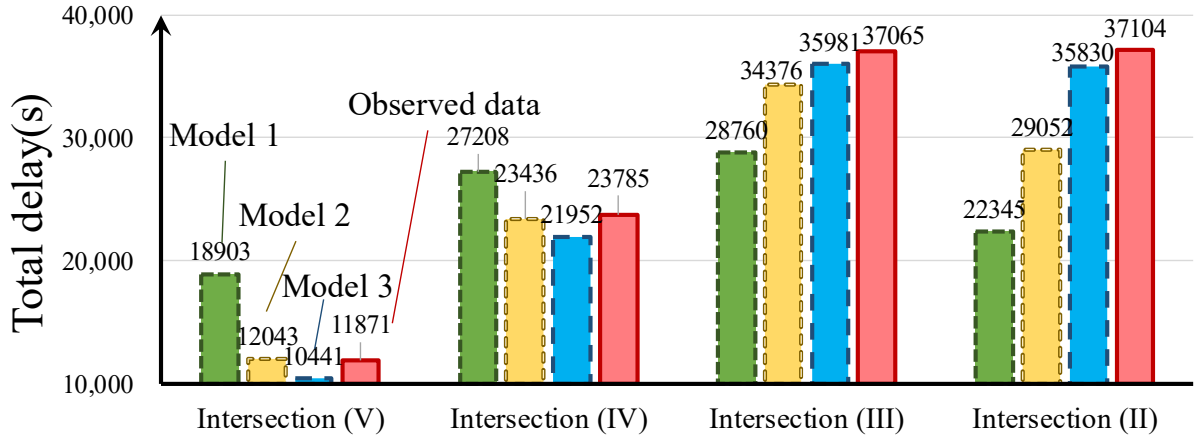

Figure 4.17 TD at each intersection

4.3 Sensitivity Analysis

4.3.1 Hypothesized Arterial and Scenario Settings

As shown in Figure 4.18, a hypothetical signalized arterial with three consecutive signalized intersections is assumed. Traffic in one direction on this road is simulated by using the proposed CTM. Parameter values of cells follow the parameter setting which was applied in model 3 (proposed CTM) of ***Chapter 4.2.2***. Based on this platform, six scenarios are created for sensitivity analysis as shown in Table 4-3. Only segment length, offset values, and input volume will be discussed in this section. For each scenario, values of the cycle length and the green ratio at all intersections are fixed with 160s and 0.6 respectively. For each scenario, offsets of AB (the offset between intersection A and intersection B, offset-AB for short) and offsets of BC (the offset between intersection B and intersection C, offset-BC for short) changes from -30 up to 30s with the same increment of 3s. A total of 2646 cases (441 cases for each scenario) were created finally.

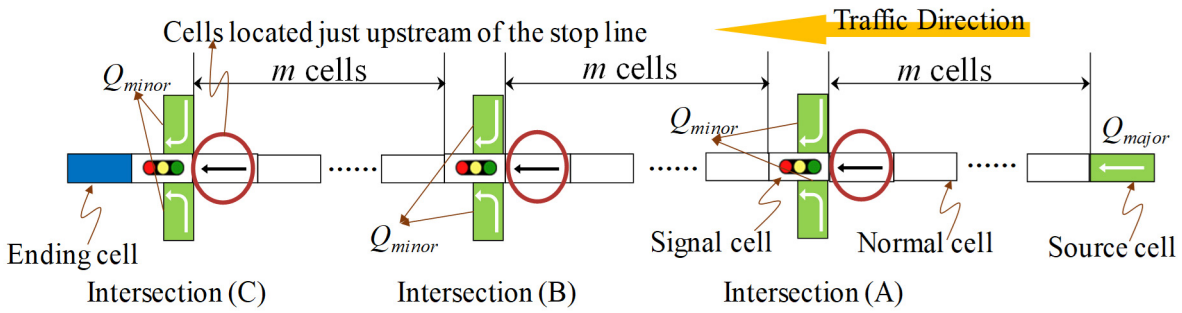

Figure 4.18 The hypothesized arterial

Table 4-3 Scenario settings in sensitivity analysis

No.	*m*	Q_{major} (*veh/h*)	*Total* Q_{minor} (*veh/h*)	Cells in red circles
1	15 (240 m)	900	0	Influenced cell (Proposed model)
2	15	900	0	Modified cell (Srivastava in 2015)
3	15	700	0	Influenced cell
4	15	700	100	Influenced cell
5	15	700	100	Modified cell
6	30 (480 m)	700	100	Influenced cell

In each case, the simulation period contains 3200s warm-up time (20 cycles) at the beginning and then 4000s measuring time (25 cycles). At intersection A, the changing of queue lengths at each cycle is recorded and maximal queue length for each cycle in the measuring period is extracted. In each case, the average value of 25 maximal queue length is calculated and this value is named as Average Maximal Queue Length at intersection A (AMQL-A or AMQL, hereinafter). In this study, AMQL is introduced to evaluate the congestion level in upstream of the assumed arterial (at intersection A). It can be easily inferred that the larger values of AMQL-A are, the greater the congestion in upstream is. The first 3200s warm-up time is set to ensure queue lengths that are measured to be a stable value for the defined case.

4.3.2 Result Analysis

The results of 6 scenarios are listed in Figure 4.19. Firstly, as shown in Figure 4.19 (a), in scenario 1, AMQLs are unchanged in a lower value (150m) in the low offset section (Offset-AB in [-30s, 5s] and Offset-BC in [-30s, 15s]). Then, when the Offset-AB increases from 5s to 30s and the Offset-BC increases from 15s to 30s, AMQL-A rapidly grows to 225m. Also, in

the increasing area, the growth rate of AMQL-A on the Offset-AB axis is faster than it on the Offset-BC axis. These findings indicate that under low negative offset values of two downstream intersections, the upstream intersection may receive less downstream influence. Whereas, large positive offset values of two downstream intersections may result in heavy traffic jams at upstream intersections. Meanwhile, discharge performances are mainly influenced by the offset of the nearest downstream intersection. Secondly, in the comparison between results of scenario 1 (Figure 4.19(a)) and scenario 2 (Figure 4.19(a)), values of AMQL-A of scenario 1 are greater than them of scenario 2, in the interval where Offset-AB belongs to [5s, 30s] and Offset-BC belongs to [-5s, 15s]. After checking the simulation result of each case in this interval, we proved that the difference of queue length is not caused by spillbacks at intersection A but is due to capacity deteriorations that are influenced by negative downstream conditions. This finding provides evidence for the conclusions that without considering downstream impacts existing models may overestimate the intersection capacity and existing simulators (modified CTM) cannot accurately predict congestions on signalized arterial. The same finding can be got by comparing scenario 4 and scenario 5. Thirdly, in Figure 4.19 (c), in the interval where Offset-AB belongs to [-30s, 15s] and Offset-BC belongs to [30s, -15s], values of AMQL-A do not increase any more like them in scenario 1. Also, in scenario 3, AMQLs are lower than them in scenario 1 when Offset-AB belongs to [15s, 30s]. It indicates that congestions in upstream sections can be obviously alleviated by reducing input volumes. Also, it can be concluded that upstream congestion would no longer be sensitive to offset values of the second downstream intersection if traffic inputs are low. Fourthly, in the comparison between scenario 3 and scenario 4 (Figure 4.19 (c) and Figure 4.19 (d)), the growth interval in scenario 4 is wider than scenario 3. Also, the increasing of queue lengths on the Offset-BC axis in scenario 4 is more drastic than it in scenario 3. It reveals that input volumes from minor street play an important role in stimulating the queue growth at the upstream intersection. Finally, the results of scenario 4 and scenario 6 are compared, as shown in Figure 4.19 (d) and Figure 4.19 (f). Scenario 4 and Scenario 6 use the same traffic input profile. However, unlike the result in scenario 4, values of AMQL-A in scenario 6 are invariant under all offset values. This finding emphasizes that long links can mitigate downstream interactions between signalized intersections.

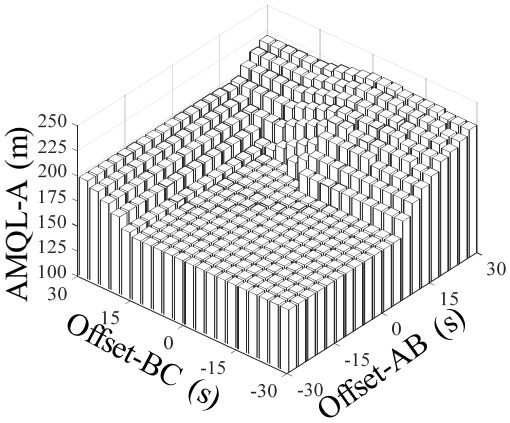

(a) Scenario 1

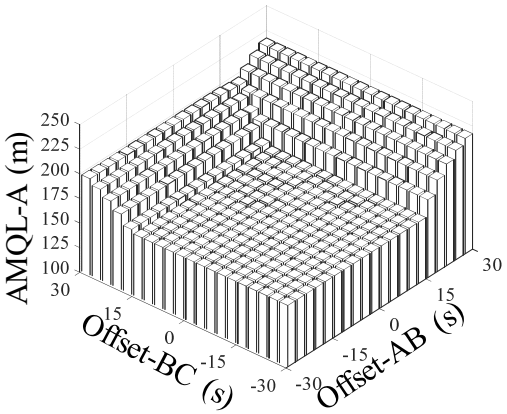

(b) Scenario 2

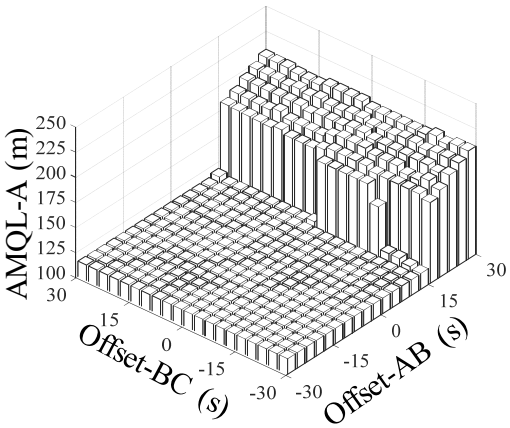

(c) Scenario 3

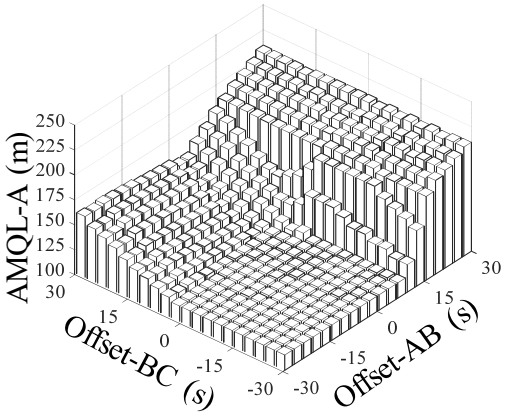

(d) Scenario 4

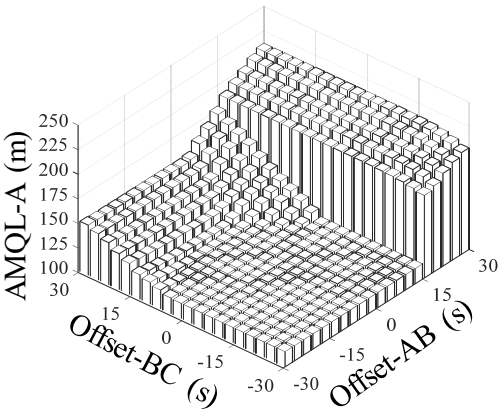

(e) Scenario 5

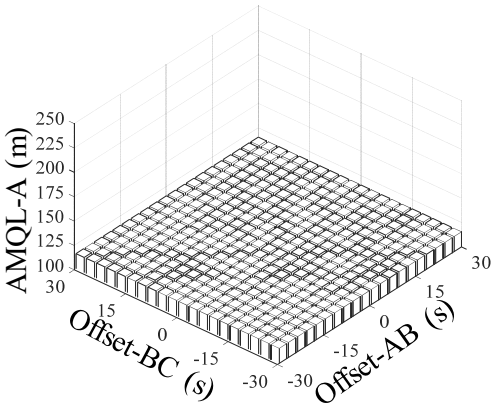

(f) Scenario 6

Figure 4.19 Sensitivity analysis: results of scenarios 1-6

4.4 Summary

The main contribution of this chapter is proposing an improved CTM. Existing CTM theories cannot simulate correctly traffic propagations on arterial. However, by the proposed procedure in this chapter, not only the discharge process at single signalized intersections can be properly reproduced but also congestion positions on signal-controlled arterials can be accurately predicted, which is very important and necessary for urban traffic modeling. Meanwhile, the research process to achieve such contribution is summarized as follows.

Regression models for the influenced SFR and SLT which are proposed in Chapter 3 are introduced to control parameters in the modified CTM. Through a virtual road section, we proved that the improved CTM model and IDM+ based simulation platform can achieve the same effect in generating influenced SFR and SLT. After that, the improved CTM is tested on the Hirokoji-tori during both peak hour and off-peak hour along with the normal CTM and the modified CTM. The proposed CTM was proved to have a better performance than previous CTM models in simulating the traffic propagation along signalized arterials. It reveals that the downstream influence can be accumulated along the upstream direction leading to severe congestion in the upstream intersection. Therefore, considering downstream impacts is an important issue for reproducing the real traffic on signalized arterials. Furthermore, a sensitivity analysis was conducted and it concluded that high traffic demand, high entry flow from the minor streets, short segment links, large positive values of both downstream and secondary downstream intersections' offsets may result in the upstream congestion of signalized corridors.

CHAPTER 5 ADJUSTMENT FACTORS ON SFR AND SLT OF DOWNSTREAM CONDITIONS

As for the model proposed in ***Chapter 3***, the core parameter l_q in Equations (3-14) and (3-15) is an instantaneous parameter that only represents the downstream situation of one signal cycle. However, adjustment factors of SFR and SLT are macroscopic indicators. In existing manuals, adjustment factors for SFR are normally estimated by long-term parameters such as traffic demand, traffic composition, road geometry design, and signal settings. These parameters can be easily got from field surveys which facilitates the model's practical application. Once their values are determined, they need to take effect not simply for a single cycle but for a long period. Until now, there is still a gap before achieving the ultimate goal. This is the reason why this research emphasizes the derivation work from downstream situation parameters to normalized traffic condition parameters.

In this chapter, another simulation experiment will be designed based on the improved CTM proposed in ***Chapter 4***. Several scenarios will be determined for this experiment to generate data that can be further used for the model derivation. The model derivation is divided into two steps and will be performed by regression analysis. The first is to analyze the relationship between queue length and traffic condition parameters (traffic demand, signal settings, and so on). In this step, two regression equations will be created based on two different assumptions and their parameters will be calibrated by GA. The second is to study the relationship between adjustment factors (SFR and SLT) and estimated queue length of the new model. In this step, both two assumed queue length models will be further studied. Then, contour line figures for SFR and SLT adjustment factors for some cases will be provided. Only one estimation model will be selected and suggested by referring to their statistical measurements and logicalities. Finally, a comparison analysis between proposed models, existing manuals, and empirical data will be done to further validate the model and prove the necessity for applying new estimation methods. The total procedure for this Chapter is shown in Figure 5.1.

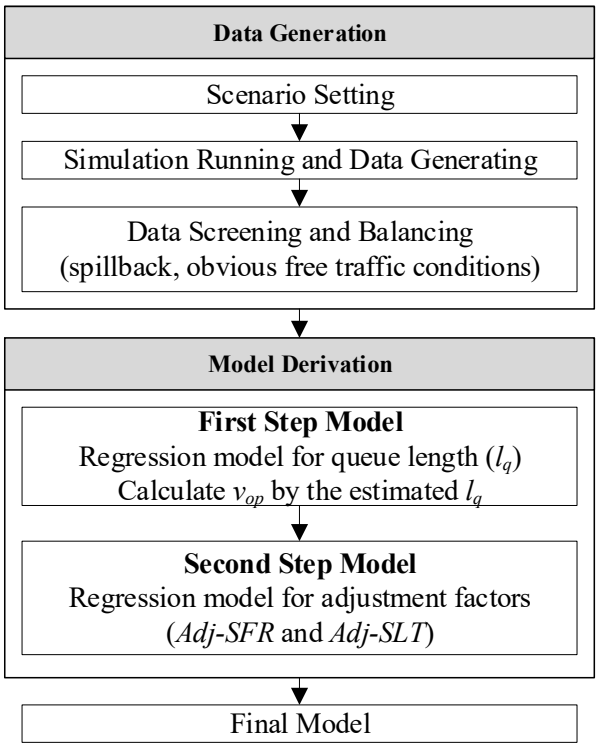

Figure 5.1 The procedure of modeling adjustment factors

5.1 Generating Experiment Data

The experiment is based on another hypothetical road as shown in Figure 5.2. Two signalized intersections connected by two-lane road with variable segment length (l_s). For simplification, the traffic discharged from the downstream intersection is assumed to be free discharge receiving zero impact from its downstream. It also means that the SFR and SLT of the downstream intersection are constant values and equal to base SFR and base SLT values respectively. Also, signals in both upstream and downstream intersections are set to be 2-phase control. For all cases, the amber time is always 3 seconds and the all-red time is 4 seconds. the traffic from the upstream major road is defined as Q_{major}. At the upstream intersection, certain traffic volume from the minor road (Right turn flow Q_{minor_R} and left turn flow Q_{minor_L}) merges into the major street during the given green time of the minor street. However, the traffic on the major will not turn into the minor road in this assumed road system.

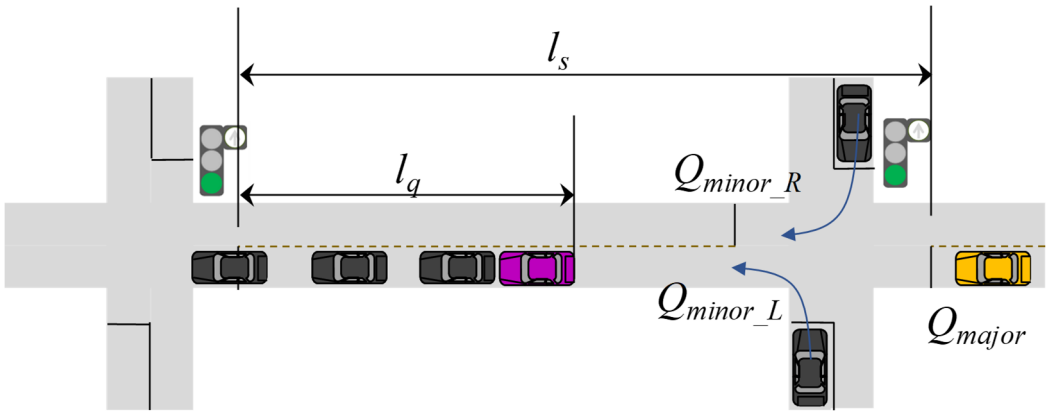

Figure 5.2 Simulation platform for data-generating

The result obtained from this road system can not only be directly applied for roads with a similar traffic arrangement (Figure 5.3 (upper)) but also be used for through lanes of multilane approaches when lane changing rate is very low (Figure 5.3 (lower)). Measurement methods of different input volumes of these two situations are shown in this figure as well.

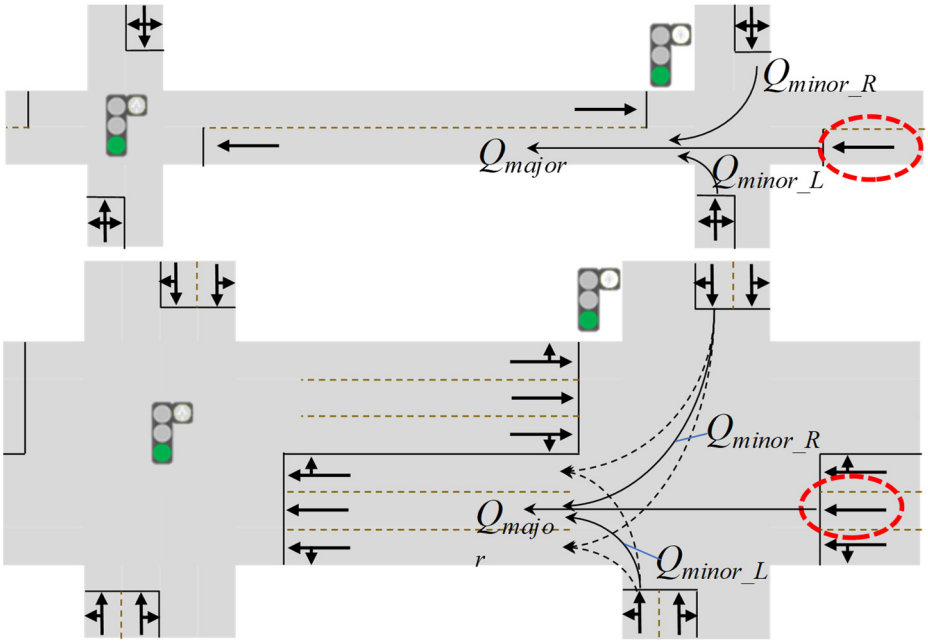

Figure 5.3 Applicable conditions of adjustment factor models

The hypothesized road is converted into a CTM based simulation platform as shown in Figure 5.4. Normal cells, modified cells, and influenced cells are set with the same parameters as those surveyed from Yasukuni-tori (mentioned in ***Chapter 4.1.3***). The traffic demand from major and minor roads is controlled by giving different values to three source cells in the platform. By changing the number of cells between two intersections, scenarios with different segment length (l_s) can be generated. Also, parameters of signalized cells can be adjusted as

well for simulating different phase plan (*Offset,* green ratio (*gr*) cycle length (*C*)). In addition, the ratio between the traffic demand from minor roads (Q_{minor_R}+ Q_{minor_L}) and the traffic demand from the major road (Q_{major}) is defined as r_{minor}.

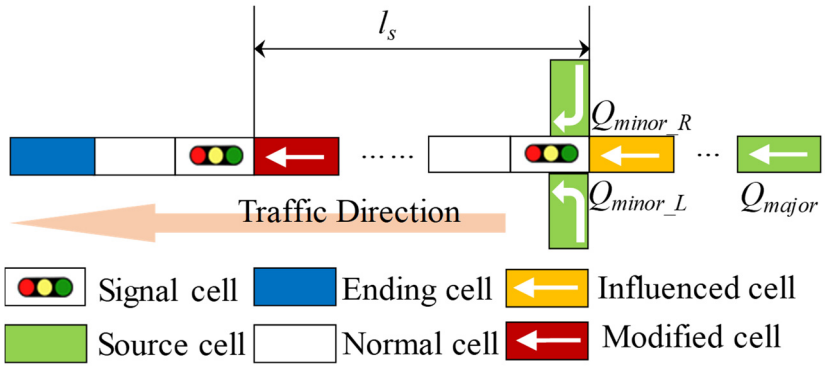

Figure 5.4 CTM based simulation platform for data-generating

By determining values for these parameters (Q_{major}, r_{minor}, l_s, C, *Offset*, *gr*), different scenarios are designed as shown in Table 5-1. In this assumed road system, when the capacity of the downstream intersection is significantly lower than the one of the upstream intersection. In one cycle, vehicles discharged from the upstream intersection cannot totally pass the downstream intersection. After several cycles, the downstream queue will definitely extend to upstream intersection incurring spillback. If the downstream capacity is higher than the upstream capacity, in most cases the whole platoon from upstream can be perfectly handled by the downstream intersection. Then it can be easily inferred that in these situations there is no long queue in the downstream link and the downstream impact is minimal. However, situations that green ratios of upstream and downstream intersections are different are important as well. It is suggested to be studied and solved in future works. Therefore, we only study situations that the green ratio of the downstream intersection equals to the green ratio of the upstream intersection. Accordingly, green ratios of upstream and downstream intersection are set to be the same value (0.4 or 0.6). For making traffic volume lower than the traffic capacity, we let the Q_{major} increase from 50 to 500veh/h/ln with an interval of 50 veh/h/ln. r_{minor} values are 20% or 40%, representing the low and high traffic volume from minor streets respectively. The segment length (l_s) increased from 48 to 320m with an interval of 16m. Cycle length (C) is 120s or 150s and *Offset* values increased from -5s to 5s with an interval of 2s.

Table 5-1 Proposed surrogate safety conflict measures in literature

Parameters	Values					
gr	Both two intersections equal to 0.4 Both two intersections equal to 0.6					
Q_{major} (veh/h/ln)	50~500 (50×10)					
r_{minor}	20%			40%		
l_s (m)	48~320 (16×18)					
C (s)	120			150		
Offset (s)	-5	-3	-1	1	3	5

Finally, a total of 8640 cases are generated and cases are numbered with variable *k*. For each case, the simulation runs for 45 cycles. The first 20 cycles are treated as warm-up time and dropped. Through this time, the traffic on this road system will become stable gradually. For the next 25 cycles, the queue length (l_q) at the onset of the upstream green of each cycle is measured. Then, for case *k*, the influenced SFR and STL for each cycle are calculated based on equation (a) and (b). The average values of SFRs and SLTs for the rest 25 cycles ($\overline{SFR_k}$ and $\overline{SLT_k}$) are calculated. Adjustment factors of SFR and SLT for case *k* (Adj_SFR_k and Adj_SLT_k) are derived by letting $\overline{SFR_k}$ and $\overline{SLT_k}$ be divided by SFR_{base} (1691 veh/h/ln) and SLT_{base} (2.5153s) as shown in Equations (5-1) and (5-2). Meanwhile, the average queue length ($\overline{l_{q\,k}}$) for the remaining 25 cycles is calculated as well, representing the ordinary queue length for case *k*.

$$Adj\_SFR_k = \frac{\overline{SFR_k}}{SFR_{base}} \tag{5-1}$$

$$Adj\_SLT_k = \frac{\overline{SLT_k}}{SLT_{base}} \tag{5-2}$$

Before modeling, all data goes through processes of data screening and balancing. In the data screening, cases in which spillback happened are removed. In the data balancing, some cases in which downstream influence (low traffic volume with large negative *Offset*) are obviously 0 are deleted. The ratio of the number of samples with downstream impacts to the number of samples with 0 downstream impact is reduced to a reasonable value. Therefore, during regression, parameters of models will not be dominated by samples without downstream impact and these samples originally account for a large proportion (more than 90%) of total

samples before the data balancing. Finally, a total of 2114 samples are selected. In addition, several variables in the following paragraph will be used which are listed and explained in Table 5-2 for the convenience of differentiation.

Table 5-2 Explanation of variables in modeling

Variables	Definition	Source	Positions
Q_{major}, r_{minor}, l_s, C, $Offset$, gr	Parameters of Traffic Condition	Scenario settings	Independent variable of the 1st step model
$\overline{l_q}$	Average queue length	Calculated by the data of simulation experiments	The actual value for the 1st step model
$\widehat{l_q}$	Estimated average queue length	Calculated by the 1st step model	The estimated value of the 1st step model
$\widehat{v_{op}}$	Estimated optimal speed	Calculated by $\widehat{l_q}$ with Equation (3-13)	Independent variable of the 2nd step model
Adj_SFR	The adjustment factor for SFR	Calculated by the data of simulation experiments	The actual value for the 2nd step model
Adj_SLT	The adjustment factor for SLT	Calculated by the data of simulation experiments	The actual value for the 2nd step model
$\widehat{Adj\text{-}SFR}$	The estimated adjustment factor for SFR	Calculated by the 2nd step model	The estimated value of the 2nd step model
$\widehat{Adj\text{-}SLT}$	The estimated adjustment factor for SLT	Calculated by the 2nd step model	The estimated value of the 2nd step model

5.2 Modeling the Queue Length (First Step Model)

Estimation of queue length is an important part of studying traffic flow characteristics and developing effective traffic control strategies. Queue length is also a key parameter when calculating the influenced SFR and SLT under different downstream situations. Input-output (I/O) model and shockwave theory are two queue length estimation methods that are widely applied. The I/O model simply calculates the queue length based on the difference between the total input and output traffic volume. The space of the measured section is not considered and it is simplified into a point with 0 lengths in the I/O methodology. The shockwave theory method derives the queue length based on analyzing traffic density changes in the measured

road section. Unlike the I/O method, real features of measured sections and arrival flows are properly considered. Many efforts have been done to reveal the relationship between these two methods. Daganzo (1983) pointed out that these two methods can get the same value if approximation errors of calculations are allowed. Chin (1996) provided a typical example. In his case, he proved that through a certain compensation method differences between these two methods can be reduced to a negligible value. Yi (2008) proposed a baseline factor to explain the discrepancies between these two methods. Compensating by this factor, two methods can reach the same results.

I/O and shockwave analysis are two basic models and can be properly applied to roadway sections. However, even for the simplest case (two consecutive intersections), the queue length on signalized arterials cannot be easily modeled, because several complicated issues are involved. The input and output flow (or traffic waves) are influenced by multiple variables such as cycle length, offset, segment length, traffic flow from minor streets as shown in Figure 5.5. Especially in this study, the input flow and output flow for an intersection should also be governed by downstream situations. Considering the above difficulties, the queue length model will be studied through regression analysis. The queue length (l_q) in this study is the distance measured from the rear bumper of the last queueing vehicle in the downstream link to the downstream stop-line at the onset of the upstream green of each cycle. But in this study, the dependent variable of the queue length estimation model is the average queue length of multiple cycles for one case. The data used for regression are generated from simulation experiments introduced in ***Chapter 5.1***.

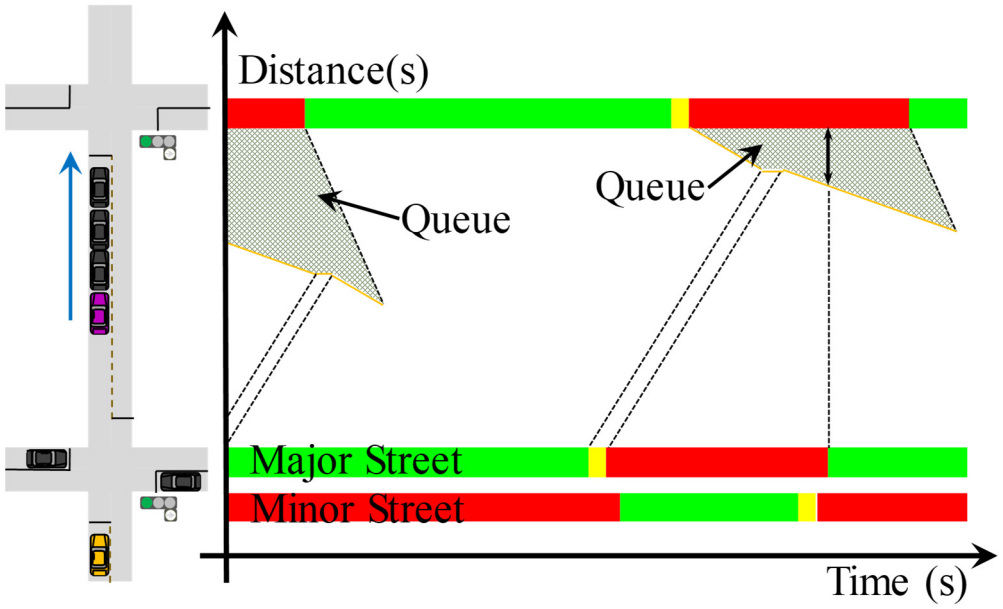

Figure 5.5 An example of queue length estimation by shockwave analysis

5.2.1 Creation of regression models for queue length estimation

In this section, functions will be produced, by which the average queue length can be estimated with variables of Q_{major}, r_{minor}, l_s, C, $Offset$, and gr. At first, some basic functions such as power, linear, logarithmic are tested. However, their regression results are far from acceptable. As discussed before, the estimation of queue length on signalized arterials a complex process s. For overcoming this problem, two special regression equations are created based on two assumptions as shown in Equations (5-3) and (5-4).

Assumption 1: queue length/input volume ratio is a measurable value

$$\hat{l}_q = min\left(CQ_{major}\left(\left(a_0 + a_1 Offset\right)\cdot gr + a_2\left(1-gr\right)r_{minor}\right),\ \ l_s\right) \tag{5-3}$$

Firstly, we considered that in common sense, the higher the input volume is, the longer the queue should be. The first formula is created based on the assumption that the ratio of queue length to volume is a constant value. a_0 and $a_1$are coefficients of the regression model. The queue length at one intersection is mainly dominated by the traffic volume from the upstream intersection which consists of two parts. The first part is the traffic volume from major street and equals to $CQ_{major}gr$. The second part is the traffic volume from minor street and equals to

$CQ_{major}(1-gr)r_{minor}$. On the other hand, we observed that in one cycle vehicles from the minor street will stay in all probability while a large proportion of vehicles from the major street has been discharged from the downstream intersection. In addition, the number of vehicles (from the upstream main street) in the downstream queue was different under different offset conditions. This mechanism may result in different queue length/input volume ratios for the major volume and the minor volume. Accordingly, $a_0 Offset$ and a_1 are introduced to represent this discrepancy. The estimated queue length should always be smaller than l_s. Therefore, the whole equation is nested into a maximal formula letting the result always be less than segment length (l_s). By constraints settings, the value of the whole equation is always limited to be larger than 0.

Assumption 2: linear formula with upper and lower constraints

$$\hat{l}_q = min\left(max\left(\left(b_0 + b_1 Offset + b_2 C + b_3 Q_{major} + b_4 gr + b_5 r_{minor} + b_6 l_s \right),\ 0 \right),\ l_s \right) \qquad (5\text{-}4)$$

As for the second regression formula, b_0, b_1, b_2, b_3, b_4, b_5, and b_6 are coefficients of the model. In this equation, the relationship between the l_q and independent variables are simply assumed to be linear. Through the maximal and minimal equations, its results are limited to space between 0 and l_s.

5.2.2 Solving Coefficients by GA

Math structures for these two equations are too complicated for statistic software such as SPSS, R, and STATA. Therefore, the regression work is transformed into an optimization problem. In this process, optimal variables are coefficients of regression models. The objective is to determine a set of parameters (Equation (5-3): a_0, a_1; Equation (5-4): b_0, b_1, b_2, b_3, b_4, b_5, and b_6) letting estimated values (the $\widehat{l_q}$ calculated by Equation (5-3) or (5-4)) fit actual values (the average queue length $\overline{l_q}$ of each case in the experiment). The optimization is solved by the genetic algorithm (GA function in Matlab (R2017b)) which has been applied in ***Chapter 3.2.3***. As shown in Equation (5-5), the fitness value is defined as the residual sum of squares (*RSS*), which measures the differences between actual values and estimated values. The fitness value is always larger than 0. The smaller the fitness value is, the higher the model's accuracy is.

$$Fitness = \sum_{k} \left(\hat{l}_{q\,k} - \bar{l}_{q\,k} \right)^2 \tag{5-5}$$

Moreover, for applied mathematics and computer science, there may be more than one suspected candidate solution within the available space. These candidate solutions are optimal for their neighboring space. However, only the best one among them is the global optimal solution, other solutions are called local optimal solutions. When applying GA, the solution's searching may fall into a certain limited area and output a local optimal solution. For preventing this happens, multiple attempts for one regression are suggested and it will be achieved by the following procedure.

Firstly, cut the solution space into several intervals by adopting different variables constraints based on the experience. Secondly, perform the GA process for each solution intervals and several solution intervals whose results are in the top 50%. Thirdly, selected solution intervals are further cut into multiple intervals. Return the second procedure again until the overall optimal solution keeps unchanged for more than three rounds.

5.2.3 Regression results and validations

An example of the GA iteration process is shown in Figure 5.6. Also, the final constraint setting and optimal solution for each coefficient and is shown in Table 5-3.

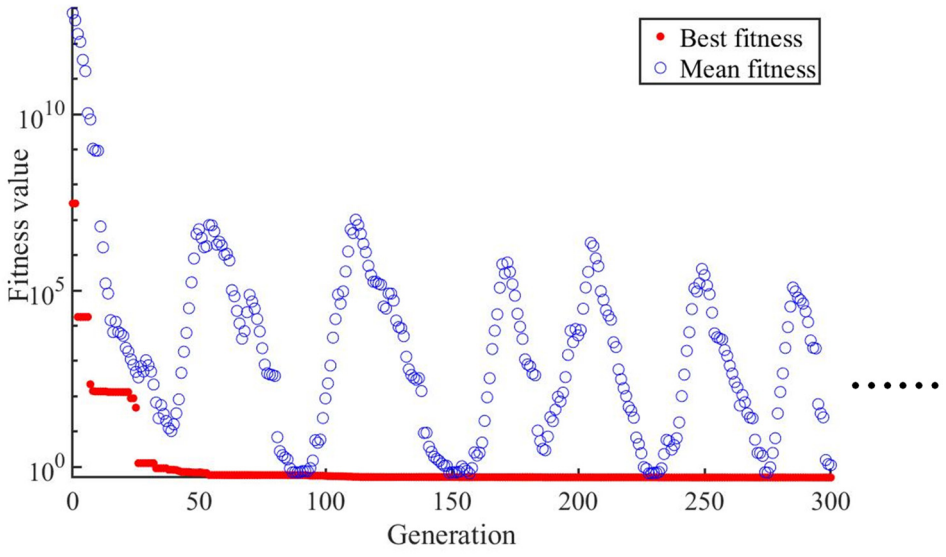

Figure 5.6 GA iteration process

Table 5-3 1st step: final constraint setting and optimal solution for each coefficient

Queue Length Model 1: Assumption 1		
Parameters	**Constraints**	**Values**
a_0	$(0, 5\times10^{-4}]$	2.6497×10^{-5}
a_1	(0, 0.5]	1.3785×10^{-4}
a_2	(0, 0.5]	1.1314×10^{-3}
Queue Length Model 2: Assumption 2		
Parameters	**Constraints**	**Values**
b_0	$(-\infty, 0]$	-10.5202
b_1	(-1, -0.5]	-0.7593
b_2	(0, 0.5]	4.344×10^{-2}
b_3	(0, 0.5]	3.352×10^{-2}
b_4	(-20, -15]	-16.0608
b_5	(15, 20]	19.5764
b_6	(0, 0.5]	8.2549×10^{-2}

Actual vs predicted comparison figures for assumptions 1 and 2 are shown in Figure 5.7 (a) and (b). In the result of assumption 1, the R^2 is 0.5820, the MAPE is 36.96%, and the RMSE is 6.00. When actual values are less than 15m, the regression model shows a good degree of fitness. However, when actual values are larger than 15m, data points are divergent on both sides of the diagonal line. It indicates that the regression model based on assumption 1 can fit the changing trend of the $\overline{l_q}$ and its estimated values can roughly reproduce actual values. For assumption 2, the R^2 is 0.9291, the MAPE is 21.01%, and the RMSE is 2.47. Data points in Figure 1b basically coincide with the diagonal line and the convergent accuracy is obviously high. Only when actual values are larger than 30m, predicted values are a little bit larger (around 5%) than actual values. It reveals that the regression model based on assumption 2 fits actual data very well and its fitting performance is better than the previous one. Finally, we concluded that model 1 is more logical and reasonable while model 2 has better prediction accuracy. Both two models are able to explain the changing trend of $\overline{l_q}$ and will be further applied to the next step derivation.

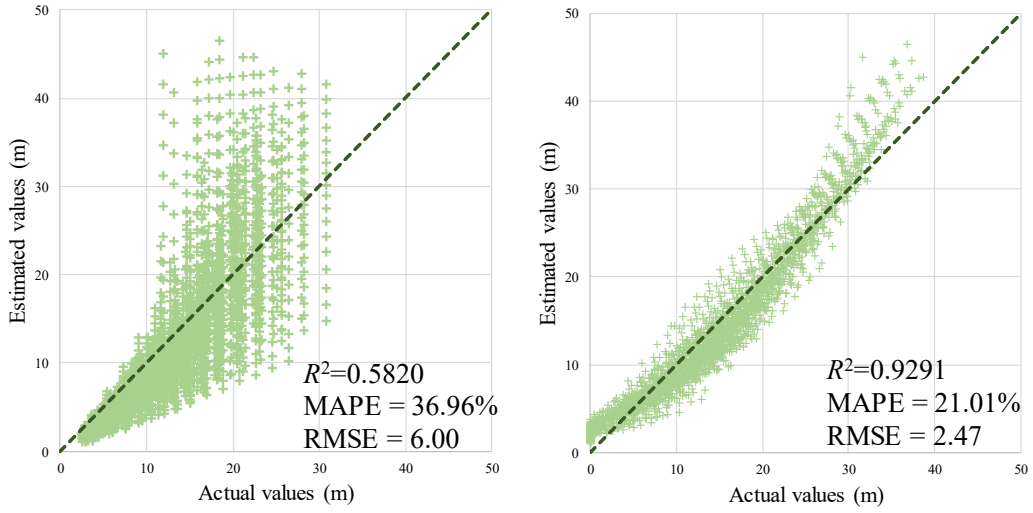

(a) Assumptions 1 (b) Assumptions 2

Figure 5.7 Actual vs predicted comparison for queue length models

5.3 Modeling Adjustment Factors (Second Step Model)

Regression models between *Adj_SFR*, *Adj_SLT,* and predicted queue length will be derived in this section. Combing with the 1st step model, models for adjustment factors will be proposed as well. In ***Chapter 3***, models for influenced SFR and SLT are two-step models. For the convenience of description, these models are also listed as follows (Equation (5-6), (5-7), and (5-8)). Firstly, v_{op} is calculated based on the parameters of downstream situations (l_q, l_s, and *Offset*). Then, influenced SFR and SLT are calculated by v_{op}. Among parameters in this model, l_s, l_q, and *Offset* should be determined by current downstream situations. In practical applications, if conditions permit, values of τ, l, and d_0 should be measured from the field data. Otherwise, they can be defined as default values (τ=1s, l=4.5m, and d_0=2m).

$$v_{op}=\begin{cases} min\left(\dfrac{l_s-l_q}{\tau\dfrac{l_q+d_0}{d_0+l}+offset},\ v_0\right) & \text{if}\quad \tau\dfrac{l_q+d_0}{d_0+l}+offset>0 \\ v_0 & \text{otherwise} \end{cases} \tag{5-6}$$

$$SFR = min\left(44.195 \times v_{op} + 997.93,\ \ 1691\right) \tag{5-7}$$

$$SLT = max\left(18.99 \times \left(v_{op}\right)^{-0.67},\ \ 2.5153\right) \tag{5-8}$$

The above equations are a micro-level model that can only be applied in the microsimulation and dynamic signal control systems. In contrast, the model for adjustment factors proposed in this section will be a macro-level model which can be applied for setting the long-term signal timing. There are similarities between these two models. The calculation procedure and equation structure of this macro-level model is designed referring to the micro-level model. For instance, the macro-level model also needs to calculate the v_{op} firstly before estimating adjustment factors.

5.3.1 Regression Models for Adjustment Factors

The estimated optimal speed ($\widehat{v_{op}}$) is calculated by estimated queue lengths ($\widehat{l_q}$) based on Equation 1. The estimated queue lengths are calculated by queue length model 1 or queue length model 2. Hence, two groups of $\widehat{v_{op}}$ are calculated at last. Parameters of τ, l, and d_0 in the calculating are determined as default values (τ=1s, l=4.5m, and d_0=2m) as shown in Equation (5-9).

$$v_{op} = \begin{cases} min\left(\dfrac{l_s - l_q}{\tau\dfrac{l_q + d_0}{d_0 + l} + offset},\ \ v_0\right) & \text{if} \quad \tau\dfrac{l_q + d_0}{d_0 + l} + offset > 0 \\ v_0 & \text{otherwise} \end{cases} \tag{5-9}$$

Considering structures of Equation (5-7) and (5-8), it is inferred that both regression models for *Adj_SFR* and *Adj_SLT* consist of flat parts (*Adj_SFR*=1 and *Adj_SLT*=1) and influenced parts. The decreasing part of *Adj_SFR* is assumed to be linear and the increasing part of *Adj_SLT* is assumed to be an exponential model. Therefore, regression models for *Adj_SFR* and *Adj_SLT* are created as shown in Equations (5-10) and (5-11).

$$\widehat{Adj\text{-}SFR} = min\left(c_0 \widehat{v_{op}} + c_1,\ \ 1\right) \tag{5-10}$$

$$\widehat{Adj\text{-}SLT} = max\left(c_2 \widehat{v_{op}}^{\,c_3},\ \ 1\right) \tag{5-11}$$

Two sets of coefficients will be solved by inputting two groups of $\widehat{v_{op}}$. Two regression models are named as "Assumption 1" and "Assumption 2" for short which correspond to two assumptions for queue length models in Chapter 5.2.1 respectively. This regression is also transformed into an optimization problem. The optimization target is to determine a set of parameters (c_0, c_1, c_2, and c_3) letting estimated values ($\widehat{Adj\text{-}SFR}$ and $\widehat{Adj\text{-}SLT}$) fit actual values (*Adj_SFR* and *Adj_SLT*). The result of the optimization is shown in Table 5-4 and Figure 5.8.

Table 5-4 2nd step: final constraint setting and optimal solution for each coefficient

Assumption 1		
Parameters	**Constraints**	**Values**
c_0	(0, 1]	2.2281×10^{-2}
c_1	(0, 1]	0.6727
c_2	(0, 10]	4.2741
c_3	(-2, 2]	-0.4812
Assumption 2		
Parameters	**Constraints**	**Values**
c_0	(0, 1]	2.4019×10^{-2}
c_1	(0, 1]	0.6047
c_2	(0, 10]	7.7491
c_3	(-2, 2]	-0.6751

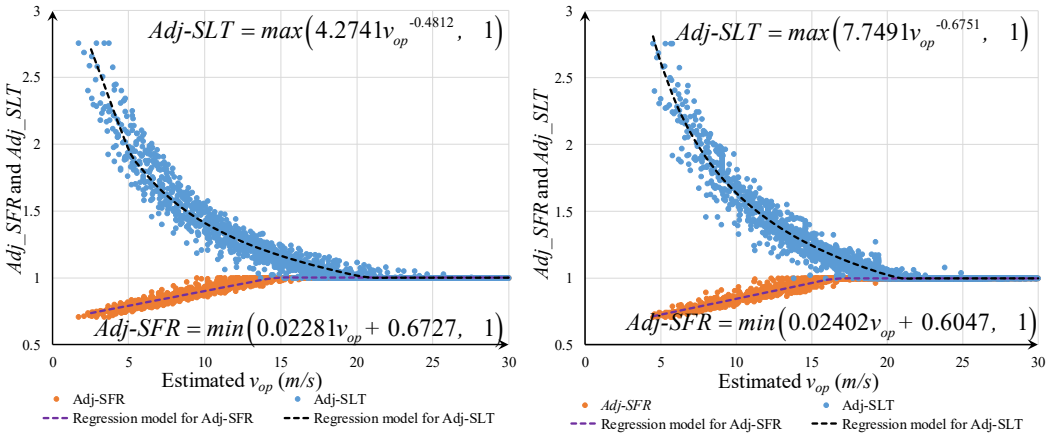

(a) Assumptions 1 (b) Assumptions 2

Figure 5.8 Regression models for *Adj_SFR* and *Adj_SLT*

Actual vs predicted comparison figures for assumptions 1 are shown in Figure 5.9 (a) and (b). In the result of SFR, the R^2 is 0.9503, the MAPE is 0.78% (0~11.11%), and the RMSE is 0.015. Data points evenly distributed on both sides of the diagonal line and the convergence performance is good. In the result of SLT, the R^2 is 0.9476, the MAPE is 2.58% (0~27.76%), and the RMSE is 0.071. Most of the data is concentrated on the diagonal line and only a few points deviate from the centerline.

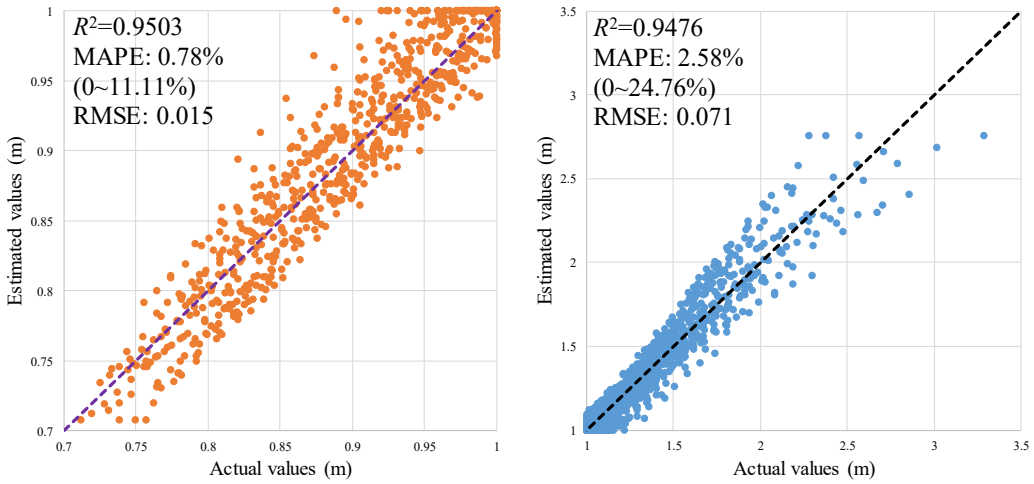

(a) SFR (b) SLT

Figure 5.9 Assumptions 1: actual vs predicted comparison for 2nd step model

As for assumption 2, actual vs predict comparison figures are shown in Figure 5.10 (a) and (b). In the result of SFR, the R^2 is 0.9999, the MAPE is 0.78% (0~11.88%), and the RMSE is 0.015. In the result of SLT, the R^2 is 0.9696, the MAPE is 2.47% (0~31.44%), and the RMSE is 0.066%. In both Figure 5.10 (a) and (b), most data points located on or near the diagonal line. When actual values of SFR are in the interval of between 0.85 and 1, it can be observed that the divergence phenomenon occurs and some data points are significantly off the centerline. This model's fitness performance is slightly better than the previous one. However, the estimation accuracy of the first model is higher than the second one. It indicates that both two models fit the changing trend of actual data and can reproduce their values accurately.

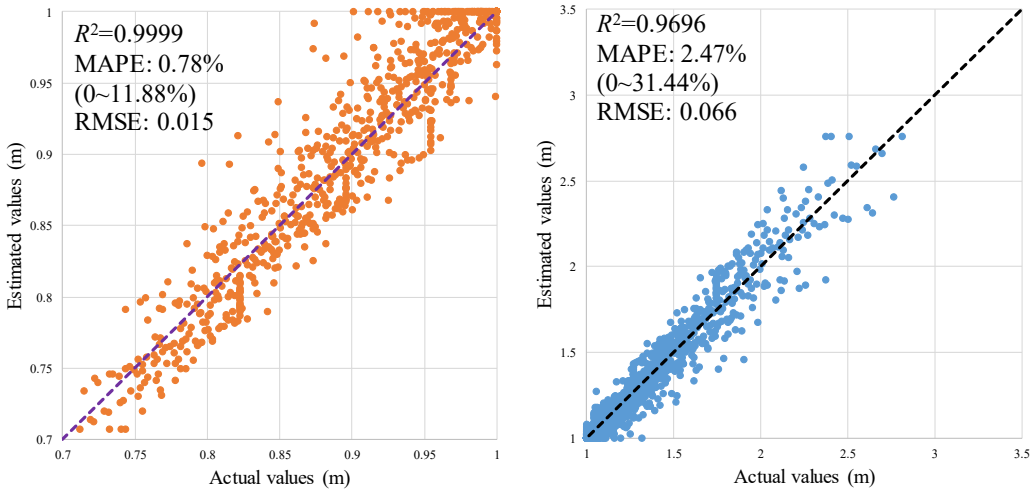

(a) SFR (b) SLT

Figure 5.10 Assumptions 2: actual vs predicted comparison for 2nd step model

5.3.2 Contour Figures for Adjustment Factors

Combining the first step model and the second step model, ultimate models are obtained as shown in Equation (5-12) and (5-13).

Adjustment Factor Model 1 (Assumption 1)

$$\begin{cases} l_q = min\left(CQ_{major}\begin{pmatrix}\left(2.6497\times10^{-5}Offset+1.3785\times10^{-4}\right)g_r \\ +1.1314\times10^{-3}\left(1-g_r\right)r_{minor}\end{pmatrix},\ \ l_s \right) \\ v_{op} = \begin{cases} min\left(\dfrac{l_s - l_q}{\dfrac{l_q+2}{6.5}+offset},\ \ 24.23 \right) & \text{if} \quad \dfrac{l_q+2}{6.5}+offset>0 \\ 24.23 & \text{otherwise} \end{cases} \\ Adj\text{-}SFR = min\left(0.02281v_{op}+0.6727,\ \ 1\right) \\ Adj\text{-}SLT = max\left(4.2741v_{op}^{-0.4812},\ \ 1\right) \end{cases} \tag{5-12}$$

Adjustment Factor Model 2 (Assumption 2)

$$
\begin{cases}
l_q = min\left(max\left(\begin{pmatrix} -10.5202 - 0.7593 Offset + 4.344\times10^{-2} C \\ +3.352\times10^{-2} Q_{major} - 16.0608 g_r \\ +19.5764 r_{minor} + 8.2549\times10^{-2} l_s \end{pmatrix}, \quad 0 \right), \quad l_s \right) \\
v_{op} = \begin{cases} min\left(\dfrac{l_s - l_q}{\dfrac{l_q+2}{6.5} + offset}, \quad 24.23 \right) & \text{if} \quad \dfrac{l_q+2}{6.5} + offset > 0 \\ 24.23 & \text{otherwise} \end{cases} \\
Adj\text{-}SFR = min\left(2.4019\times10^{-2} v_{op} + 0.6047, \quad 1 \right) \\
Adj\text{-}SLT = max\left(7.7491 v_{op}^{\,-0.67511}, \quad 1 \right)
\end{cases}
\tag{5-13}
$$

In order to further compare these two assumptions, several scenarios are designed for contour line figures drawing as shown in Table 5-5. Among offset types in different scenarios, green wave means the offset value under which upstream platoon with free-flow speed can reach the downstream stop line at the onset of downstream green. Queue clear 2s or 4s defines offset value under which upstream platoon with free-flow speed can reach the downstream stop line 2s or 4s after the onset of downstream green. For each scenario, the Q_{major} increases from 50 veh/h/ln to 450 veh/h/ln. Within this range, all cases will not be influenced by the spillback phenomenon.

The simulation platform in ***Chapter 5.1***, adjustment factor model 1, and adjustment factor model 2 perform for all 6 scenarios respectively. Based on results from them, contour line figures of all 6 scenarios are drawn separately for three methods. Figure 5.11 shows contour line figures for SFR and Figure 5.12 shows contour line figures for SLT.

Table 5-5 Scenarios are designed for contour line figures

No.	*C*	Offset type	r_{minor}	*gr*	l_s (m)	Q_{major} (veh/h/ln)
1	150	Green wave	0.4	0.6	48-320	50~450
2	150	Green wave	0.4	0.4	48-320	50~450
3	150	Green wave	0.2	0.6	48-320	50~450
4	120	Green wave	0.4	0.6	48-320	50~450
5	150	Queue Clear 2s	0.2	0.4	48-320	50~450
6	150	Queue Clear 4s	0.2	0.4	48-320	50~450

gr: downstream=upstream=0.4 or 0.6
Offset types:

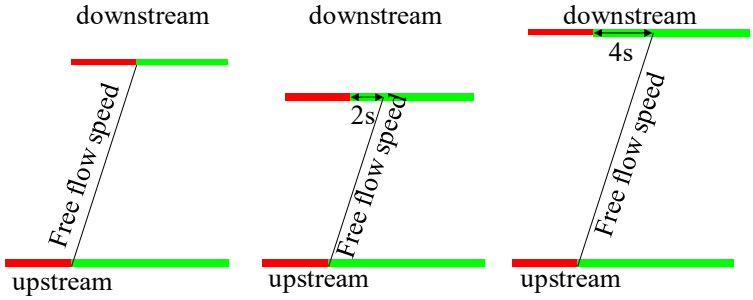

Firstly, the analysis focuses on the first column. In scenarios 1, 2, 3, and 4, with the l_s decreases from 320 to 48, the *Adj_SLT* increases and the *Adj_SFR* decreases. With Q_{major} increases from 50 to 450, it is found that the *Adj_SLT* increases and the *Adj_SFR* decreases as well. It confirms that the capacities of intersections with shorter downstream links under higher traffic demand are more easily influenced by downstream. Comparing the results of scenario 1 and 2, values of *Adj_SFR* with same l_s and Q_{major} is lower in scenario 1 than them in scenario 2. Meanwhile, values of *Adj_SLT* with the same l_s and Q_{major} are higher in scenario 1 than them in scenario 2. Because the g_r in scenario 2 (0.4) is lower than scenario 1 (0.6), capacities of upstream intersections in scenario 2 are lower than scenario 1. In scenario 2, fewer vehicles can be discharged from upstream intersections to form the downstream queue than them in scenario 1. Accordingly, the SLT and SFR are more likely influenced by downstream at intersections with higher *gr*. Comparing results of scenario 1 and 3, for same points, values of *Adj_SFR* in the scenario 1 is lower than them in the scenario 3 and values of *Adj_SLT* in the scenario 1 is higher than them in the scenario 3. It reveals that lower r_{minor} can mitigate downstream impacts. While comparing scenario 1 and scenario 4, it is found that, in the same position, the *Adj_SFR* in scenario 1 is lower than it in scenario 4 and the *Adj_SLT* in scenario 1 is higher than it in scenario 4. Larger cycle lengths can result in more serious downstream impacts. By comparisons between scenario 1, scenario 5, and scenario 6, it can be clearly

observed that downstream influence for cases (Q_{major}≤150 veh/h/ln) are 0 in scenario 5. When the queue clear time increases from 2s to 4s, the range of the Q_{major} under which downstream impacts are 0 expands to (0, 300) veh/h/ln. It indicates that green wave timings perform badly on short link arterials or under high traffic demand because of the downstream influence. Letting downstream queue discharge firstly can eliminate the downstream influence. The longer the queue clear time is, the lighter the downstream impact is. However, longer queue clear time may result in the green time of downstream intersection being wasted (downstream queue already being discharged however upstream platoon hasn't arrived). It is necessary to discuss the relationship between wasted green time and improved upstream capacity. Then, the offset value can be determined comprehensively and reasonably.

Figure 5.11 Contour line figures for SFR

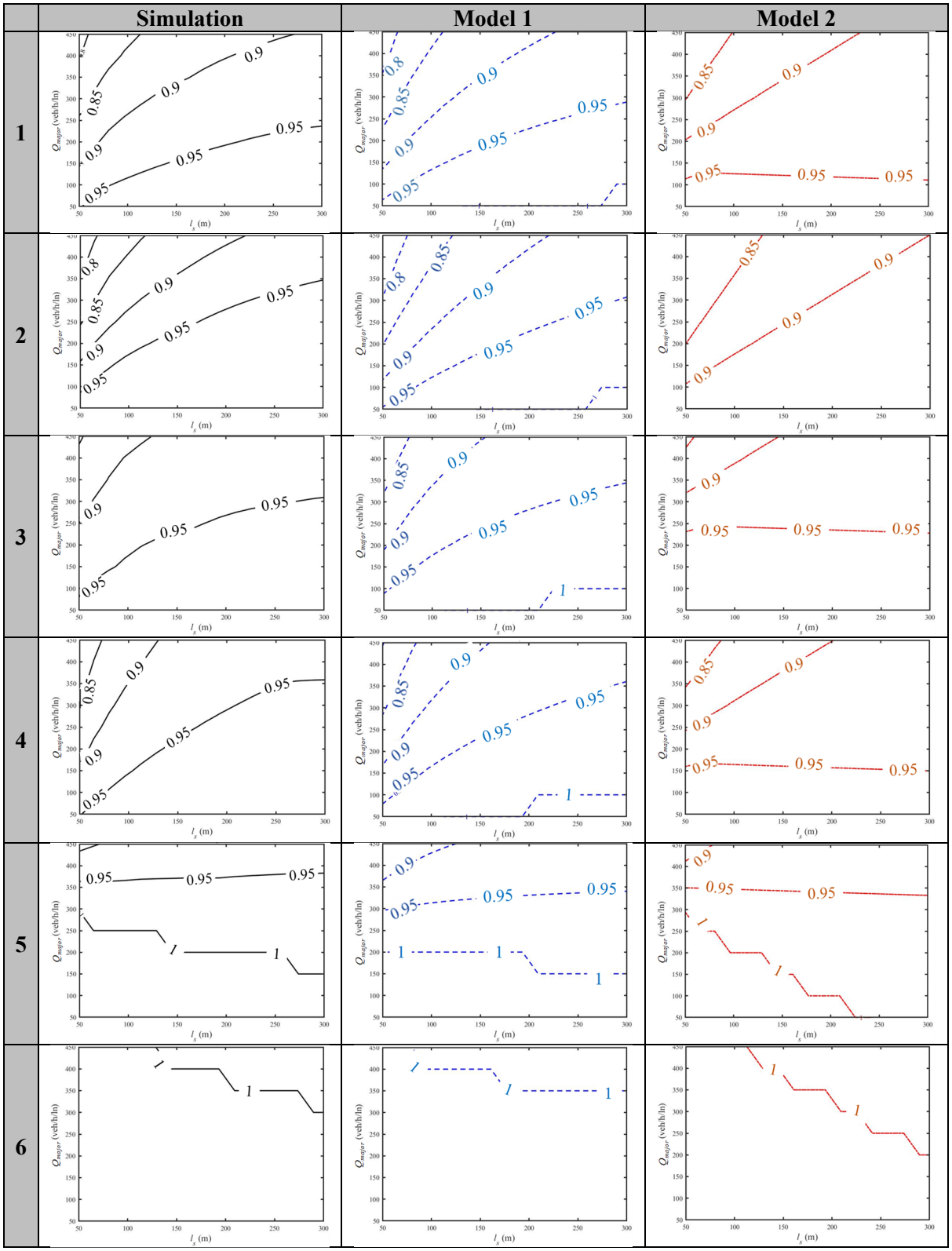

Figure 5.12 Contour line figures for SLT

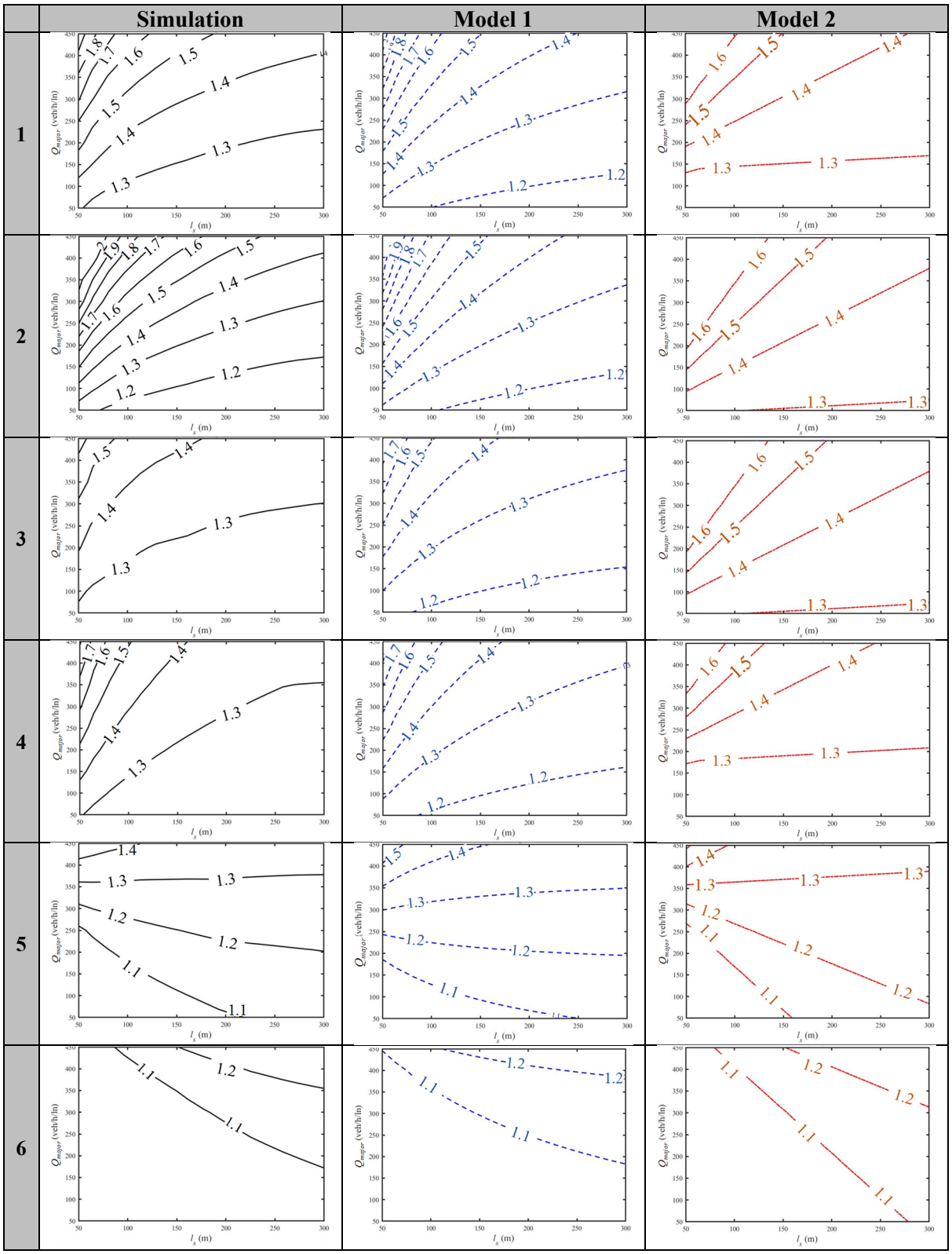

On the other hand, attention should be focused on comparisons between results of these three methods. For scenario 1,2, and 6, shapes of contour line figures from the simulation experiments are similar to those from model 1 and model 2. Model 1 is more similar to the

simulation results than model 2. In scenarios 3, 4, and 5, results from simulations still show good consistency to results from the model. On the contrary, there are obvious differences between the shapes of contour lines from the simulations and those from model 2. For all 6 scenarios, differences between values of each position and border are smaller than 0.05 for SFR figures and 0.1 for SLT figures. Model 2 has better fitness value, but it lacks logicality. Regression data is perfectly fitted. However, when the model 2 is applied for other situations (different offset types), its shortcomings will be exposed. Model 1 has good fitness value and logicality. It can not only fit the regression model well but also be reasonably applied in other scenarios. Therefore, model 1 is suggested to be applied finally.

5.3.3 Comparison with Existing Manuals and Empirical Data

In order to further validate the proposed model, a comparison analysis is done on Hirokoji-tori between the proposed model, existing manuals, and empirical data. The empirical data is only extracted from the 2nd (through) lane of approach WB 4 and EB 7 in Figure 4.8. They are selected because they fit the applicable conditions of the proposed estimation model. Firstly, the upstream green ratio equals to downstream green ratio. Secondly, based on our observation, vehicles on selected lanes are mainly from the turning volume of the minor street and major volume of corresponding upstream through lanes. Lane changing (vehicles from other lanes merging into this lane or vehicles on this lane diverging into adjacent lanes) rarely happens in their downstream during this period. 15 cycles between 8:30 and 9:30 are randomly chosen. SFR and SLT for these 15 cycles are measured by the method mentioned in ***Chapter 3.1.3***. Mean values for them are calculated to represent the actual SFR and the actual SLT for the selected period. Meanwhile, volume profiles are measured for selected lanes. Along with signal settings and segment length, they will be used in calculating adjustment factors of downstream influence as shown in Table 5-6.

The calculation of estimated SFR (SFRest) is based upon the MTSCJ methodology described in ***Chapter 2.2.1***. Among all the adjustment factors, only adjustment factor for lane width (f_w) and adjustment factor for approach gradient (f_g) are considered and the other adjustment factors equal to 1. The surveyed site is located in the urban area so that considering the adjustment factor for area type (f_a) is feasible. However, MTSCJ does not include this factor. The result of the estimated SFR by MTSCJ methodology and Table 5-7. On the other hand, no

available estimation method for SLT can be found in existing manuals. SFR estimated by MTSCJ calculated by Equation (5-14) and adjusted SFR on MTSCJ is calculated by Equation (5-15).

$$SFR_{MTSCJ} = s_0 f_w f_{HVg} f_{bb} f_{LU} f_{LT} f_{RT} f_{Lpb} \tag{5-14}$$

$$Adjusted\ SFR_{MTSCJ} = s_0 f_w f_{HVg} f_{bb} f_{LU} f_{LT} f_{RT} f_{Lpb} \cdot Adj\_SFR \tag{5-15}$$

Meanwhile, some other factors that should be included may not be taken into account by the MTSCJ. For fair comparisons, we also calculate adjusted SFR on base SFR as well which equal to 1631 veh/h/ln as shown in Equation (5-16). Also, adjusted SLT on base SLT is calculated by Equation (5-17). The value of the base SLT is 2.95s which is consistent with Equation (4-24). Finally, estimated SFRs by MTSCJ (MTSCJ), adjusted SFR on MTSCJ, adjusted SFR on base SFR, and observed SFRs are compared in Figure 5.13. Regarding the SLT, because no available SLT estimation method can be found, only observed SLT and adjusted SLT on base SLT are compared in Figure 5.13.

$$Adjusted\ SFR_{base\ SFR} = base\ SFR \cdot Adj\_SFR \tag{5-16}$$

$$Adjusted\ SLT_{base\ SLT} = base\ SLT \cdot Adj\_SLT \tag{5-17}$$

Table 5-6 Calculating adjustment factors of downstream influence

Approach	C	$Offset$	l_s (m)	gr	Q_{major} (veh/h/ln)	r_{minor}	Adj_SFR	Adj_SLT
WB 4	160	0	154	0.55	1001.25	0.50	0.95	1.22
EB 7	160	0	160	0.55	1102.5	0.51	0.92	1.34

Table 5-7 Estimated SFRs by the MTSCJ methodology

Approach	s_0	Lane width (m)	f_w	Gradient (%)	f_g	SFR_{est} by MTSCJ	Adjusted SFR
WB 4	2,000	3	0.95	-0.08	1	1,900	1796
EB7	2,000	3.2	1	0.45	1	2,000	1834

In Figure 5.13, for both two approaches, estimated SFRs by MTSCJ and adjusted SFRs on MUTCJ are extremely larger than actual values. Adjusted SFRs on base SFR are close to but a little larger than actual SFRs. These indicate that the estimation method in the MTSCJ may overestimate the actual SFR. It is important to consider the downstream influence when

estimating the SFR. In the MTSCJ equation, not only the downstream adjustment factor but also some other necessary factors are left out. We speculate that the adjustment factor for area type (f_a) and the factor involving elderly drivers can be discussed and taken into account. Meanwhile, adjusted SLT on based SLT and observed SLTs are almost equal in both two selected approaches, which further proves the usability of the proposed method.

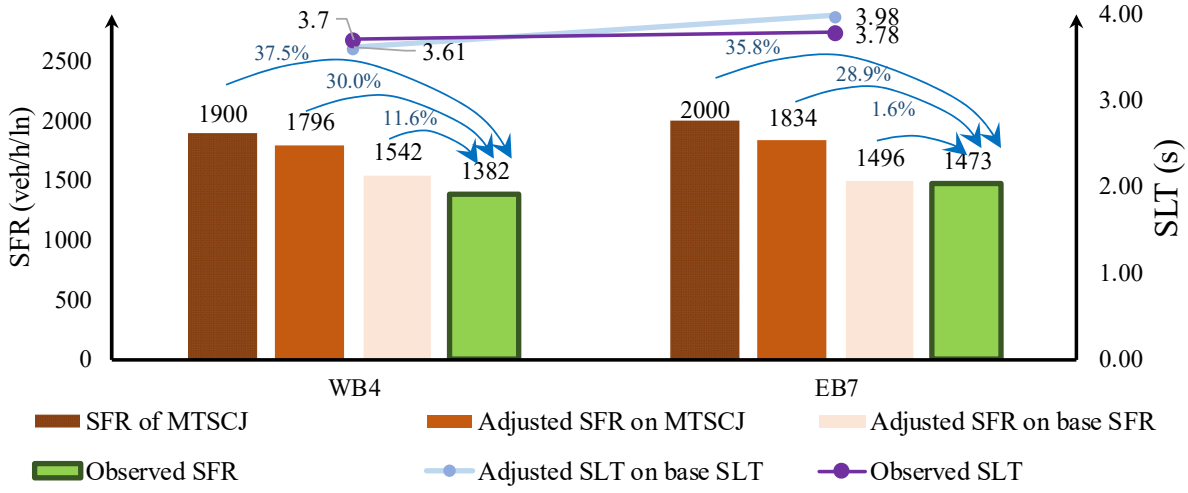

Figure 5.13 Comparison between proposed method, MTSCJ, and empirical data

5.4 Summary

This chapter established models of adjustment factors for influenced SFR and SLT considering downstream conditions. By this model, factors adjusting SFR and SLT for downstream influence can be calculated by parameters of traffic volumes, road geometry, and signal settings. Then the influenced SFR and SLT can be calculated accordingly by these adjustment factors. Before this research, none of the estimation models in existing manuals can properly calculate the influenced SFR and SLT considering downstream impacts.

The model of adjustment factors proposed in this Chapter is a two-step model that is studied by regression analysis. The raw data used for modeling was from the simulation experiment. The first step is to estimate the downstream queue length considering downstream impacts. The second step is to estimate adjustment factors based on the newly proposed queue

length model. During the analysis, it was found that the model in two steps can reduce the computational complexity. Also, one regression fitting target was set for each step, which helped to improve the accuracy of the final model. In this process, the basic changing trend of queue length was reproduced in the first step and fitting errors were reduced to a good level in the second step. Finally, two models that are based on two different assumptions separately were got. Simulation platform and two models were performed on 6 designed scenarios. Based on contour line figures of these 6 scenarios, it was found that lower green ratio, smaller cycle length, and more flow from minor street result in more serious downstream impacts. Through comparison, model 1 (more logical, assumption: constant queue/volume ratio) is proved to be better than model 2 (more fitting, assumption: linear with upper and lower constraints). Through this process, it revealed that the model's logicality is as important as the model fitting performance. The proposed model was further applied in real-world approaches along with the methodology prescribed in MTSCJ. Results indicate that proposed adjustment factors are reasonable and necessary to be included.

CHAPTER 6 CONCLUSIONS AND FUTURE WORKS

6.1 Conclusions

This research provided solid scientific evidence by empirical studies and appropriate methodology by theoretical studies for estimating the influenced SFR and SLT. The existing manuals and simulators overestimated capacities at signalized intersections. Also, previous research before this study did not comprehensively discuss the downstream influence. Therefore, the major contribution of this research is creating models for adjustment factors that can properly adjust SFR and SLT considering downstream conditions. The adjustment factors are calculated with parameters of traffic volumes, road geometry, and signal settings so that the model can be applied in practice easily. Furthermore, they can be included in the estimation models of existing manuals such as HCM 6th edition and MTSCJ letting predicting results more accurate. The improved car-following model created in chapter 3 and the improved cell transmission model proposed in chapter 4 are also important achievements of this research. The proposed car-following model can provide revising ideas for the core models of existing simulators and newly established CTM is a good tool for simulating traffic propagation on signal-controlled arterials. In this study, not only the car-following model and CTM but also simulation experiment and regression analysis are applied. These models and research methods are used to solve the relationship model between influenced SFR, SLT, and macro traffic indicators which is also the most important difficulty that has been overcome by this research. Meanwhile, significant findings of this study are summarized as follows.

6.1.1 Influenced Discharging Behavior Considering Downstream Impacts

This research proposed an improved car-following model (IDM+) that can properly reproduce influenced discharging behaviors under different downstream conditions. The main idea of this model is to consider the human subconscious. When they clearly understood that they must stop soon, drivers may reduce the speed to avoid completely stops and uncomfortable

deceleration. This influence was measured by a virtual speed optimal speed (v_{op}, the speed by which the upstream platoon reaches the endpoint of the queue ahead when the last vehicle in the downstream queue just starts). Treating v_{op} as the core indicator, the improved model was designed. This model was calibrated by empirical driving data. The model's characteristics are tested by a sensitivity analysis. Results showed that facing with long queue and red signals in downstream links, drivers' ambitions of rapid acceleration and quickly running will be discouraged. For the same length of the queue, this impact is more significant in a shorter segment link. Under these situations, accelerations and speeds of upstream vehicles are lower than uninfluenced ones. Accordingly, discharging efficiencies of upstream platoons are impacted. This subconscious is not only limited at signalized intersections in urban areas but also suitable for explaining some phenomena on freeway sections. For instance, when approaching the downstream jam section on a freeway, the speed of the upstream platoon tends to decrease.

6.1.2 SFR and SLT Influenced by Downstream Conditions

Studying on the influenced SFR and SLT firstly started from an empirical analysis on Yasukuni-tori. Results indicated that with queues in downstream links become longer, SFRs tend to be lower and SLTs tend to be higher. SFRs of data points with large offset values are lower than others and SLTs of data points with large offset values are higher than others. Also, downstream impacts are more significant for intersections with short downstream links. Then downstream influence is theoretically studied. Based on these findings, the downstream module in IDM+ was designed. The IDM+ was further designed into a simulation experiment. Simulation results showed that this experiment can properly reproduce the phenomena that were found in the empirical analysis. Meanwhile, simulated SFR and SLT. Trends modeled by IDM+ were further summarized into two-step models by doing regression analysis on the simulation data. In these models, downstream influence is measured by v_{op}. Then, influenced SLT and SFR are calculated by v_{op} based on two piecewise models. Influenced SFR and SLT calculated by regression models not only are the same as simulated values but also fitted the empirical data very well.

6.1.3 Downstream Influence on the Signalized Arterial

For introducing the downstream influence into traffic modeling along signalized arterials, models of influenced SFR and SLT were combined with modified CTM. Unlike the traditional CTM, the newly composed model can simulate real discharge features at signalized intersections. By adjusting cells' parameters regarding current downstream conditions, influenced SFR and SLT can be reproduced as well. Firstly, the proposed CTM was proved to have the equivalent performance as the IDM+. Then it was validated on a real-world road (Hirokoji-tori). Results proved that considering the downstream influence is quite a necessary procedure for traffic simulations. Because only by this, the simulation platform can accurately reproduce the evolution of queue length at each intersection, simulation the congestion section, and estimate the delay that happened on the corridor. Furthermore, how the downstream effect evolves along the signalized arterial was explored on a CTM based platform by the sensitivity analysis. It found that the degree of congestion in one road section is related to input volume (from minor and major streets), downstream links length, offsets of downstream, and secondary downstream intersections.

6.1.4 Adjustment Factors of SFR and SLT

Based on the proposed CTM theory, adjustment factors of SFR and SLT were modeled into two-step models. The queue length was estimated by regression analysis based on data that were from simulation experiments and then estimated v_{op} was calculated by the estimated queue length. Adjustment factors of SFR and SLT were further modeled by estimated v_{op}. By this procedure, *Adj_SLT* and *Adj_SFR* can be directly calculated by variables of traffic conditions (road geometry, traffic demand, and signal settings). Contour line figures revealed that high traffic demand (from major and minor streets) and short downstream link length lead to a lower *Adj_SLT* and higher *Adj_SFR*. Green ratios and large cycle length can aggravate the downstream influence. Meanwhile, it also indicated that green wave timings are not suitable for roads with short segments or under high traffic demand. Instead, queue clear timings (letting downstream queue discharge firstly before upstream platoon arrives) work well and are suggested for these cases. Finally, a comparison analysis was made at a real-world approach. Results showed that after including the *Adj_SFR*, the accuracy of the existing SFR model (MTSCJ) was improved. Also, SLT calculated by the proposed procedure is basically

consistent with observed SLT. Hence, it could be concluded that proposed models can be applied in practice for some specific road conditions.

6.2 Limitations and Future Works

The main limitation of this study is the exclusion of cases with several factors. Through data screening, some influencing factors have been excluded, such as heavy vehicles, motorcycles, cutting-in effect, and overtaking behaviors. Therefore, during experiment simulations, a simple two-intersections two-lane road was built. The assumed simulation platform can avoid discussing the impacts of cut-in effects and overtaking issues. However, these factors are necessary to be incorporated when the method is applied in practice. The other limitation is the basic assumption of this research. This study assumed that the subject and downstream intersection will not further be influenced by the secondary downstream intersection. However, the downstream intersection maybe not isolated from the impact of the secondary downstream intersection. Meanwhile, for short links, drivers can observe traffic conditions in the secondary downstream link. Hence, drivers may be influenced by two downstream intersections simultaneously. If all the above issues are considered there be infinite varieties of study cases. From the beginning, it is appropriate and necessary to explore the research with some simplifications. In the future, this research should be further improved by deleting the assumption gradually. The following is suggested as significant future studies in order to achieve the global objective of dynamic network traffic control considering downstream influence.

6.2.1 Adaptability to Multi-lane Arterials

As prescribed in ***Chapter 5.1***, the final estimation model can mainly be applied to approaches on two-lane arterials. For approaches on multi-lane arterials, only when lane changing behaviors rarely happens in the corresponding downstream lane, the estimation model can be used. Before this model can be fully applied to approaches of multi-lane arterials, it is necessary to overcome the following points. Firstly, in empirical studies, cutting-in effect and overtaking behaviors are neglected. Also, in theoretical studies, models were built based on an assumed two-lane arterial where cutting-in effect and overtaking are not allowed. In order

to build a more compatible model, cutting-in and overtaking behaviors should also be included in the designing of the micro-simulation platform. Secondly, considering OD pairs of input flows, using rates of lanes in downstream links are different in reality. In terms of this, the queue length estimation model in ***Chapter 5.2*** can be updated and improved as well in future studies. This point is also important for simulating the traffic on multi-lane arterials. In addition, on multi-lane arterials, one approach may consist of different types of lane groups (right or left turn lane, shared right or left turn lane). Although it can be inferred that discharge flows on through lanes are most susceptible to downstream influence. Other lane types might be impacted to some extent and should be investigated as well.

6.2.2 Stochastic Feature of Calibrated Parameters in Car Following Model

In Figure 3.29, only one point for each case was modeled and empirical data points distributed over a wide range surrounding modeled lines. This phenomenon can be explained by drivers' stochasticity. In the IDM based micro-simulation platform, the same parameters were adopted for all drivers in the simulation to represent the average behavior. In the real world, these parameters might differ for different drivers. For instance, the reaction time for young drivers might be lower than old drivers. Assuming certain distributions (such as normal distribution) for model parameters might help in understanding the stochasticity of driver behavior. Distribution shapes should be estimated from empirical data. Adopting different parameters for different drivers and letting the experiment be performed based on the Monte Carlo method, more convincing results can be got. However, no available calibration methodology that can output distribution shapes for parameters of multi-variable car-follow has ever been proposed. This technical difficulty is expected to be solved in the future.

6.2.3 Clearing Vehicles and Clearance Lost Time

During collecting field data from video, it was observed that in some cases when platoon started to discharge there were some vehicles from the last phase still in the intersection as shown in Figure 6.1. These vehicles are called clearing vehicles and their presence may block or interfere the forwarding route of the discharge flow, resulting in high SLT. in observed streets, inter-green times of all intersections are up to 8 seconds which are long enough for vehicles clearing the intersection. Therefore, clearing vehicles occurred rarely. Their influence

was treated as random events and excluded from this research. However, at intersections under large traffic volumes, this phenomenon can be frequently observed. It is necessary to build a theoretical model for impacts from clearing vehicles. In addition, for now, it can be inferred that this phenomenon is related to lengths of inter-green times and traffic volumes from minor streets.

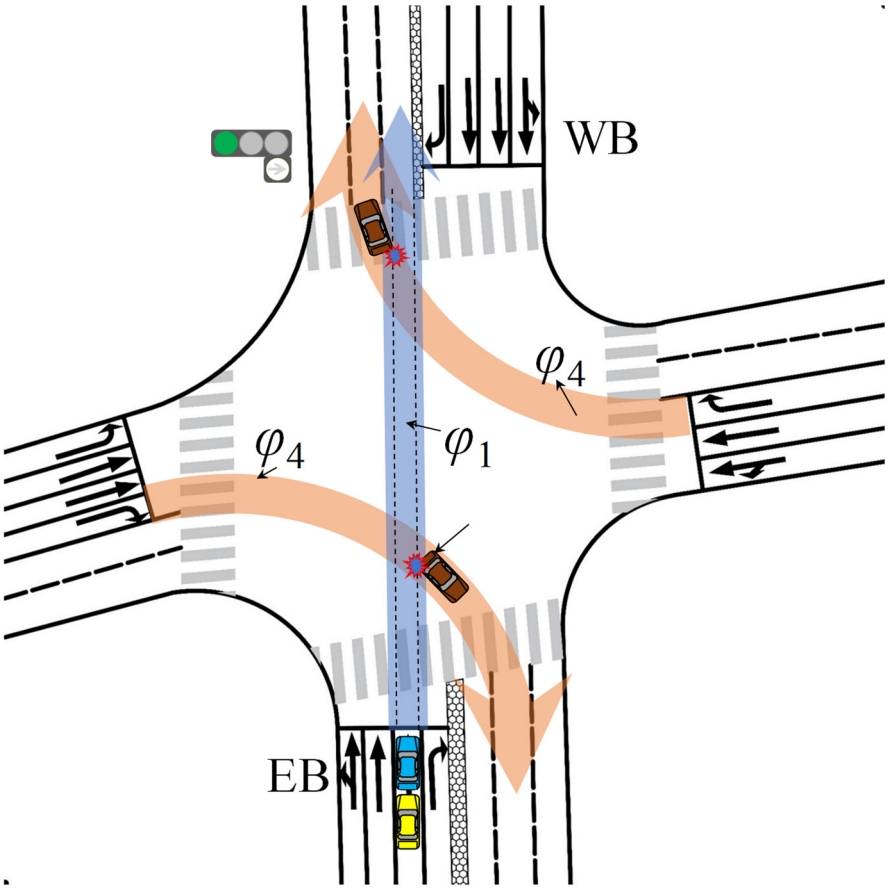

Figure 6.1 Discharging flow influenced by clearing vehicles

On the other hand, clearance lost time (CLT, hereinafter) also serves as important parameters in the capacity estimation of signalized intersections. CLT defines the time between signal phases during which an intersection is not used by any critical movements. Since clearance lost time is often not observable since observation requires that some vehicles which were waiting at the start of a green phase still be waiting when the green phase ends, it is simply defined as a default value of 2.0 seconds in HCM (2016). ALDOT's Traffic Signal Design

Guide and Timing Manual (2006) determines CLT to be half of the yellow interval plus the entire all-red interval. How could CLT be influenced by downstream influence is also an interesting topic in the future.

6.2.4 Autonomous Vehicle Flow

In the future, human-driven vehicles (HV, hereinafter) will be gradually substituted by autonomous vehicles (AV, hereinafter). With the improvement of related technologies, AVs can not only handle vehicles for humans during whole driving processes but even be completely superior to human drivers' skills. Definitely, in the future, AVs will be able to have abilities that human drivers can't do. For example, unlike human drivers, AVs don't have emotions therefore they will not be impacted by downstream queues. Meanwhile when running AVs may share driving status information with other vehicles and communicate with control systems of signalized intersections. How would traffic propagations be distributed, if flows on the signalized arterial are 100% consisted of AVs? According to my imagination, for the AVs' discharge platoon, all waiting vehicles will start quickly simultaneously at the onset of green indication and the platoon will operate as a train. Therefore, SLTs may simply equal to machine starting time and SFRs will always equal to a constant value. The traffic jam along a signalized arterial can be mitigated to some extent. But if congestion happened, the distribution of traffic along arterials will be different from what is shown in Figure? (due to the downstream influence, heavy traffic occurs in the upstream section). It can be inferred that congestion would happen only after bottleneck intersections (e.g. small green ratio). The above image assumes that all vehicles are AVs. "How results would be if only part of them (e.g. 10~90%) is AVs?" is also an interesting topic for future studies.

REFERENCES

Abuamer, I. M., Sadat, M., Silgu, M. A., and Celikoglu, H. B. (2017) *Analyzing the effects of driver behavior within an adaptive ramp control scheme: a case-study with ALINEA*, In 2017 IEEE International Conference on Vehicular Electronics and Safety (ICVES), pp.109-114.

Abuamer, I. M., Silgu, M. A., and Celikoglu, H. B. (2016) *Micro-simulation based ramp metering on Istanbul freeways: an evaluation adopting ALINEA*, In 2016 IEEE 19th International Conference on Intelligent Transportation Systems (ITSC), pp.695-700.

Ahmed, K. and Abu-Lebdeh, G. (2005) *Modeling of Delay Induced by Downstream Traffic Disturbances at Signalized Intersections*, Transportation Research Record, 1920, 1, pp.106-117.

Akyol, G., Silgu, M. A., and Celikoglu, H. B. (2019) *Pedestrian-friendly traffic signal control using Eclipse SUMO*, Proceedings of the SUMO User Conference 2019, EPiC Series in Computing, 62, pp.101-106.

Akçelik, R., Besley, M. and Roper, R. (1999) *Fundemantal relationships for traffic flows at signalized intersections*, ARRB Transportation Research Ltd., Research Report ARR340.

Antoniou, C., Barceló, J., Brackstone, M., Celikoglu, H. B., Ciuffo, B., Punzo, V., Sykes, P., Toledo, T., Vortisch, P., and Wagner, P. (2014) *Traffic simulation: case for guidelines*, JRC Scientific and Technical Report, EUR 26534 EN, Publications Office of the European Union, Luxembourg.

Behbahani, H., Samet, M. J., Gilani, V. N. M. and Amini, A. (2017) *Determining of the Parking Manoeuvre and the Taxi Blockage Adjustment Factor for the Saturation Flow Rate at the Outlet Legs of Signalized Intersections: Case Study from Rasht City (Iran)*, In IOP Conference Series: Materials Science and Engineering, IOP Publishing, 245, 4.

Bonneson, J.A. (1992) *Modelling queued driver behavior at signalized junctions*, Transportation Research Record, 1365, pp.99-107.

Branston, D. (1979) *Some factors affecting the capacity of signalised intersections*, Traffic Engineering and Control, 20, pp.8-9.

Çalışkanelli, S. P., Atasever, F. C. and Tanyel, S. (2017) *Start-up Lost Time and its Effect on Signalized Intersections in Turkey*, Promet -Traffic&Transportation, 29, 3, pp.321-329.

Çalişkanelli, S.P., and Tanyel, S. (2016) *Investigating the driver's response time at signalized intersections*, Transport, doi: 10.3846/16484142.2016.1250106.

Chand, S., Gupta, N. J. and Velmurugan, S. (2017) *Development of saturation flow model at signalized intersection for heterogeneous traffic*, Transportation Research Procedia, 25, pp.1662-1671.

Chin, H. C. (1996) Reexamination of the analysis of freeway bottlenecks, ITE Journal, 66, 1, pp.30–35.

Chodur, J., Ostrowski, K. and Tracz, M. (2011) *Impact of saturation flow changes on performance of traffic lanes at signalised intersections*, Procedia-Social and Behavioral Sciences, 16, pp.600-611.

Cohen, S. (2002) *Application of Car-Following Systems to Queue Discharge Problem at Signalized Intersections*, Transportation Research Record, 1802, 1, pp.205-213.

Daganzo, C. F. (1983) *Derivation of delays based on input-output analysis*, Transportation Research Part A, 17, 5 pp.341–342.

Daganzo, C. F. (1994) *The cell transmission model: A dynamic representation of highway traffic consistent with the hydrodynamic theory*, Transportation Research Part B: Methodological, 28, 4, pp.269-287.

Daganzo, C. F. (1995) *The cell transmission model, part II: network traffic*, Transportation Research Part B: Methodological, 29, 2, pp.79-93.

Davoodi, S. R., Sadeghiyan, S. and Faezi, S. F. (2015) *The Analysis the Role of Motorcycles on Saturation Flow Rates at Signalized Intersections in Gorgan*, Indian Journal of Science and Technology, 8, 13.

Deng, H. and Zhang, H. (2012) *Driver anticipation in car following*, Transportation Research Record, 2316, pp. 31-37.

Erdağı, İ. G., Silgu, M. A., and Çelikoğlu, H. B. (2019) *Emission Effects of Cooperative Adaptive Cruise Control: A Simulation Case Using SUMO*, Proceedings of the SUMO User Conference 2019, EPiC Series in Computing, 62, pp.92-100

FHWA – Federal Highway Administration (2008) *The Traffic Signal Timing Manual*, U.S.

Hashemi, A. H., Nakamura, H. and Goto, A. (2017) *Influence of Downstream Conditions over Saturation Flow Rate*, Proceedings of the 37th Conference of Japan Society of Traffic Engineers, pp.467-472.

Herman, R., Montroll, E.W., Potts, R.B. and Rothery, R.W. (1959) *Traffic Dynamics: Analysis of Stability in Car Following*, Operations Research, 7, 1, pp.86-106.

Institute of Transportation Engineers (1994) *Determination of Vehicle Signal Change and Clearance Intervals*, Publication IR-073, Washington, D.C.

JSTE – Japan Society of Traffic Engineers (2006) *Revised Edition of Manual on Traffic Signal Control*, JSTE, Tokyo.

Kesting, A. and Treiber, M. (2008) *Calibrating Car-Following Models Using Trajectory Data: Methodological Study*, Transportation Research Record, 2088, 1, pp.148-156.

Li, H. and Prevedouros, P.D. (2002) *Detailed Observations of Saturation Headways and Start-up Lost Times*, Transportation Research Record, 1802, pp.44-53.

Little, J. D., Kelson, M. D. and Gartner, N. M. (1981) *MAXBAND: a program for setting signals on arteries and triangular networks*, Transportation Research Record, 795.

Liu, Y., Yu, J., Chang, G. L., et al. (2008) *A lane-group based macroscopic model for signalized intersections account for shared lanes and blockages*, 11th International IEEE Conference on Intelligent Transportation Systems, Beijing.

Lo, H. K., Chang E. and Chan, Y. C. (2001) *Dynamic network traffic control*, Transportation Research Part A: Policy and Practice, 35, 8, pp.721-744.

Messer, C.J. and Fambro, D.B. (1977) *Effects of Signal Phasing and Lengths of Left-Turn Bay on Capacity*, Transportation Research Record, 644, pp.95-101.

Minh, C.C. and Sano, K. (2003) *Analysis of motorcycle effects to saturation flow rate at signalized intersection in developing countries*, Journal of Eastern Asia Society for Transportation Studies, 5, pp.1211-1222.

PTV – Planung Transport Verkehr (2015) *PTV VISSIM 8 User Manual*, PTV AG, Karlsruhe, Germany.

Roess, P.R., Prassas, E.S. and McShane, W.R. (2004) *Traffic Engineering 3rd ed*, Pearson Prentice Hall, New Jersey, USA.

Rouphail, N. M. and Akcelik, R. (1992) *A Preliminary Model of Queue Interaction at Signalized Paired Intersections*, Australian Road Research Board Ltd (ARRB) Conference, 16, 5.

Sadat, M. and Celikoglu, H. B. (2017) *Simulation-based variable speed limit systems modelling: an overview and a case study on Istanbul freeways*, Transportation Research Procedia, 22, pp.607-614.

Sando, T., and Moses, R. (2009) *Influence of intersection geometrics on the operation of triple left-turn lanes. Journal of transportation engineering*, 135, 5, pp.253-259.

Shao, C.Q., Rong, J. and Liu, X.M. (2011) *Study on the saturation flow rate and its influence factors at signalized intersections in China*, Procedia-Social and Behavioral Sciences, 16, pp.504-514.

Silgu, M. A., Muderrisoglu, K., Unsal, A. H., and Celikoglu, H. B. (2018) *Approximation of Emission For Heavy Duty Trucks In City Traffic*. Proceedings of the 2018 IEEE International Conference on Vehicular Electronics and Safety (ICVES2018)

Srivastava, A., Jin, W. L. and Lebacque, J. P. (2015) *A modified cell transmission model with realistic queue discharge features at signalized intersections*, Transportation Research Part B: Methodological, 81, pp.302-315.

Sun, H., Yang, J., Wang, L., Li, L. and Wu, B. (2013) *Saturation Flow Rate and Start-up Lost Time of Dual-left Lanes at Signalized Intersection in Rainy Weather Condition*, Procedia-Social and Behavioral Sciences, 96, pp.270-279.

Suzuki, K. and Nakamura, H. (2006) *Development and performance evaluation of a video image processing system for traffic flow analysis - TrafficAnalyzer*. [In Japanese.] Doboku Gakkai Ronbunshu D, Japan Society of Civil Engineers, 62, 3, pp.276-287.

Tong, H.Y. and Hung, W.T. (2002) *Neural network modelling of vehicle discharge headway at signalized intersection: model descriptions and results*, Transportation Research Part A: Policy and Practice, 36, 1, pp.17-40.

TRB – Transportation Research Board (2016) *Highway Capacity Manual 6th Edition*, National Research Council, Washington, D.C.

Treiber, M., Hennecke, A. and Helbing, D. (2000) Congested traffic states in empirical observations and microscopic simulations, Physical Review E, 62, 2, pp.1805-1824.

TSS-Transportation Simulation Systems (2010) *Aimsun 6.1 User Manual*.

Wang, X., Zheng, J., Liu H. X. et al (2019) E*stimating Saturation Flow Rate for Signalized Intersection Using Trajectory Data*, 98th Annual Meeting of the Transportation Research Board (TRB), Washington, D.C., January.

Yi, P., Tian, Z. Z. and Zhao, Q. (2008) Consistency of Input-Output model and shockwave analysis in queue and delay estimations, J Transpn Sys Eng & IT, 8, 6, pp.146-152.

Yu X., and Sulijoadikusumo, G. (2012) *Analysis of Downstream Queues on Upstream Capacity Expansion of Urban Signalized Intersection*, Journal of Transportation Systems Engineering and Information Technology, 12, 3, pp.98-108.